BMP nanocapsule formulation in treating Glioblastoma and BMP-antagonists interaction studies

Thesis submitted for the degree of

DOCTOR OF PHILOSOPHY

By

Kesaban Sankar Roy Choudhuri

Department of Biochemistry
School of Life Sciences
University of Hyderabad
Hyderabad-500046, INDIA

Enrolment No. 15LBPH14

University of Hyderabad
(A central university established in 1974 by act of parliament)
Hyderabad- 500046, INDIA

CERTIFICATE

This is to certify that Mr. **Kesaban Sankar Roy Choudhuri** has carried out the research work embodied in the present thesis under my supervision and guidance for a full period prescribed under the Ph.D. ordinance of this University. We recommend his thesis entitled "BMP nanocapsule formulation in treating Glioblastoma and BMP-antagonists interaction studies" for submission for the degree of Doctor of Philosophy of this University.

Dr. Seema Mishra
Research Supervisor

Head
Department of Biochemistry

Dean
School of Life Sciences

DEAN
School of Life Sciences
University of Hyderabad
Hyderabad - 500 046.

University of Hyderabad
(A central university established in 1974 by act of parliament)
Hyderabad- 500046, INDIA

DECLARATION

I, **Kesaban Sankar Roy Choudhuri**, hereby declare that the work embodied in this thesis entitled "**BMP nanocapsule formulation in treating Glioblastoma and BMP-antagonists interaction studies**" has been carried out by me under the supervision of Dr. Seema Mishra and this has not been submitted for any degree or diploma of any other university earlier.

Kesaban Sankar Roychoudhuri
18/1/21

Kesaban Sankar Roy Choudhuri
(Research Scholar)

University of Hyderabad
(A central university established in 1974 by act of parliament)
Hyderabad- 500046, INDIA

CERTIFICATE

This is to certify that the thesis entitled "**BMP nanocapsule formulation in treating Glioblastoma and BMP-antagonists interaction studies**" submitted by **Kesaban Sankar Roy Choudhuri** registration number **15LBPH14** in partial fulfillment of the requirements for award of Doctor of Philosophy in the School of Life Sciences is bonafide work carried out by him/her under my supervision and guidance.This thesis is free from plagiarism and has not been submitted previously in part or in full to this or any other university or institution for award of any degree or diploma.

Further, the student has the following publication(s) before submission of the thesis/ monograph for adjudication and has produced evidence for the same in the form of reprint in the relavent area of his research.

1. Kesaban Sankar Roy Choudhuri, Seema Mishra. Structural basis of BMP-2 and BMP-7 interactions with antagonists Gremlin-1 and Noggin in Glioblastoma tumors. J Comput Chem. 2020;1–18.

And has made presentations in the following conferences:

1. K. S. Roy Choudhuri, Mishra S. BMP microsphere formation in treating glioblastoma and BMP-antagonist interaction studies: Poster presented in "Biomolecular Interactions in Development and Disease", a seminar organized by the Department of Biochemistry, University of Hyderabad on 28 September, 2019.
2. K. S. Roy Choudhuri, Mishra S. BMP microsphere formation in treating glioblastoma and BMP-antagonist interaction studies: Presented poster in Inspire Fellowship review meet organized by DST Inspire on 20 June, 2019.
3. K. S. Roy Choudhuri, Mishra S. BMPs and its antagonist interaction studies in glioblastoma: A computational approach, BioQuest 2017 on 12 Oct, 2017.

Further, the student has passed the following courses towards fulfillment of coursework requirement for Ph.D.

Course code	Name	Credits	Pass/Fall
BC801	Analytical Techniques/ Research methodology	4	passed
BC802	Biostatistics, Research ethics and Data analysis	3	passed
BC803	Lab seminar and Record	5	passed

Supervisor

Head of the Department

HEAD
Dept. of Biochemistry
SCHOOL OF LIFE SCIENCES
UNIVERSITY OF HYDERABAD
HYDERABAD-500 046

Dean of School

DEAN
School of Life Sciences
University of Hyderabad
Hyderabad - 500 046

Acknowledgments

I express my deepest sense of gratitude to my mentor, Dr. Seema Mishra, for giving me an opportunity to work under her able guidance, providing the lab facilities and constant support throughout my work. It gives me immense pleasure to admit that Dr. Seema Mishra, my mentor with integrity, patience and perseverance, has been a constant source of inspiration throughout my doctoral discourse.

I would like to forward my gratitude to Professor A. Kondapi, for allowing his student, Mr. Satyajit Mukhopadhyay, to work in collaboration for few works in the thesis (Chapter 4: Section 4.2.3 & Section 4.3.4, Chapter 5: Section 5.2.5 & Section 5.3.4). I would like to forward my gratitude to the Department of physics for allowing me to use instruments for doing DLS and FESEM studies (Section 5.2.2. & 5.3.1).

I would like to thank the former head, N. Siva Kumar, Prof. Mrinal Bhattacharya Department of Biochemistry and the present head, Prof. Krishnaveni Mishra.

I would like to thank former and present Dean, School of Life Sciences Prof. Kolluru V A Ramaiah and Prof. Dayananda Siddavattam for allowing me to use the facilities of the school.

I wish to thank all my cooperative lab mates A. SaleemBhasha, Santosh Kumar, Euphinia, Praveena, Rohan and Ayang for their timely help and support. I wish them all success and happiness in their lives

I thank Prof. Tushar Jana, Prof. D.B. Ramachary, Prof M. Durga Prasad and other faculty members of School of Chemistry for the knowledge they have shared with me.
I thank Prof R.K.Mishra for offering me a project position and share me knowledge in the field of cognitive science.

I thank all my teachers since my childhood whose guidance and encouragement at each step was instrumental in shaping my career.

I acknowledge DST INSPIRE, New Delhi for providing JRF and SRF in the form of financial assistance.

I fall short of words to thank my family members, especially my brother Sandipan Sankar Roy Choudhuri, and my aunt Dr. Suparna Bhattacharjee for their blessings, inseparable support, prayers and love.

I take this opportunity to thank my intimate friends, N. Anurag, Samuel Anurag, Sham Bharadwaj, Omkar, Tathagata, Sahith, Rajarshi, Varna; Sai kumar Yamarthi, Neshat Haq, Tejaswi Naidu, Satyajit, Suraj, Neha, Pankaj,Ranjan and Ganesh. I wish them all success and happiness in their lives.

Finally, I express my gratitude to my mother, Sutapa Roy Choudhuri and my father Krishna Sankar Roy Choudhuri for providing me the moral strength to lead the life against all the odds. I owe all my success to them.

Kesaban Sankar Roy Choudhuri

Dedicated to my parents

Table of content

i. Abbreviations

GBM	:	Glioblastoma Multiforme
WHO	:	World Health Organization
ALL	:	Acute Lymphoid Leukemia
BMP	:	Bone Morphogenetic Proteins
TGF-β	:	Transforming growth factor beta
DAN	:	Differential screening-selected gene abbreviative in Neublastoma
Tsg	:	Twisted gastrulation
Chd	:	Chordin
Nog	:	Noggin
Fst	:	Follistatin
Fstl3	:	FLRG-follistatin-related gene
Grem-1	:	Gremlin-1
R-Smads	:	Regulatory Smads
Co-Smad	:	Common Smad
I-Smads	:	Inhibitory Smads
ERK	:	Extracellular signal-regulated kinase
NFkB	:	Nuclear factor kappa beta
JNK	:	c-Jun N-terminal kinase
BRAM1	:	Bone Morphogenetic Protein Receptor Associated Molecule 1
XIAP	:	X-linked Inhibitor of Apoptosis Protein
TAK1	:	TGF- β Activated Kinase 1
TAB1	:	TAKI Binding protein
PK	:	Protein kinase
TMZ	:	Temozolomide
PDB	:	Protein Data Bank
SL2	:	Superlooper2
CHARMM	:	Chemistry at Harvard Macromolecular Mechanics
EEEF	:	Empirical effective energy function
GICs	:	Glioblastoma initiating cells

CSCs	:	Cancer Stem Cells
PPIM	:	Protein-protein interaction modulators
NSs	:	Neurospheres
PLGA	:	poly(lactic-co-glycolic acid)
FESEM	:	Field Emission Scanning Electron Microscope
DLS	:	Dynamic Light Scattering
SDS-PAGE	:	Sodium dodecyl sulphate-polyacrylamide gel electrophoresis
ELISA	:	Enzyme-linked immunosorbent
BME	:	Beta-mercaptoethanol
PBS	:	Phosphate buffered saline
DMEM	:	Dulbecco's Modified Eagle Medium
FITC	:	Floroscein isothiocyanate
ALA	:	Alanine
ARG	:	Arginine
ASN	:	Asparagine
ASP	:	Aspartate
CYS	:	Cysteine
GLU	:	Glutamate
GLN	:	Glutamine
GLY	:	Glycine
HIS	:	Histidine
ILE	:	Isoleucine
LEU	:	Leucine
LYS	:	Lysine
MET	:	Methionine
PHE	:	Phenylalanine
PRO	:	Proline
SER	:	Serine
THR	:	Threonine
TYR	:	Tyrosine

VAL	:	Valine
TRP	:	Tryptophan

ii. List of figures and tables

Figures

Chapter 3

Chapter 4

Chapter 5

Tables

Chapter 3

Chapter 4

Chapter 5

Chapter-1: Introduction and Review of literature

1.1. Glioblastoma Multiforme

Glioblastoma Multiforme (GBM) can be characterized as a primary brain tumor in its most malignant form which accounts for 60% of all brain tumors in adults (1). Despite advancements as well as an increase in therapeutic strategies in the treatment of glioblastoma, the median survival period is approximately 15-23 months with a 5-years survival rate below 6% (2). The World Health Organization (WHO) has designated glioblastoma as a Grade IV glioma based on its aggressive and invasive nature (3, 4).

The global incidence rate of GBM is less than 10 per 100,000 people and has significantly shown a steady increase over the last decade (5-7). GBM can present itself at any age, although the peak incidence age remains between 55 to 60 years (8). The incidence of GBM varies across genders, regions, races, and ethnicity. The ratio of GBM occurring in men is higher than in women (6, 8). It has been observed that most cases of GBM are recounted in the western world as compared with the less developed countries due to reasons like under-reporting and lack of proper public health care facilities, among others (6).

1.1.1. Etiology of GBM

In the context of the etiology of GBM, very little is known until now. The only risk factor confirmed till date is exposure to high doses of ionizing radiations (9-11). More than 116 cases have been recorded since the 1960s, due to exposure from radiation. It has been claimed that the risk of developing GBM after exposure to radiotherapy is 2.5% (12). Even administered low doses of radiation in infants with tinea capitis and skin hemangioma have been identified to cause risks of developing GBM (13). Previous research data also clearly indicates that the pediatric population, exposed to therapeutic intracranial radiation, have high chances of developing GBM. Studies have also suggested that patients with acute lymphoid leukemia (ALL) are prone to developing GBM. This can be due to the action of chemotherapeutic agents used to treat ALL (14). But in the case of GBM, any direct relation between environmental factors such as smoking, electromagnetic field, severe head injury, dietary risk factors, pesticide exposure, etc. and GBM incidence was not established (11, 15-18). Few studies have mentioned that ovarian steroid hormone can be related to the incidence of GBM (19). For people suffering from allergies, the risk of them developing GBM is

comparatively low (20). Although in the context of GBM, genetic predisposition was observed to be only in 5-10% cases, which is very low. Group of genes such as *TNN*, *ERBB2* and *LAMA1* has been linked with GBM development. Besides, studies also found polymorphism in *CR1 (CD35)* and mutation in *TP53* to be engaged actively in GBM development (21).

1.2. BMP signaling pathway

1.2.1. BMPs

BMPs or Bone Morphogenetic Proteins, form the largest constituent of the transforming growth factor beta (TGF-β) superfamily, which is phylogenetically conserved (22, 23). BMPs are reported to be involved in inhibiting the recurrence and the growth of glioblastoma (24). So far, 20 types of BMPs have been distinguished. Initial studies of BMP showed them to be involved in only ectopic bone formation, but later it was found that they are involved in various other developmental processes to the extent that they came to be known by the name of Body Morphogenetic Proteins (25, 26). BMPs could be distinguished into at least four subgroups on the basis of their sequence similarity and their functions. BMP2 and BMP4 are included in one subgroup while BMP5, BMP6, BMP7, BMP8a, and BMP8b are included in another subgroup. BMP9 and BMP10 form another sub-group and the last sub-group includes BMP12, BMP13, and BMP14 (27, 28).

BMP precursors consist of around 400-500 amino acid residues, and their structure includes a single peptide at the N-terminal region, a prodomain region that would facilitate proper folding, and a mature peptide in the C-terminal region (29, 30). The C-terminal region of the protein is proteolytically cleaved from the prodomain by serine endoproteases (exception: furin, PC6, and PC7 [31]). This proteolytic cleavage takes place at the ARG-X-X-ARG sequence region. Active BMPs consist of around 50-100 amino acid residues. The primary structural feature of an active BMP is made up of seven cysteines that help in formation of strong dimeric stable structures. The exceptions are shown by BMP3, GDF9, and BMP15 which have only six cysteines, instead of seven. Among the seven cysteines available in an active BMP, six of them form three intracellular disulfide bonds while the seventh cysteine forms a covalent disulfide linkage with another monomer during dimerization (32). Except for BMP3, GDF9, and BMP15, all dimers are

biologically active as either homo-dimers or hetero-dimers. Among all the BMPs, BMP2/5, BMP2/6, BMP2/7, and BMP4/7 heterodimers have been observed to facilitate active BMP signaling pathways more effectively as compared with their respective homodimeric counterparts (30, 33, 34).

1.2.2. Extracellular regulation of BMP proteins

Post cleavage of the protein from their prodomain, studies have shown that the prodomain area in BMP4, BMP7, BMP9, BMP10, and BMP11 remains non-covalently bound in a complex with the active BMP (35-37). Exceptions exist for BMP-2 and BMP-4 where their prodomain region fails to form a complex with the active BMP (35). The association of the prodomain with the active mature BMP is beneficial due to the fact that it facilitates the binding of the complex with the fibrillins in the extracellular membrane (ECM). Fibrillins are glycoproteins secreted in the extracellular membrane to which the complex formed between the prodomain and the active mature BMP is targeted at, post secretion (35, 38). This would suggest that the mature active BMPs are introduced as proteins that are soluble and capable of diffusion. But, the BMPs which have stably formed complex with the prodomain will remain concentrated within the extracellular membrane unless the BMPs or their prodomains have other active binding sites. In BMP-2 and BMP-4, a secondary cleavage takes place in the prodomain region, producing a long sized prodomain and a short sized prodomain. These long and short prodomains then dictate whether the active BMP be released in a soluble form or in a tethered form (31, 39-42). An active BMP has two active binding sites through which it binds to its receptors. This receptors are distinguished as Type-I receptor and Type-II receptor. Type I receptors are characterized as those which bind at the concave hydrophobic pocket in the mature active BMP while Type II receptors are characterized as those which bind at the convex hydrophobic pocket in the mature active BMP. In the presence of the prodomain-dimer complex when the complex is immobilized, Type I receptor binding remains unaffected while Type II receptor binding gets significantly affected and it actively gets severely diminished (35).

In context of interactions within the tissue, the presence of prodomain would reduce the affinity of the complex towards the Type II receptor, thereby disrupting the potentiality of the complex in

promoting the congregation of the heterodimeric receptor complex required for the activation of the receptors. Thus, BMP needs to either dissociate itself from the prodomain/fibrillin complex or the prodomain/dimer complex for full bioactivity (38). BMPs can be released upon disruption of matrix vesicles of which certain BMPs (BMP1-7) have been detected to be a component (43). These matrix vesicles are a type of shedding vesicle that originate from the plasma membrane and serve as a center of mineralization which can contribute to the bioavailability of the BMPs (44-47).

The bioavailability of mature active BMP dimers can also be further restricted by the presence of antagonists. So far, 15 antagonists have been identified. These include members of DAN (Differential screening-selected gene abbreviative in Neublastoma) family, Tsg (twisted gastrulation), Chd (chordin), Nog (noggin), (Chrd11) Ventroptin, Fst (follistatin) and Fstl3 (FLRG-follistatin-related gene) (48, 49). Besides these Xnr3, Lefty, BMP3, and BMP15 are also found which can antagonize BMPs by directly interacting with them (49, 50). The reason cited for the antagonism by Xnr3, Lefty, BMP3, and BMP15 is attributed to the missing seventh cysteine, which is required for forming the covalent disulfide bond during dimerization, although the exact nature of their antagonist interactions is completely unknown (51). Limited studies on BMPs and their antagonists suggest that the BMP-antagonism can happen by antagonists, either by binding at the epitope binding sites on BMPs or by antagonists like Inhibin, BMP3, etc. binding at the BMP receptors and blocking BMPs from binding in the process (52).

1.2.3. **Regulation of BMPs at the cell surface**

BMPs bind with their receptors at the cell surface to facilitate the activation of a signaling assembly. In this section, a detailed discussion on the interactions between BMP ligands and the extracellular domains of BMP receptors is given.

- **BMP receptors**

BMP receptors include a short extracellular domain containing 10-12 cysteine residues, a transmembrane domain, and an intracellular serine/threonine kinase domain. There are five Type-I receptors, three Type-II receptors for BMPs (32, 53). Type-I BMP receptors include ALK-1

(Acvr11), ALK-2 (ActRI), ALK-3 (BRIa), ALK-4 (ActRIb), and ALK-6 (BRIb) while Type-II BMP receptors include BRII, ActRIIa, and ActRIIb (30). The specificity of these receptors is not only limited to BMPs but also other members of the TGF-β superfamily. Although members of both BMPs and TGF-β superfamily share the same fundamental structure, it is the distinction in their binding interfaces that directs different binding interactions (54, 55).

The assembly of the BMP signaling complexes occurs due to membrane localization, as the receptors have varied affinities towards BMP ligands. This is contrary to the event that takes place with other members of the TGF-β superfamily. In the case of members of the TGF-β superfamily, the ligand and the Type-II receptor forms an interactive interface that allows Type-I receptor to come and bind, thereby being both sequential and cooperative (56).

The specificity of the Type-I BMP receptor towards BMP ligand is dependent on the structure and the nature of residues residing in the interface of the ligand & receptor. In certain cases, it is dependent on the modifications that occur post-translationally such as N-glycosylation in BMP6, which directs the interaction between BMP6 and ActR-I (57). BMPs interact with specific receptors with varied affinities although relative affinities are not known for all BMPs yet. BMPs would bind to the dimeric Type-I receptor before binding to the Type-II receptor at low effective concentrations, due to high relative binding affinity. However for BMP7, which shows no clear preferences, various studies have shown that it has either a high affinity towards Type-II receptor or equal affinity for both Type-I and Type-II receptors (55, 58-60).

- **BMP receptor activation**

Constitutively active Type-II kinase phosphorylates Type-I kinase within the glycine and the serine-rich juxta membrane region (GS box) of its cytoplasmic domain, following the assembly and engagement of the ligands. It is considered that this assembly and engagement of the BMP ligands causes a change in conformation which in turn activates the Type-I and Type-II kinases. Ligand assembly initially incites the activation of the Type-II receptor, that prompts the activation of the Type-I receptor. The activation of both Type-I and Type-II receptors is responsible for the initiation of the BMP signaling pathway. When compared between activation of the Type-I BMP

receptor kinase and the Type-I TGF-β receptor kinase, there are both similarities and differences. For instance, not all Type-I receptors used by BMPs bind to FKBP12 as can be seen in the case of Type-I TGF-β receptors, despite the leucine/proline binding motif being conserved in both the Type-I receptors (61). But unfortunately, very less is known about the placement of the BMP receptors at the cell surface, except in the case of BMP-2 receptors.

- **Signaling**

BMPs affect gene transcription by activating Smad-dependent and Smad-independent pathways. These signaling pathways activations originate from the heteromeric complex of Type-I and Type-II BMP receptors and are dependent on BMP ligands binding to Type-I receptors (62, 63). Smad proteins are of three types namely Regulatory Smads (R-Smads), Common Smad (Co-Smad), and Inhibitory Smads (I-Smads). When compared between TGF-β and BMP Smad-dependent signaling pathways, the specific activation of the R-Smads is important (30, 64-66).

<u>Smad-dependent pathway</u>

In Smad-dependent BMP signaling pathway, also known as the canonical signaling pathway, BMPs bind to the cell surface receptors initially and form a hetero-tetrameric complex. The serine/threonine kinase cell surface receptors are of two types, namely Type I and Type II, each of which exists in dimeric form. After the formation of the hetero-tetrameric complex, initially, the Type II receptor trans-phosphorylates the Type I receptor at the glycine-serine-rich GS domain region. The phosphorylated Type I receptor, in turn, phosphorylates the receptor-regulated Smads proteins (Smad-1, Smad-5, and Smad-8) at the C –terminal of the SSXS motif (67). These R-Smads proteins, which are now phosphorylated, combine with Smad4 that acts as co-mediator, and move to the nucleus. This complex, along with other co-activators and co-repressors, then are involved in gene expression regulation (68). Different BMPs can bind in different ways with the receptor molecules to form a tetrameric signaling complex that is heterogeneous in characteristics. For instance, while BMP2 and BMP4 would preferentially bind with Type I receptors first and thereafter activate the Type II receptors, BMP6 and BMP7 would prefer the exact opposite and bind with Type II receptors first and thereafter Type I receptors (69). It has been also noticed that while most of the BMPs are capable of activating Smads 1, 5, and 8 without any selective

specificity, some BMPs (11 and 16) instead activate Smad 2 and Smad 3 due to their binding preferences with TGF- β receptors (70-82).

Smad-independent pathways

In Smad-independent or non-canonical signaling pathway, the only difference lies in the fact that BMPs are not dependent on Smad proteins for the regulation of gene expression. It has been observed that activated BRIa complexes initiates other downstream signaling pathways like p38 of MAP kinase, extracellular signal-regulated kinase (ERK), nuclear factor kappa beta (NFkB), and c-Jun N-terminal kinase (JNK) pathway. It is presumed that the pathway activation happens via protein-protein interactions of BRIa with Bone Morphogenetic Protein Receptor Associated Molecule 1 (BRAM1). It can also occur through X-linked Inhibitor of Apoptosis Protein (XIAP) and TGF- β Activated Kinase 1 (TAK1) and TAKI Binding protein (TAB1) which are downstream signaling molecules (82-87). BRAM1 links BRIa to TAB1 by binding with the cytoplasmic tail of BRIa, while BRIa links itself to the complex of TAB1 and TAK1 by recruiting XIAP (88). In other pathways like ERK, Protein kinase (PK), etc., it is unknown how BMPs activate the signaling pathways. These pathways might help BMPs to exhibit their effects on cell survival, migration, apoptosis, and differentiation (63, 89-93).

1.3. BMPs as a therapeutic strategy against glioblastoma

Various studies have shown BMPs as a potential treatment against glioblastoma. *Chirasani et al.* mentioned in 2010 that BMP-7, released from neural precursor cells, could activate BMP signaling in GICs and arrest cell cycle in glioblastoma, thereby suppressing the tumorigenic capacity and self-renewal ability of the tumorigenic cells (94). In another study in 2011, *Klose et al.* observed that treatment with BMP-7 can facilitate the arrest of the cell cycle in the G1 phase and cause a 50% reduction in cell proliferation (95). In 2012, another study observed that treatment with a combination of BMP-2 and Temozolomide (TMZ) caused significant cell death (96).

1.4. Reference

1. Rock K, McArdle O, Forde P, *et al.* A clinical review of treatment outcomes in glioblastoma multiforme the validation in a non-trial population of the results of a randomised Phase III clinical trial: has a more radical approach improved survival? Br J Radiol. 2014; 85:729–729.
2. Ostrom QT, Gittleman H, Xu J, Kromer C, Wolinsky Y, Kruchko C, and Barnholtz- Sloan JS (2016) CBTRUS statistical report: primary brain and other central nervous system tumors diagnosed in the United States in 2009-2013. Neuro-oncol 18: v1–v75.
3. Louis DN, Ohgaki H, Wiestler OD, *et al.* The 2007 WHO classification of tumours of the central nervous system. Acta Neuropathol. 2007; 114:97–97.
4. Gurusinghe, K.R.D.S.N.S., Mishra, A. & Mishra, *Sci. Rep*., **2018**, 8**,** 54, 87.
5. Dobes M, Khurana VG, Shadbolt B, Jain S, Smith SF, Smee R, *et al.* Increasing incidence of glioblastoma multiforme and meningioma, and decreasing incidence of Schwannoma (2000–2008): findings of a multicenter Australian study. *Surg Neurol Int.* (2011) 2:176.
6. Thakkar JP, Dolecek TA, Horbinski C, *et al.* Epidemiologic and molecular prognostic review of Glioblastoma. Cancer Epidemiol Biomarkers Prev. 2014; 23:1985–1985.
7. Iacob G, Dinca EB. Current data and strategy in glioblastoma multiforme. J Med Life. 2009; 2:386.
8. Ohgaki H, Kleihues P. Epidemiology and etiology of gliomas. Acta Neuropathol. 2005; 109:93–93.
9. Inskip PD, Tarone RE, Hatch EE, *et al.* Cellular-telephone use and brain tumors. N Engl J Med. 2001; 344:79–79.
10. Bondy ML, Scheurer ME, Malmer B, *et al.* Brain tumor epidemiology: consensus from the brain tumor epidemiology consortium. Cancer. 2008; 113:1953–1953.
11. Ohgaki H. Epidemiology of brain tumors. Methods Mol Biol. 2009; 472:323–323.
12. Salvati M, Frati A, Russo N, *et al.* Radiation-induced gliomas: Report of 10 cases and review of the literature. Surg Neurol. 2003; 60:60–60.
13. Wrensch M, Minn Y, Chew T, Bondy M, Berger MS. Epidemiology of primary brain tumors: current concepts and review of the literature. Neuro-Oncol. 2002; 4:278–278.
14. Salvati M, Frati A, Russo N, *et al.* Radiation-induced gliomas: Report of 10 cases and review of the literature. Surg Neurol. 2003; 60:60–60.

15. Inskip PD, Tarone RE, Hatch EE, *et al.* Cellular-telephone use and brain tumors. N Engl J Med. 2001;344:79–79
16. Fisher JL, Schwartzbaum JA, Wrensch M, Wiemels JL. Epidemiology of brain tumors. Neurol Clin. 2007; 25:867–867.
17. Adamson C, Kanu OO, Mehta AI, *et al.* Glioblastoma multiforme: a review of where we have been and where we are going. Expert Opin Investig Drugs. 2009; 18:1061–1061.
18. Agnihotri S, Burrell KE, Wolf A, *et al.* Glioblastoma, a brief review of history, molecular genetics, animal models and novel therapeutic strategies. AITE. 2013; 61:25–25.
19. Kabat GC, Etgen AM, Rohan TE. Do steroid hormones play a role in the etiology of glioma? Cancer Epidemiol Biomarkers Prev. 2010; 19:2421–2421.
20. Linos E, Raine T, Alonso A, Michaud D. Atopy and risk of brain tumors:a meta-analysis. J Natl Cancer Inst. 2007; 99:1544–50.
21. Christina Backes, Christian Harz, Ulrike Fischer *et al.* New insights into the genetics of glioblastoma multiforme by familial exome sequencing Oncotarget. 2015 Mar 20; 6(8): 5918–5931.
22. K. Lavery, et al., J. Biol. Chem. 283 (30) (2008) 20948.
23. M. Kawabata, T. Imamura, K. Miyazono, Cytokine Growth Factor Rev. 9 (1) (1998) 49.
24. Piccirillo, S.G., Reynolds, B.A., Zanetti, N., Lamorte, G., Binda, E., Broggi, G., Brem, H., Olivi, A., Dimeco, F., Vescovi, A.L. *Nature.* **2006**, 444 761–765.
25. M.R. Urist, Science 150 (698) (1965) 893.
26. WagnerD.O. et al., Sci. Signal. 3 (107) (2010) mr1.
27. S. Mazerbourg, A.J. Hsueh, Hum. Reprod. Update 12 (4) (2006) 373.
28. A. von Bubnoff, K.W. Cho, Dev. Biol. 239 (1) (2001) 1.
29. Y.T. Xiao, L.X. Xiang, J.Z. Shao, Biochem. Biophys. Res. Commun. 362 (3) (2007) 550.
30. C. Sieber, et al., Cytokine Growth Factor Rev. 20 (5–6) (2009) 343.
31. S.M. Nelsen, J.L. Christian, J. Biol. Chem. 284 (40) (2009) 27157.
32. A. Nohe, et al., Cell. Signal. 16 (3) (2004) 291.
33. S.C. Little, M.C. Mullins, Nat. Cell Biol. 11 (5) (2009) 637.
34. D.I. Israel, et al., Growth Factors 13 (3–4) (1996) 291.
35. G. Sengle, et al., J. Biol. Chem. 283 (20) (2008) 13874.
36. M.A. Brown, et al., J. Biol. Chem. 280 (26) (2005) 25111.
37. G. Sengle, et al., J. Mol. Biol. 381 (4) (2008) 1025.

38. F. Ramirez, D.B. Rifkin, Curr. Opin. Cell Biol. 21 (5) (2009) 616.
39. S. Sopory, et al., J. Biol. Chem. 281 (45) (2006) 34021.
40. C. Degnin, et al., Mol. Biol. Cell 15 (11) (2004) 5012.
41. Y. Cui, et al., Genes Dev. 15 (21) (2001) 2797.
42. D.C. Goldman, et al., Development 133 (10) (2006) 1933.
43. N.N. Nahar, et al., J. Bone Miner. Metab. 26 (5) (2008) 514.
44. L.N. Wu, et al., J. Biol. Chem. 268 (33) (1993) 25084.
45. H.C. Anderson, J. Cell Biol. 41 (1) (1969) 59.
46. E. Bonucci, J. Ultrastruct. Res. 20 (1) (1967) 33.
47. Z. Xiao, et al., J. Proteomics 72 (1) (2009) 34.
48. U.A. Vitt, S.Y. Hsu, A.J. Hsueh, Mol. Endocrinol. 15 (5) (2001) 681.
49. E. Di Pasquale, A.H. Brivanlou, J. Biol. Chem. 284 (38) (2009) 26127.
50. L.W. Gamer, et al., Dev. Biol. 285 (1) (2005) 156.
51. WalshD.W. et al., Trends Cell Biol. (2010).
52. V. Rosen, Ann. NY Acad. Sci. 1068 (2006) 19.
53. F. Liu, et al., Mol. Cell. Biol. 15 (7) (1995) 3479.
54. Y. Shi, J. Massague, Cell 113 (6) (2003) 685.
55. K. Heinecke, et al., BMC Biol. 7 (2009) 59.
56. J. Groppe, et al., Mol. Cell 29 (2) (2008) 157.
57. S. Saremba, et al., FEBS J. 275 (1) (2008) 172.
58. B.B. Koenig, et al., Mol. Cell. Biol. 14 (9) (1994) 5961.
59. P. Knaus, W. Sebald, Biol. Chem. 382 (8) (2001) 1189.
60. J. Greenwald, et al., Mol. Cell 11 (3) (2003) 605.
61. F. Kugimiya, et al., Biochem. Biophys. Res. Commun. 338 (2) (2005) 872.
62. A. Nohe, et al., J. Biol. Chem. 277 (7) (2002) 5330.
63. Q. Zhou, et al., Cardiovasc. Res. 76 (3) (2007) 390.
64. B. Song, K.D. Estrada, K.M. Lyons, Cytokine Growth Factor Rev. 20 (5–6) (2009) 379.
65. C.S. Hill, Cell Res. 19 (1) (2009) 36.
66. S. Itoh, P. ten Dijke, Curr. Opin. Cell Biol. 19 (2) (2007) 176.
67. Horbelt D, Denkis A, Knaus P. A portrait of transforming growth factor b superfamily signalling: background matters. Int J Biochem Cell Biol. 44(3) (2012) 469-474.

68. Heldin C-H, Moustakas A. Role of Smads in TGFβ signaling. Cell Tissue Res. 347(1) (2012) 21-36.
69. De Caestecker M., The transforming growth factor-beta superfamily of receptors. Cytokine Growth Factor Rev. 15(1) (2004) 1–11.
70. A.S. Pachori, et al., J. Mol. Cell. Cardiol. 48 (6) (2010) 1255.
71. K. Miyazono, S. Maeda, T. Imamura, Cytokine Growth Factor Rev. 16 (3) (2005) 251.
72. S. Mazerbourg, et al., J. Biol. Chem. 280 (37) (2005) 32122.
73. T. Ebisawa, et al., J. Cell Sci. 112 (Pt 20) (1999) 3519.
74. C. Kersten, et al., BMC Immunol. 6 (1) (2005) 9.
75. V. Zuzarte-Luis, et al., Dev. Biol. 272 (1) (2004) 39.
76. R. Motazed, et al., Pharm. Res. 25 (10) (2008) 2440.
77. T.W. Axelrad, T.A. Einhorn, Cytokine Growth Factor Rev. 20 (5–6) (2009) 481.
78. P.D. Upton, et al., J. Biol. Chem. 284 (23) (2009) 15794.
79. L. David, et al., Blood 109 (5) (2007) 1953.
80. M. Sammar, et al., Genes Cells 9 (12) (2004) 1227.
81. A.M. Sullivan, G.W. O'Keeffe, J. Anat. 207 (3) (2005) 219.
82. R.K. Moore, F. Otsuka, S. Shimasaki, J. Biol. Chem. 278 (1) (2003) 304.
83. J.H. Shim, et al., EMBO J. 28 (14) (2009) 2028.
84. K.M. Wu, et al., J. Biomed. Sci. 13 (3) (2006) 345.
85. H. Shibuya, et al., EMBO J. 17 (4) (1998) 1019.
86. K. Yamaguchi, et al., EMBO J. 18 (1) (1999) 179.
87. K. Kurozumi, et al., Genes Cells 3 (4) (1998) 257.
88. P.J. Chung, et al., J. Biol. Chem. 277 (42) (2002) 39850.
89. K. Sugimori, et al., J. Bone Miner. Metab. 23 (6) (2005) 411.
90. Y.S. Lee, C.M. Chuong, J. Cell. Physiol. 170 (2) (1997) 153.
91. J. Lemonnier, et al., J. Biol. Chem. 279 (1) (2004) 259.
92. G.C. Reilly, et al., Cell Commun. Signal 3 (1) (2005) 3.
93. C. Gamell, et al., J. Cell Sci. 121 (Pt 23) (2008) 3960.
94. S. R. Chirasani, A. Sternjak, P. Wend et al., “Bone morphogenetic protein-7 release from endogenous neural precursor cells suppresses the tumourigenicity of stem-like glioblastoma cells,” *Brain*, vol. 133, no. 7, pp. 1961–1972, 2010.

95. A. Klose, Y. Waerzeggers, P. Monfared et al., “Imaging bone morphogenetic protein 7 induced cell cycle arrest in experimental gliomas,” *Neoplasia*, vol. 13, no. 3, pp. 276–285, 2011.
96. L. Persano, F. Pistollato, E. Rampazzo et al., “BMP2 sensitizes glioblastoma stem-like cells to Temozolomide by affecting HIF-1alpha stability and MGMT expression,” *Cell Death and Disease*,vol. 3, p. e412, 2012.

Chapter 2: Databases and Tools

2.1. Databases

RCSB PDB: The Protein Data Bank (PDB) was established in the year 1971 at Brookhaven National Laboratory, as an open-access platform that provided access to 3D structure data of large biomolecules like protein, DNA, and RNA (1,2). The PDB archive is managed by an international collaboration between the United States of America, Asia, and Europe. Currently, data shows that the archive size grows at a rate of nearly 10%. The RCSB PDB database provides support for data depositors to submit their crystal-solved structures. The database also provides outreach and education services for all consumers on their PDB-101 website.

PDBePISA: PDBePISA is a web-based interactive tool that is used to explore macromolecule interfaces (3-5). A user can find pre-calculated data for the entire PDB archive using PDBePISA. PDBePISA can help in investigating the chemical and structural properties of surfaces and interfaces of macromolecules. It can also help predict the probable quaternary structures and their possible dissociation patterns. PDBePISA can also be used to search for interfaces which are formed by structural homologs. They have a wide range of options included in their server which would enable the investigation of the multimeric-state, the symmetry-number, the space-group, the accessible or buried surface area, the free energy of dissociation, the presence or absence of salt-bridges, etc of the target protein. It is also possible to access the biological role of interfaces of macromolecules. PDBePISA considers structures only in either PDB or mmCIF format for analysis.

Superlooper2 (SL2): Superlooper2 (SL2) is a web-based interactive tool which can be used to visualize and select missing loop in a protein structure (6,7). SL2 selects missing loop from a pre-calculated database which contains approximately 700 million protein loop segments with residue length varying from 3 to 35. This database extracts segments from the structural coordinates of more than 100,000 protein structures that exist in the RSCB PDB archive. SL2 uses the NGL viewer to facilitate visualization of selected fragments. It gives an output of around 100 fragments in response to a single missing segment search. The relationship between the number of available segments and the missing segment size is inversely proportional. For instance, for a missing fragment length of 3 amino acid residues, 23 million fragments are available. On the contrary, for

a missing fragment length of 35 amino acid residues, the available fragments drastically decrease to 18 million. SL2 uses a second database which contains fragments from helical-membrane proteins. This database has around 3,90,000 fragments and is updated every three months to include more structures and keep pace with the fast-growing number of helical transmembrane proteins deposited in the PDB archive. The list of selected loop segments is enlisted based on their score.

2.2. Tools

ModLoop: Modloop is a web-based server for modeling loop in a protein structure (8,9). It uses MODELLER to predict loop conformations. MODELLER predicts loop conformations by optimizing the position of all non-hydrogen atoms that are present in the loop. The protocol of optimization includes conjugate gradient minimization as well as molecular simulation with simulated annealing. The restraints used by MODELLER is based on statistical distribution obtained from known proteins. These restraints which includes bonds and angles (including dihedral angles) are governed by corresponding terms in the potential energy function, the CHARMM-22. CHARMM-22 is the force field function of CHARMM that deals with a protein system. CHARMM or Chemistry at Harvard Macromolecular Mechanics is a program, with a set of energy functions known as Force fields, which was developed to carry our molecular dynamics simulation on diverse-particle systems. The inputs include specifying the details of starting and ending amino acid residues of the target loop segment and atomic coordinates of the target protein structure PDB format. ModLoop can model multiple loop segments simultaneously provided, the length of a loop segment or the sum of lengths of multiple loop segments do not exceed 20 amino acid residues.

ClusPro 2.0: ClusPro 2.0 is web-based server used for automated protein-protein docking. The ClusPro server's docking is established on three computational steps (10-13). The first step includes the docking of rigid bodies by the sampling of a billion conformations. The second step is to identify the largest clusters which will conclude the most probable models of the protein-protein docking. For that, ClusPro performs pairwise interface root mean square deviation (IRSMD) based clustering, considering 9Å as the clustering radius, of the 1000 lowest energy

docked structures. In the third step, ClusPro performs energy minimizations to remove steric clashes in the docked structures. ClusPro offers various options like antibody mode docking, multimer mode docking, SAXS mode docking, restraints mode docking, and peptide mode docking. It provides the option to identify unstructured residues in the tail of a protein structure and also allows the option to specify constraints like attraction and repulsion among amino acid residues in the receptor and the ligand structures. ClusPro output results come in four categories namely balanced, electrostatic-favored, hydrophobic-favored, and (VanderWaal + electrostatic)-favored. The structure among all the predicted structures with the least optimization energy value needs to be considered.

PyMol: PyMol is a software used for molecular visualization (14). It was created by Warren Lyford Delano. For our research, PyMol was used to identify interface residues between protein-protein complexes. A python script (https://pymolwiki.org/index.php/InterfaceResidues) was used in PyMol to identify the residues. Initially, the area of the complex was calculated along with the chain-only surface area. Finally, the difference between the area of the complex and the chain-only based surface areas was calculated. The amino acid residues whose difference value (the difference between the area of the complex and the chain-only based surface areas) was more than the allowed cut-off, was considered as interface residues. The cut-off used for our research was 1.0 $Å^2$.

FoldX: FoldX was developed to evaluate the effect of the mutation rapidly, on the stability, folding, and dynamics of a protein or a nucleic acid (15). FoldX can be used to calculate the free energy of a macromolecule, the stability of a high-resolution 3D protein structure, predict the number of water bridges, the position of protons, the metal-binding site within a macromolecule, and the free energy of complex formation. Along with point mutations, FoldX also provides an option for alanine screening. The method used by the FoldX force field is known as an empirical effective energy function (EEEF). It is based on empirical data which are taken from experimental works on proteins.

The free energy calculation by FoldX is based on the equation given below.

$$\Delta G = a.\Delta G_{backbone_{Hbonds}} + b.\Delta G_{sidechain_{Hbonds}} + c.\Delta G_{vdw} + d.\Delta G_{el} + e.\Delta G_{solvP} + f.\Delta G_{solH} + g.\Delta G_{vdwclash} + h.T\Delta S_{sc} + i.T\Delta S_{mc} + j.\Delta G_{wb} + k.\Delta G_{helix_{dipole}} + l.\Delta G_{cis_{bonds}} + m.\Delta G_{disulfide} + n.\Delta G_{kn} + o.\Delta G_{partial_{covalent_{interactions}}} + p.\Delta G_{ionization} + q.T\Delta S_{complex}$$

The terms *a*-*q* carry the relative weights of the energy terms in the equation above.

Here $\Delta G_{backbone\_Hbonds}$ term indicates the contribution of the backbone H-bonds to the energy of the complex, while $\Delta G_{sidechain\_Hbonds}$ indicates the contribution of sidechain-sidechain interactions and sidechain-backbone hydrogen-bonds interactions. Vanderwaals energy is indicated by the energy term ΔG_{vdw} while inter-residue vanderwaals clashes are represented by the energy term $\Delta G_{vdwclash}$. While ΔG_{el} energy term indicates the electrostatic contribution to free energy calculations, ΔG_{helix_dipole} indicates the electrostatic contribution of helix dipole. An additional electrostatic term ΔG_{kn} is used to calculate electrostatic contribution between atoms of different chains within protein complexes. To calculate the contribution of hydrophobic and polar groups in a protein, ΔG_{solvP} and ΔG_{solvH} energy terms are being used respectively, in the calculation for free energy. While $T\Delta S_{complex}$ indicates the cost of forming a complex, $T\Delta S_{sc}$ and $T\Delta S_{mc}$ indicates the entropy cost of fixing side chains and main chains respectively. ΔG_{wb} indicates the contribution of water bridges, while ΔG_{cis_bonds} indicates the cost of having a cis peptide bond and $\Delta G_{disulfide}$ indicates the contribution of a disulfide bond. The interaction with metal-bound is calculated by $\Delta G_{partial\_covalent\_interactions}$. An additional energy term $\Delta G_{ionization}$ is used to calculate the contribution of ionization energy to the free energy calculation for the protein complex.

Discovery Studio: Discovery studio, which is commercialized by Dassault Systemes BIOVIA, is a software with multiple applications (16). Its applications broadly includes simulations (including molecular dynamics, molecular mechanics, and quantum mechanics), ligand design, pharmacophore (creation, validation, and virtual screening), structure-based designing (receptor-ligand docking, fragment-based placement, and refinement), macromolecule design, and macromolecule engineering. For our research, Discovery studio was used to study interactions post

mutation so as to have a clearer insight into the effect of the mutations on inter as well as intra-residue interactions.

InterEvDock2: InterEvDock2 is a web based docking server which is specifically designed for docking heterodimeric protein interfaces. It uses the InterEvScore potential that combines evolutionary information with a residue based multibody statistical potential while performing protein-protein dockings. InterEvDock2 uses three scoring programs that gives us three different sets of results. These programs include FRODOCK2, InterEvScore and SOAP_PP atom based statistical potential (17-19).

2.3 Reference

1. H.M. Berman, J. Westbrook, Z. Feng, G. Gilliland, T.N. Bhat, H. Weissig, I.N. Shindyalov, P.E. Bourne.(2000) The Protein Data Bank *Nucleic Acids Research*, 28: 235-242.

2. Stephen K Burley, Helen M. Berman, *et al.* RCSB Protein Data Bank: biological macromolecular structures enabling research and education in fundamental biology, biomedicine, biotechnology and energy (2019) *Nucleic Acids Research* 47: D464–D474.

3. E. Krissinel and K. Henrick (2007). *Inference of macromolecular assemblies from crystalline state.* J. Mol. Biol. 372, 774—797.

4. E. Krissinel and K. Henrick (2005). *Detection of Protein Assemblies in Crystals*. In: M.R. Berthold *et.al.* (Eds.): CompLife 2005, LNBI 3695, pp. 163—174.

5. E. Krissinel (2009). *Crystal contacts as nature's docking solutions*. J Comput Chem. 2010 Jan 15;31(1):133-43.

6. Hildebrand, P.W. *et al.* SuperLooper--a prediction server for the modeling of loops in globular and membrane proteins. Nucleic Acids Res. (2009) 37, W571—4.

7. Jochen Ismer, Alexander S. Rose, Johanna K. S. Tiemann, SL2: an interactive webtool for modeling of missing segments in proteins, Nucleic Acids Research 2016, 1-5.

8. A. Fiser, R.K.G. Do and A. Sali, Prot Sci, (2000) *9*, 1753-1773.

9. A. Fiser, and A. Sali, Bioinformatics, (2003) *19*, 2500-01.

10. Vajda S, Yueh C, Beglov D, Bohnuud T, Mottarella SE, Xia B, Hall DR, Kozakov D. New additions to the ClusPro server motivated by CAPRI. *Proteins: Structure, Function, and Bioinformatics.* 2017 Mar; 85(3):435-444.

11. Kozakov D, Hall DR, Xia B, Porter KA, Padhorny D, Yueh C, Beglov D, Vajda S. The ClusPro web server for protein-protein docking. *Nature Protocols.* 2017 Feb;12(2):255-278.

12. Kozakov D, Beglov D, Bohnuud T, Mottarella S, Xia B, Hall DR, Vajda, S. How good is automated protein docking? *Proteins: Structure, Function, and Bioinformatics.* 2013 Dec; 81(12):2159-66.

13. Mishra S, Computational prediction of protein-protein complexes, BMC Research Notes **volume 5**, 495 (2012).

14. The PyMOL Molecular Graphics System, Version 1.1r1, Schrödinger, LLC.

15. Schymkowitz, J., Borg, J., Stricher, F., Nys, R., Rousseau, F., Serrano, L. *Nucleic Acids Research.* 2005, Vol. 33, W382–W388.

16. *Dassault Systèmes BIOVIA, Discovery Studio Modeling Environment, Release 2017, San Diego: Dassault Systèmes, 2016.*

17. Quignot C, Rey J, Yu J, Tufféry P, Guerois R, Andreani J. InterEvDock2: an expanded server for protein docking using evolutionary and biological information from homology models and multimeric inputs. Nucleic Acids Res. 2018 Jul 2;46(W1):W408-16.

18. Yu J, Vavrusa M, Andreani J, Rey J, Tufféry P, Guerois R. InterEvDock: A docking server to predict the structure of protein-protein interactions using evolutionary information. Nucleic Acids Res. 2016 Jul 8;44(W1):W542-9.

19. Andreani J, Faure G, Guerois R. InterEvScore: a novel coarse-grained interface scoring function using a multi-body statistical potential coupled to evolution. Bioinformatics. 2013 29(14):1742-9.

Chapter 3: Structural investigations into the protein-protein complex interactions between BMP homodimers (BMP-2, BMP-7) and antagonists (Noggin, Gremlin-1)

3.1. Introduction

BMPs or Bone Morphogenetic Proteins are the largest subgroups of the Transforming Growth Factor Beta (TGF-β) superfamily (1, 2). BMPs are regulated by a class of soluble, extracellular secreted molecules known as BMP antagonists (3-6). These antagonists can be divided into three broad classes based on the nature of their binding: antagonists which bind directly to BMPs, antagonists which bind to the pro-regions of the BMP (mature BMP), and antagonists which bind to BMP receptors, thereby preventing BMPs from binding with its receptors (7, 8). BMP antagonists can also be divided into three subgroups based on its cysteine-knot ring size: chordin and noggin (10-membered ring); twisted gastrulation (9-membered ring) and the DAN family (8-membered ring) (7, 9-18). The DAN family of antagonists are further divided into four categories based on the additional cysteine residues that are conserved outside the cysteine knots: gremlin and PRDC; Cer1, coco, and homolog of Xenopus Cerebus; Dan; USAG-1 and sclerostin (9, 10, 19-24). The phylogenetic tree of the BMP antagonists based on sequence similarity (amino acid) is depicted in Fig. 1.

Among various antagonists, in the case of glioblastoma, elevated expression levels of BMP antagonists could be observed for only Noggin and Gremlin-1 (25). Both these antagonists are observed to inhibit BMP signaling, thereby inhibiting cell differentiation and in turn, maintaining hierarchy in cancer stem cells (CSCs) (26-30). In another study it was observed that Gremlin-1 expression levels were significantly higher than Noggin expression level in CSCs in glioma cells, thereby making Gremlin-1 the primary antagonists responsible for maintaining tumor hierarchy in cancer stem cells (31). Thus it becomes very important to have a detailed understanding of the nature of interactions, these two antagonists have with BMPs. Previous studies on the structural interaction between BMP-7 and Noggin suggests that it engages in a dimer-dimer interaction.

BMP-7 forms a butterfly-shaped homodimer with two pairs of anti-parallel β-strands as its wings (finger 1 and finger 2) (Fig.2) (32). The core of the homodimer contains 7 disulfide bonds (Fig. 3).

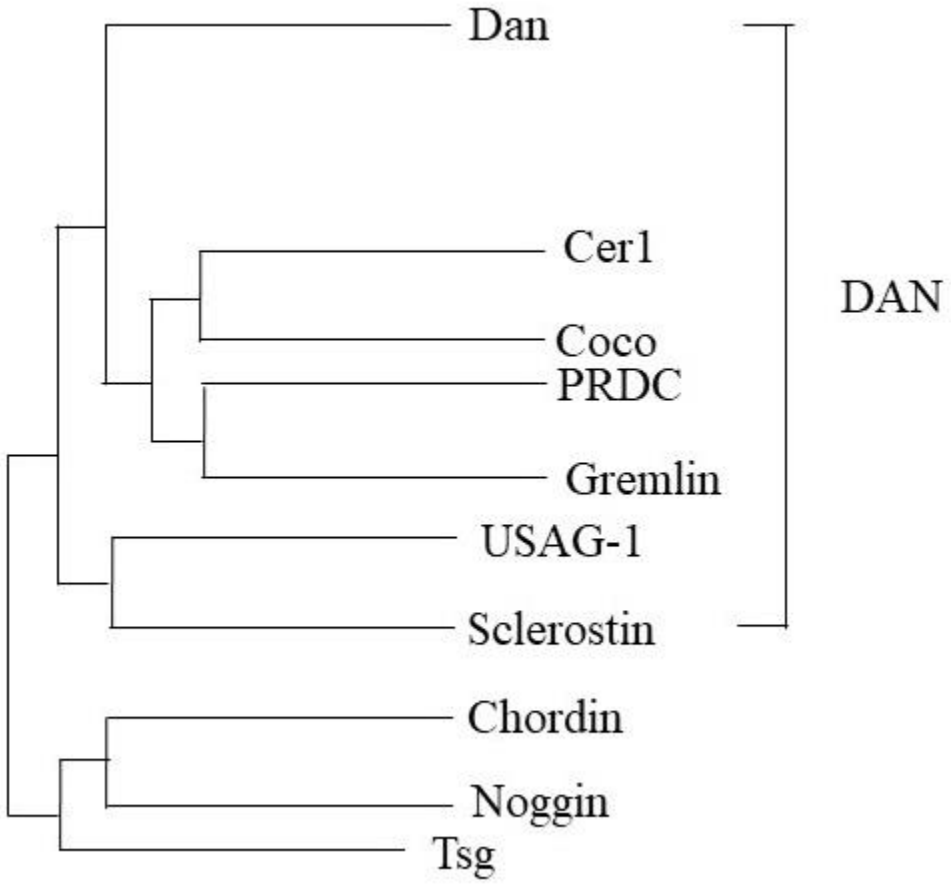

Fig 1. The BMP antagonists' phylogenetic tree (M. Yanagita *Cytokine & Growth Factor Reviews* 2005*).*

Each monomer forming the core contains 3 disulfide bonds between CYS67-CYS136, CYS71-CYS138, and CYS38-CYS104 giving a total count of 6 disulfide bonds and two 10-membered cysteine knots (Fig. 3). These two 10-membered cysteine knots join together through CYS103-CYS103 disulfide bond accounting for a total of 7 disulfide bonds forming the core of the homodimer. In the case of Noggin, it has two β-strands (Fig.3) extending out of the core containing 7 disulfide bonds similar to that in BMP-7. Unlike BMP-7, the disulfide bonds in the core of the

Noggin homodimer form a 12-membered cysteine knot (Fig. 3). The disulfide bonds include bonds between amino acid residues CYS155-CYS192, CYS178-CYS228, CYS184-CYS230, and between CYS232 of each monomer. The residues in the BMP-7_Noggin complex structure ranging from GLN28 to ASP39, which belongs to the clip like segment in Noggin, insert through the hydrophobic pocket formed by TYR52, TRP55, VAL87, TYR128, and MET131 amino acid residues of BMP at the receptor-binding site I. The residues in the other clip-like region in the Noggin ranging between ASN40 and GLU 48, bind at the Type II receptor binding site that passes through the finger-like region of the BMP-7 (namely the Finger-1 region and the Finger-2 region).

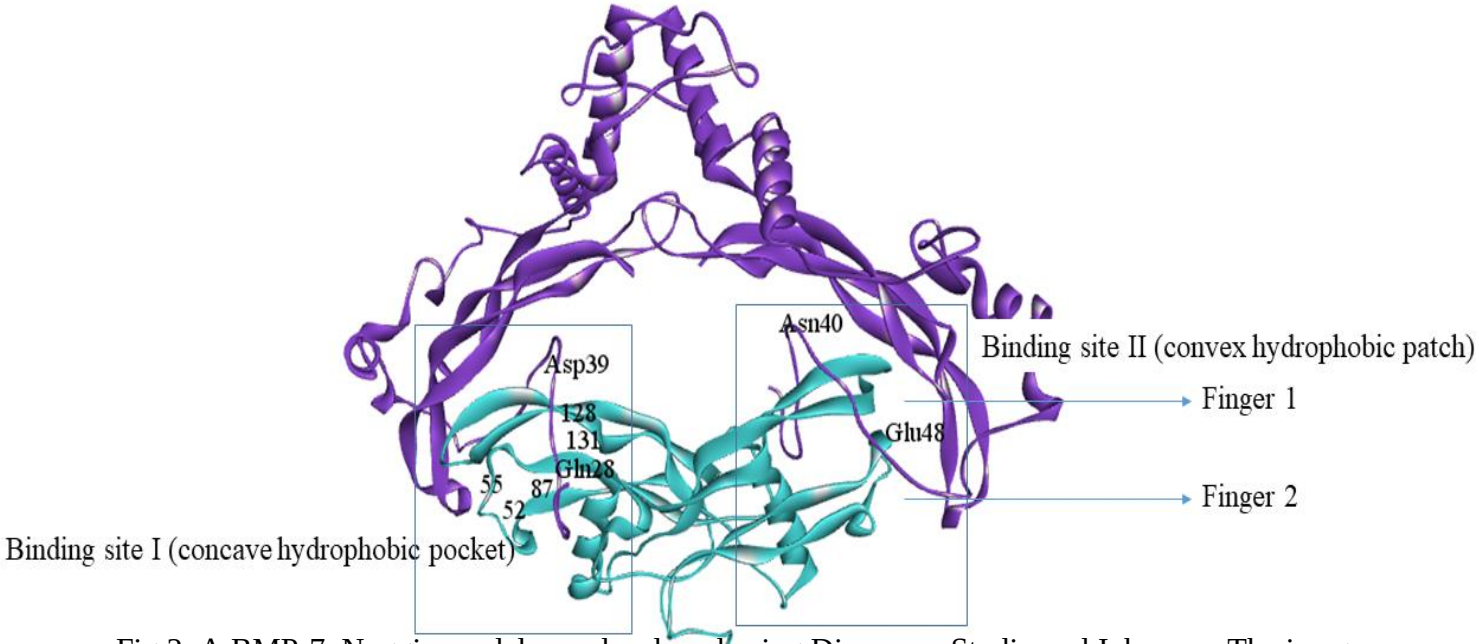

Fig 2. A BMP-7_Noggin model was developed using Discovery Studio and Inkscape. The image depicts the two β-strands of Noggin and that of BMP-7 (Finger1, Finger 2) and the two receptor-binding sites of BMP-7.

In context to Gremlin-1, previous studies between BMP-2 and Gremlin-1 suggest that the N-terminal sequence of Gremlin-1 is not engaged in its interaction with BMP-2 (33). The study also suggests that the middle region in Gremlin-1, from F117 to I127, is responsible for stable dimerization of gremlin-1 and that the structure of Gremlin-1 is like a bent rod with exposed concave and convex surfaces (33). The concave and the convex surfaces which are represented by F1, F2, and W region (Fig. 4) might remain the only regions where Gremlin-1 can interact with BMP-2.

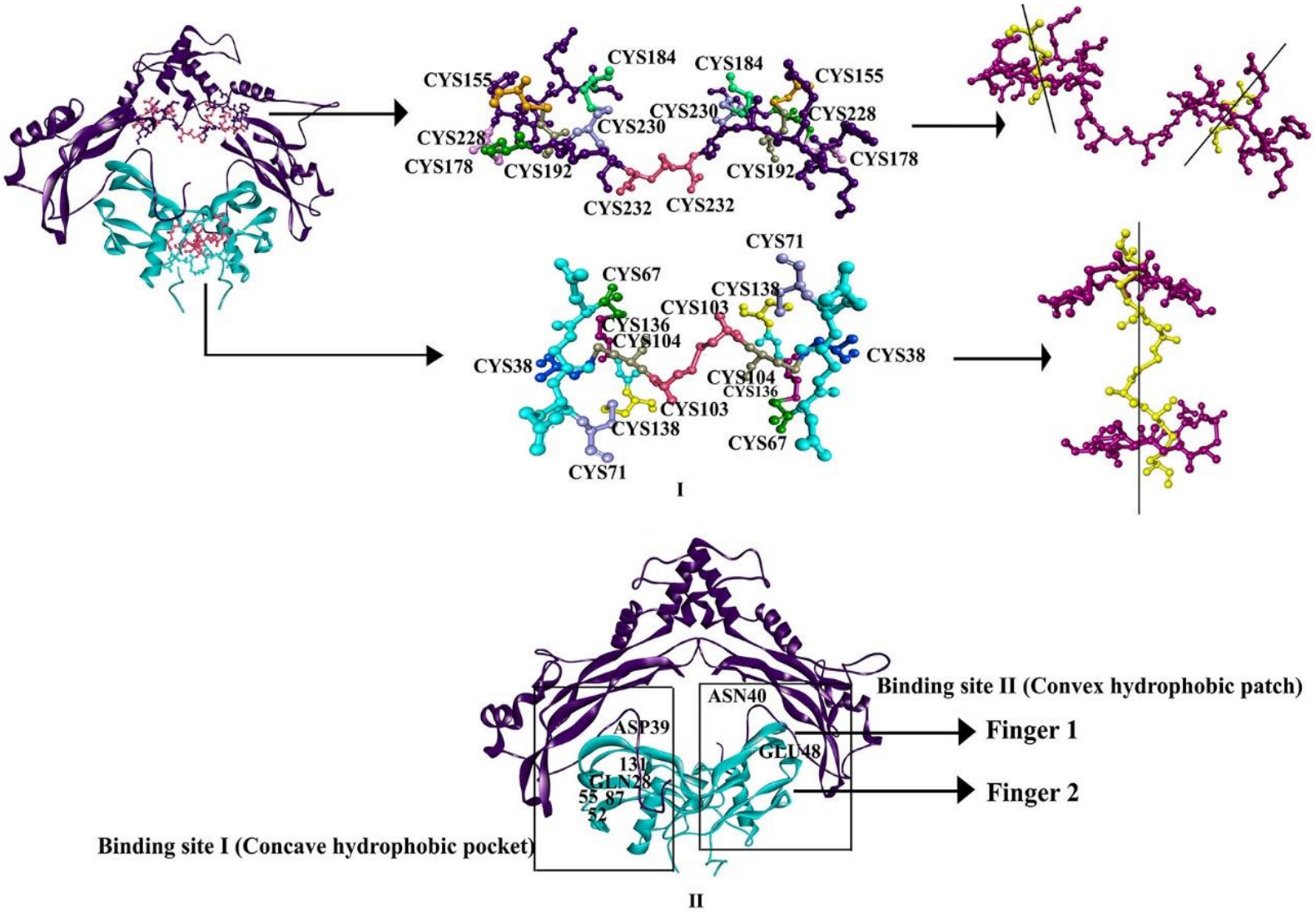

Fig 3. (I)The core of the BMP-7 homodimer (top most right corner, 10-membered cysteine knot) and the core of the Noggin homodimer (bottom most right corner, 12-membered cysteine knot) is depicted in this figure. The seven cysteines forming the cysteine knots in each of the cores are simultaneously represented. (II) The receptor binding sites in BMP-7 and the essential amino acid residues in the interface required for binding is depicted in this figure. Finger 1 and Finger 2 represents the two wings of BMP-7 engaged in the interactions with the Noggin. Discovery studio and inkscape were used to develop the images of these structures. Various shades of coloring were used to distinguish between BMP-7 and Noggin. Purple color strands represent Noggin dimer, while sky-blue colored strands represent BMP-7.

The study also suggested that Gremlin-1 and BMP-2 can be involved in side-side oligomeric binding, by placing the α-helix of Gremlin-1 in the BMPR1A binding pocket (receptor-binding site I) of BMP-2, while the knuckle epitope (receptor-binding site II) of BMP-2 can be shielded by the convex face of Gremlin-1 (33).

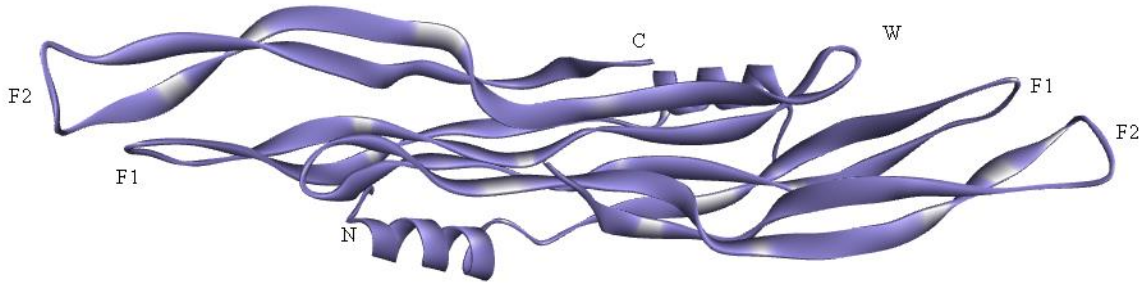

Fig 4. Image showing the C-terminal region, the N-terminal region, the F1 region, the F2 region, and the W region of Gremlin-1 homodimer structure.

As seen above, although there has been few previous studies on the interactions between the BMPs and its antagonists, the present knowledge is still very vague and inadequate, thereby signifying the need for a much detailed study in this context. The interaction study of Gremlin-1_BMP-2 also remained very speculative and definitive interactive models was not made. In our study, we try to computationally investigate the nature of these interactions. We have limited our studies to only BMP-2 and BMP-7 (representing two separate classes of BMPs) in case of the BMPs and Gremlin and Noggin in context to the antagonists. We also tried to have a detailed investigation into interfacial amino acid residues, which upon point mutation can destabilize the predicted interactive models of the BMPs with their antagonists. As discussed before, the interactions of these antagonists with BMPs inhibit BMP signaling and thereby try to maintain the tumor hierarchy in cancer stem cells. Therefore, designing a probable way to destabilize these interactions between BMPs and their antagonists can help us prevent these antagonists from regulating the tumor-morphology in CSCs.

3.2. Materials and methods

3.2.1. Predicting models for the protein-antagonist interactive complex structures

ClusPro 2.0 was used to develop an interactive model of the protein-antagonists complexes (34-36). In ClusPro 2.0 besides blind docking, we also did advanced docking where we used the "attraction and repulsion" feature of ClusPro 2.0 which enabled us to distinguish the interfacial residues of the complexes for targeted docking.

For modelling the BMP-7_Noggin structure, we initially searched the RCSB Protein Data Bank with Protein Data Bank (PDB) and obtained a monomeric structure of the protein complex with the PDB ID of 1M4U (resolution: 2.42 Å). We then used PDBePISA for probable assemblies (37-39). The probable assembly obtained from PDBePISA as well as the monomeric structure of the complex obtained from the protein data bank had a missing loop between Proline-88 and Glycine-96. The probable assembly was then uploaded to the SL2 server for predicting the missing loop fragment (40, 41). To further refine the modeled loop, we uploaded the final structure obtained from the SL2 server in ModLoop (42, 43). FoldX was used for energy optimization of the final structure (44). For modeling the BMP-2_Noggin complex structure, initially BLASTp analysis was done between BMP-7(1M4U_L, UniProtKB: P18075) and BMP-2 (2QJ9_A, UniProtKB: P12643), and advanced docking was done using the information of the residues in BMP-2 corresponding to the interfacial residues in BMP-7. The BLASTp results indicate a 54 % sequence identity of BMP-2 with BMP-7 (Fig. 5). For modeling complex structures between BMPs and Gremlin-1, we used the residues in the F1 region, the F2 region, and the W region as inputs for advanced docking using ClusPro 2.0. It is known that Gremlin-1 would prefer BMP-2 to BMP-7 in the context of binding, according to studies conducted previously (45). Also as mentioned before, BMP-2 prefers binding to the receptor-binding site-I while BMP-7 prefers binding to the receptor-binding site II (33, 46). But since Gremlin-1 weakly binds to BMP-7 as compared to its binding across BMP-2, we think that this might be because of binding at the receptor-binding site I instead of its preferential receptor-binding site II. So in context to Gremlin-1 interactions, we investigate the models where Gremlin-1 would bind across the receptor-binding site I in both BMP-2 and BMP-7 proteins. For the convenience of our study, we have labeled each chain

involved in formation of the multimeric interactive models. In the case of BMP-2, the chains were identified as “B” and “C”. In the case of BMP-7, the chains were identified as “A” and “D”, while the chains in Noggin were identified as “G” and “H”. In Gremlin-1, we deal with two dimeric units. Therefore, the two chains in one case were identified as “G” and “H” while for the other two chains, the labels used were named “K” and “L”.

Range 1: 1 to 115 Graphics ▼ Next Match ▲ Previous Match

Score	Expect	Method	Identities	Positives	Gaps
147 bits(370)	8e-52	Compositional matrix adjust.	63/116(54%)	84/116(72%)	1/116(0%)

```
Query  23   MANVAENSSSDQRQACKKHELYVSFRDLGWQDWIIAPEGYAAYYCEGECAFPLNSYMNAT  82
            MA          + +CK+H LYV F D+GW DWI+AP GY A+YC GEC FPL  ++N+T
Sbjct  1    MAQAKHKQRKRLKSSCKRHPLYVDFSDVGWNDWIVAPPGYHAFYCHGECPFPLADHLNST  60

Query  83   NHAIVQTLVHFINPETVPKPCCAPTQLNAISVLYFDDSSNVILKKYRNMVVRACGC  138
            NHAIVQTLV+ +N + +PK CC PT+L+AIS+LY D++  V+LK Y++MVV  CGC
Sbjct  61   NHAIVQTLVNSVNSK-IPKACCVPTELSAISMLYLDENEKVVLKNYQDMVVEGCGC  115
```

Fig. 5: BLAST analysis between BMP-7 and BMP-2. Here BMP-7 sequence is taken as a query, and the BMP-2 sequence is taken as a subject.

3.2.2. Interfacial residues

Interfacial residues are very important for maintaining the stability of a protein-protein complex structure by directing both intermolecular and intramolecular interactions at the interface. They form the backbone of any protein-protein complex structure. Using a python script “InterfaceResidue.py” (https://pymolwiki.org/index.php/InterfaceResidues) in PyMol, we were able to specify the interfacial residues (47). These interfacial residues were then selected in Discovery Studio for interaction studies (48).

3.2.3. Energy optimization and mutation studies

Energy optimization is a crucial step to investigate interactions in the protein-protein interfaces as well as to compare between multiple structures. FoldX was used for both energy optimization and mutation studies (44). Extensive averaging of data is performed to develop a crude generalization to predict trends in interactions within the interactive models.

The free energy calculation done by FoldX is given as follows

$$\Delta G = a.\Delta G_{backbone_{Hbonds}} + b.\Delta G_{sidechain_{Hbonds}} + c.\Delta G_{vdw} + d.\Delta G_{el} + e.\Delta G_{solvP} + f.\Delta G_{solH} + g.\Delta G_{vdwclash} + h.T\Delta S_{sc} + i.T\Delta S_{mc} + j.\Delta G_{wb} + k.\Delta G_{helix_{dipole}} + l.\Delta G_{cis_{bonds}} + m.\Delta G_{disulfide} + n.\Delta G_{kn} + o.\Delta G_{partial_{covalent_{interactions}}} + p.\Delta G_{ionization} + q.T\Delta S_{complex}$$

The terms a-q carry the relative weights of all energy parameters in the equation above. The energy parameters are expanded in Table 1.

For optimizing the structures, the command "Optimize" was used while for mutation studies, the command "PositionScan" was used in FoldX. "PositionScan" mutates all the input residues to all the amino acids that occur naturally and then calculates the free energy upon mutation using the formulae: $\Delta\Delta G = \Delta G_{wt} - \Delta G_{mut.}$

A schematic diagram of the step-wise processes involved in the mutation studies is depicted below in Fig. 6.

SYMBOLIC TERMS	ENERGY TERMS FOR FREE ENERGY CALCULATION
$\Delta G_{BACKBONE\_HBOND}$	Backbone Hydrogen bonds
$\Delta G_{SIDECHAIN\_HBOND}$	Sidechain-sidechain and sidechain-backbone Hydrogen bonds
ΔG_{VDW}	Vander Waals energy
$\Delta G_{VDWCLASH}$	Inter residue Vander Waals clashes
ΔG_{EL}	Electrostatic contribution
ΔG_{HELIX_DIPOLE}	Electrostatic contribution of helix dipole
ΔG_{KN}	Additional electrostatic contribution between atoms of different chains within protein complexes
ΔG_{SOLVP}	Energy contribution by polar group atoms of proteins
ΔG_{SOLH}	The energy contribution of the hydrophobic group in the protein
$T\Delta S_{COMPLEX}$	The cost function for forming the complex
$T\Delta S_{SC}$	Entropy used in fixing sidechains
$T\Delta S_{MC}$	Entropy cost for mainchain fixation
ΔG_{WB}	The energy contribution of water bridges
ΔG_{CIS_BONDS}	Cost of having a cis peptide bond
$\Delta G_{DISULFIDE}$	Energy from disulfide bonds
$\Delta G_{PARTIAL\_COVALENT\_INTERACTIONS}$	Interactions with metal-bound
$\Delta G_{IONIZATION}$	Contribution of ionization energy

Table 1: Expanding the energy terms used in the equation for calculating free energy in FoldX.

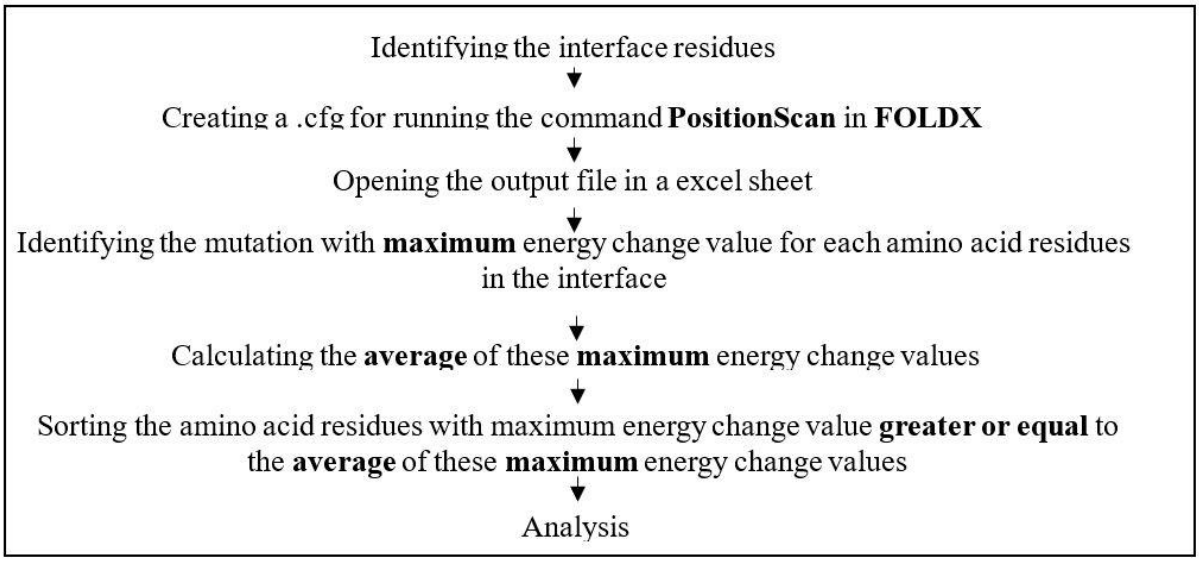

Fig. 6. Flowchart showing various filtering techniques involved in the mutational studies to get a proper trend of effects on the structure and stability of protein complexes upon mutation.

3.3. Results

3.3.1. BMP-7_Noggin complex reconstruction.

The structures, both from the PDB and from PDBePISA, have a missing loop fragment "GGGGGAA" between amino acid residues PRO88 and GLY96 (Fig. 7). To model the missing loop, the protein complex from PDBePISA was uploaded in the SL2 server and then ModLoop webserver was considered for further refinement of the complex structure (Fig. 7).

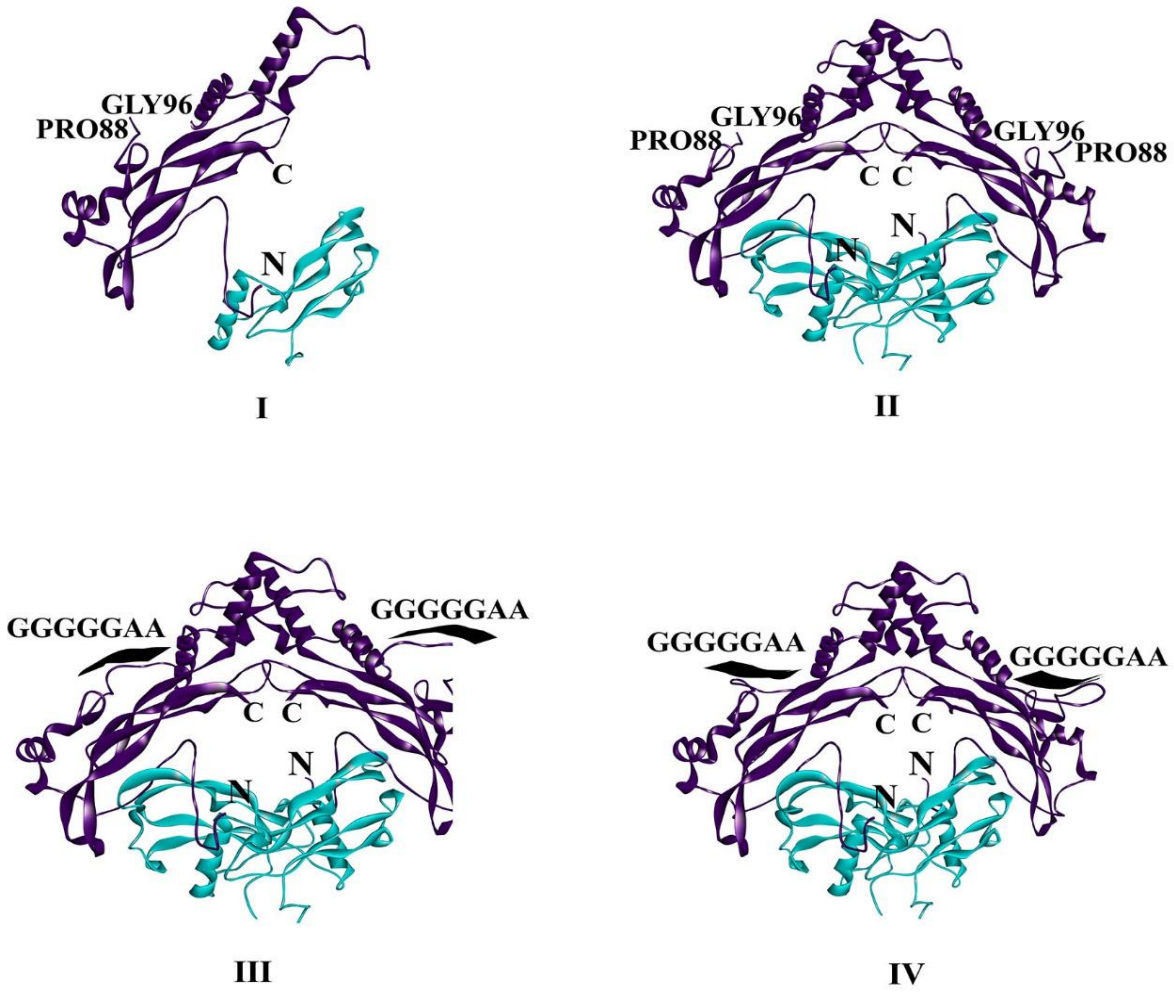

Fig. 7: I: Structure obtained after removing hetero atoms using Notepad++ from PDB structure 1M4U. II: Structure obtained after searching for probable assemblies in PDBePISA. III: Structure after adding loop fragment obtained from SL2 webserver. IV: ModLoop output.

SL2 webserver gave a list of loop fragments that were analyzed, based on maximum score, maximum similarity, and minimum clash score between various templates and the target loop fragment. For our study, a segment from the A-chain of the protein with ID 3BOG was considered as a template for loop construction (Fig. 8).

ID	D(	Sc...	PDB	Cl...	Template...	Se...	Seq position
1		0.22	3bog	3	GKGGSGT	42.86	64-70:A
2		0.17	4n75	9	DAVGGNA	42.86	704-710:B
3		0.15	2z7f	0	GWGLLGR	28.57	140-146:E
4		0.15	5cer	7	GKVEGEG	28.57	42-48:A
5		0.15	4wum	10	LFGFGPG	28.57	370-376:A
6		0.15	2p0u	8	LIGFGPG	28.57	388-394:A
7		0.14	1z1e	8	LFGFGPG	28.57	370-376:A
8		0.14	2ns9	11	EGNVGGL	28.57	119-125:A
9		0.14	5g0g	6	ALEGGYN	28.57	358-364:A
10		0.14	5ikk	10	SLEGGYN	28.57	362-368:A
11		0.14	2r5v	9	ATIGGFG	28.57	114-120:A
12		0.14	3c0y	8	ALEGGHD	28.57	838-844:B
13		0.14	3riq	4	GFFFGTD	28.57	648-654:A
14		0.13	2vkx	4	EGQRGED	28.57	607-613:E
15		0.12	1tq7	4	IVSAGAG	28.57	212-218:B
16		0.12	2i3g	7	GALTAAT	28.57	43-49:A
17		0.12	3etc	8	YFSSGTA	28.57	208-214:B
18		0.12	4y7o	5	RPGTAAG	28.57	982-988:A
19		0.12	3syb	6	HTGDTGA	28.57	281-287:A
20		0.11	3obl	2	GTMTYAG	28.57	116-122:A
21		0.11	4z17	15	PSGASTG	14.29	39-45:B
22		0.11	3e0n	1	IVSWGDA	28.57	212-218:B

Fig. 8: The first 22 outputs from the SL2 webserver for both the chains of Noggin.

Once we obtained the modeled structural complex of the BMP-7_Noggin, we investigated all the information of interactions which are mentioned in the previous work stated before [Fig. 3 (32)]. The 10-membered cysteine knot in the case of BMP-7 and 12-membered cysteine knot in the case of Noggin in our predicted structure can be shown as Fig. 3. Our predicted structure also has residues ranging from M27 to D39 in Noggin, that have been involved in binding with the receptor-binding site I, which is constructed by the residues with residue number 52, 55, 87, 128, and 131 in BMP-7. A similar pattern, as mentioned in the literature, is also seen in the case of binding site-II (32). The free energy value post optimization for the BMP-7_Noggin complex was found to be 592.438 kcal/mol.

3.3.2. BMP-2_Noggin complex model prediction

We obtained a total of approximately 150 structures after doing both default and advanced targeted docking using ClusPro 2.0. We considered various amino acid residues at the binding sites in different combinations, to reach these 150 different structures. We further narrowed it down to a single structure based on the free energy value post-optimization. The structure having the minimum energy following optimization is considered. The energy value of the top-most three structures having the least energy value following optimization is listed in table 2.

Modelled structures	**Energy post optimization (kcal/mol)**
Model_X	336.532
Model_Y	338.512
Model_Z	350.426

Table 2: The three top-most structures with minimum energies following optimization.

3.3.3. BMP-2_Gremlin-1 complex model prediction

Using ClusPro 2.0, we obtained approximately 150 models which accounted for outputs from both default and advanced docking. The outputs are presented with two types of distinctive conformers. One conformer indicated parallel binding where two Gremlin-1 dimers bonded in a parallel sense across the BMP-2 while the other conformer indicated anti-parallel binding where the two Gremlin-1 dimers bonded in an anti-parallel nature across the BMP-2. We considered the model with the minimum energy post optimization (Table 3).

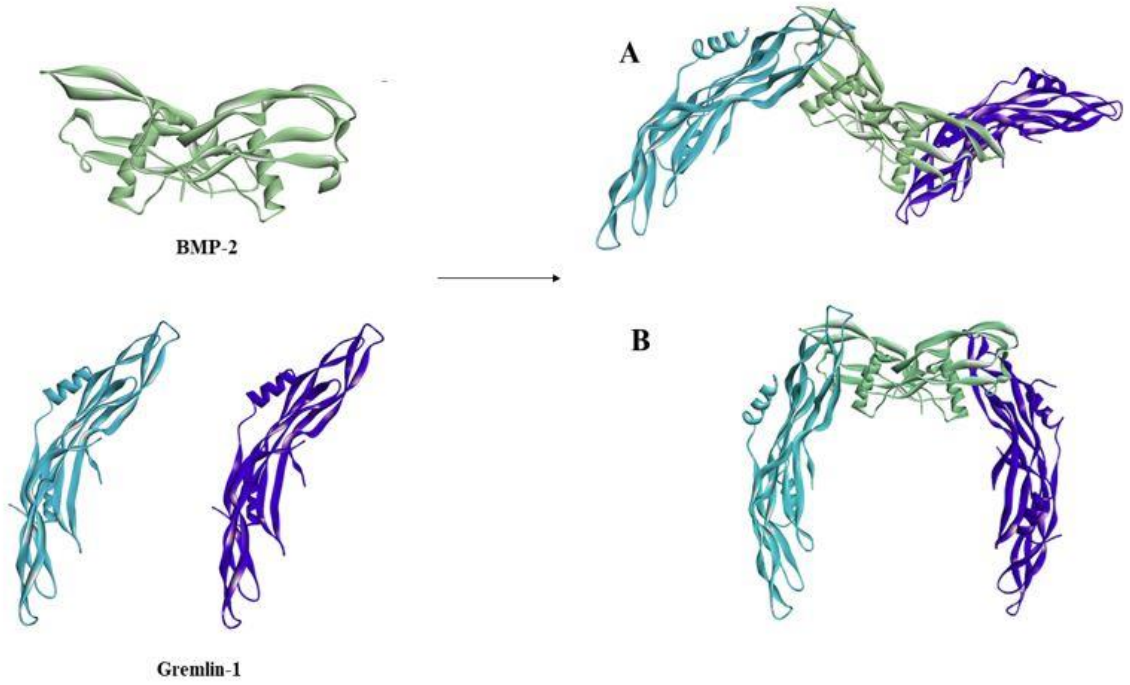

Fig. 9: The two distinctive conformations in which Gremlin-1 might bind across BMP-2 as per our results. (A) Conformer projecting anti-parallel binding. The minimum energy of the optimized structure in this conformation, post optimization, is 365.401 kcal/mol. (B) conformer projecting parallel binding. The minimum energy of the optimized structure in this conformation, post optimization, is 457.998 kcal/mol.

Models projecting anti-parallel binding	**Energy value post optimization (kcal/mol)**
Model_X	365.401
Model_Y	373.529
Model_Z	389.10

A

Models projecting parallel binding	**Energy value post optimization (kcal/mol)**
Model_X	457.998
Model_Y	482.444
Model_Z	485.721

B

Table 3. (A) Table showing the energy values of the three top-most optimized structures in case of anti-parallel binding. (B) Table showing the energy values of the three top-most optimized structures in case of parallel binding.

3.3.4. BMP-7_Gremlin-1 complex model prediction

After default and advanced docking using ClusPro 2.0 for the BMP-7_Gremlin complex, we obtained a total of approximately 150 docked structures. Here we were able to find three distinctive conformers which can be broadly classified into parallel and anti-parallel binding of Gremlin-1 across BMP-7 (Fig. 10). As indicated in some studies that Gremlin-1 prefers binding with BMP-2 in comparison with BMP-7, the minimum energy of the predicted model for BMP-7_Gremlin-1 should have a higher value than that of the minimum energy of the predicted model for BMP-2_Gremlin-1 (365.401 kcal/mol) (47). For further studies, we have considered Model_Z (Conformer "A") with a post-optimization energy value of 386.06 kcal/mol (approx. 20 kcal/mol energy value more than energy value of the BMP-2_Gremlin-1 predicted model).

Models projecting anti-parallel binding (Conformer "A" in Fig. 4.)	**Energy value, post-optimization (kcal/mol)**
Model_X	364.541
Model_Y	373.521
Model_Z	386.06

A

Models projecting anti-parallel binding (Conformer "B" in Fig. 4.)	**Energy value, post-optimization (kcal/mol)**
Model_X	403.088
Model_Y	413.054
Model_Z	421.975

B

Models projecting parallel binding (Conformer "C" in Fig. 4.)	Energy value, post-optimization (kcal/mol)
Model_X	371.104
Model_Y	372.088
Model_Z	376.110

C

Table 4: The minimum energy of the optimized structures in each category of conformer.

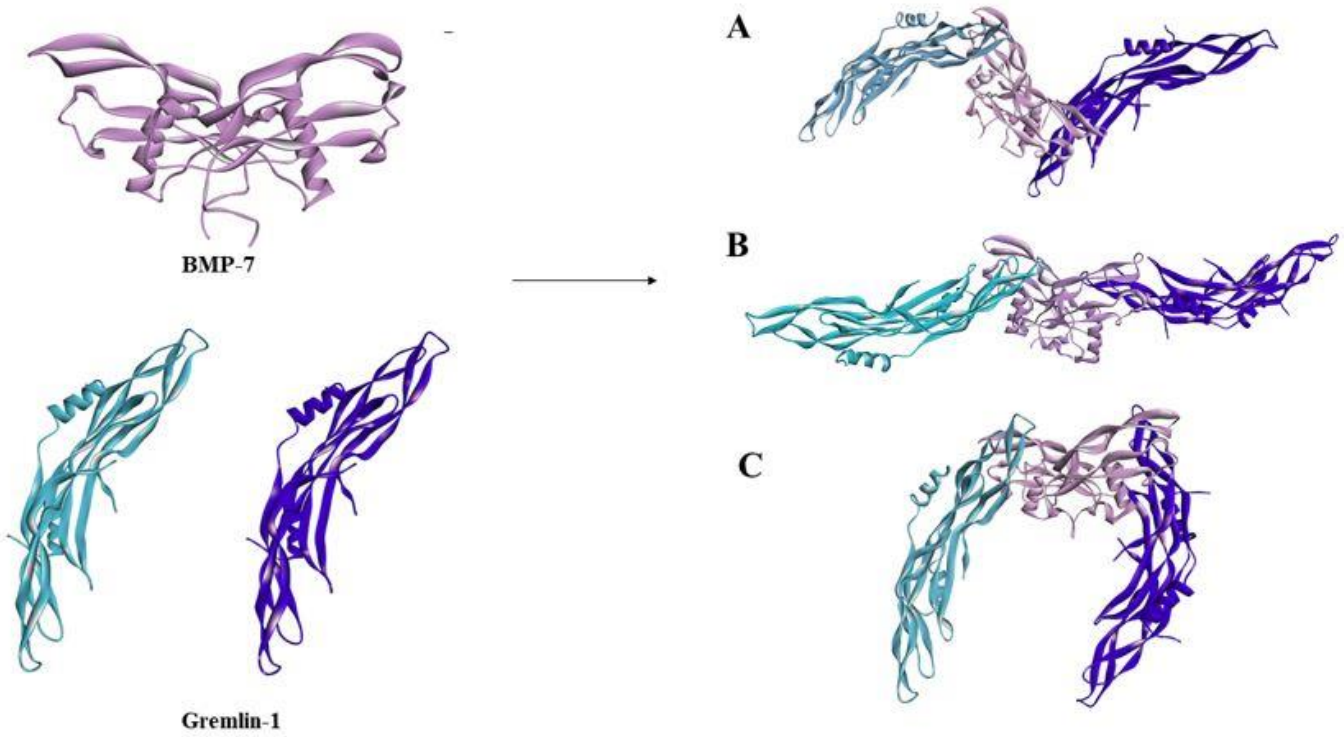

Fig. 10: The three distinctive conformers BMP-7_Gremlin-1. **A** and **B** depict an anti-parallel binding while **C** depicts the parallel binding.

3.3.5. Post-optimization-energy values of the modeled complexes of BMPs with their antagonists

The predicted structures were optimized to repair the side chains and to minimize the van der Waals clashes. FoldX was used for energy optimization of these structures. The free-energy value of the BMP-7_Noggin model, after optimization, was calculated to be 592.438 kcal/mol whereas, for the BMP-2_Noggin model, the free-energy value post-optimization calculated to be 336.532 kcal/mol. We investigated these two structures to analyze the energy parameters that had a significant influence associated with the formation of the complexes. Once we obtained the energy values, we considered the differences in energy values between the complexes and did an average of the values in two categories. In one category, we have considered those energy parameters which have positive energy values and averaged all those values; while in another category, we have considered those which have negative values. The positive energy values averaged to 40.464 kcal/mol, while the negative energy values averaged -48.589 kcal/mol. We considered those values which measured greater than (or equal to) 40.464 kcal/mol or less than (or equal to) -48.589 kcal/mol as significant. Our study also showed that the contribution of hydrogen bonds towards stability of BMP-2_Noggin is much more when compared with BMP-7_Noggin. The higher energy of BMP-7_Noggin can be attributed to the high Van der Waals clashes as compared with BMP-2_Noggin (Fig. 11, Table 5).

Similar minimization procedures were repeated for Gremlin-1 and BMP complexes. The free-energy calculation for BMP-2_Gremlin-1, following optimization was measured to be 365.401 kcal/mol, whereas for BMP-7_Gremlin-1 the energy value was 386.06 kcal/mol. The positive energy values averaged to 10.487 kcal/mol, while the negative energy values averaged -13.537 kcal/mol. In the case of BMP-2_Gremlin-1, It can be concluded from Fig. 12 and Table 6 that stability is largely directed by hydrogen bonding and Van der Waals interactions.

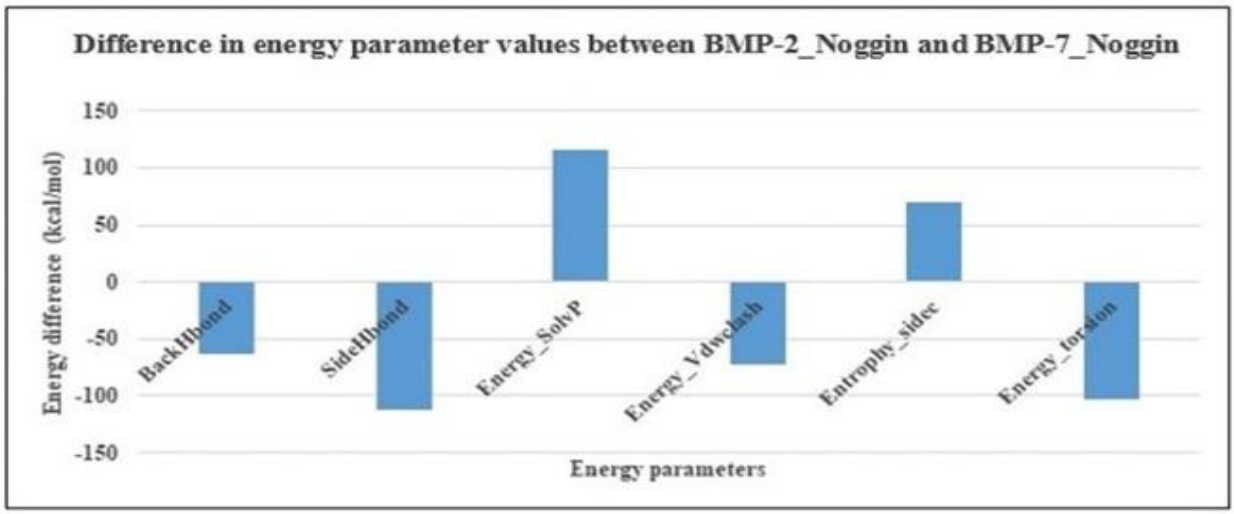

Fig. 11. Graphical representation of energy differences between BMP-2_Noggin and BMP-7_Noggin, which are considered significant.

Energy parameters	BMP-2_Noggin (kcal/mol)	BMP-7_Noggin (kcal/mol)	Difference (kcal/mol)
BackHbond	-356.994	-294.206	**-62.788**
SideHbond	-184.428	-72.035	**-112.393**
Energy_Vdw	-732.682	-698.236	-34.446
Electro	-54.6121	-11.9325	-42.6796
Energy_SolvP	1048.33	932.666	**115.664**
Energy_SolvH	-930.32	-913.58	-16.74
Energy_Vdwclash	122.424	195.571	**-73.147**
Entrophy_sidec	417.147	346.44	**70.707**
Entrophy_mainc	1007.74	992.699	15.041
cis_bond	11.2406	11.2406	0
Energy_torsion	54.6228	157.234	**-102.6112**
Backbone_vdwclash	344.338	372.003	-27.665
Helix dipole	-4.37262	-4.73647	0.36385
Disulfide	-60.4735	-50.7338	-9.7397
kn electrostatic	-3.69798	-0.0126311	-3.6853489
Energy ionization	2.60785	2.05991	0.54794

Table 5: Table showing various energy parameters associated with both complexes.

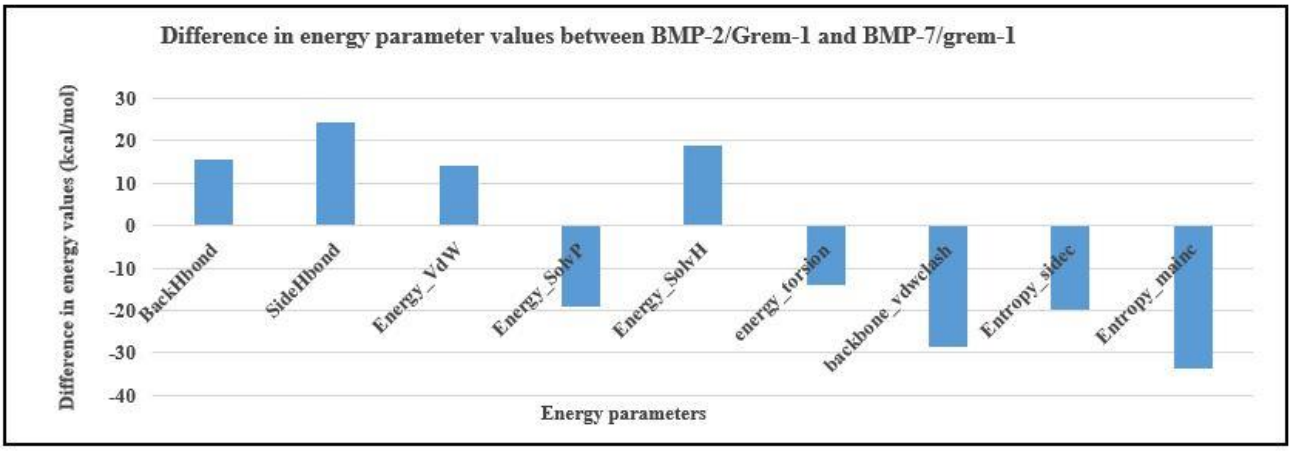

Fig. 12: Graphical representation of energy difference between BMP-2_Gremlin-1 and BMP-7_Gremlin-1, which are considered significant.

Energy parameters	BMP-2_Gremlin-1 (kcal/mol)	BMP-7_Gremlin-1 (kcal/mol)	Difference (kcal/mol)
BackHbond	-405.67	-421.2	**15.53**
SideHbond	-225.73	-250.08	**24.35**
Energy_Vdw	-840.71	-854.76	**14.05**
Electro	-39.27	-36.85	-2.42
Energy_SolvP	1224.36	1243.33	**-18.97**
Energy_SolvH	-1058.06	-1076.93	**18.87**
Energy_Vdwclash	149.79	152.97	-3.18
Entrophy_sidec	76.7	90.53	**-13.83**
Entrophy_mainc	241.16	269.68	**-28.52**
cis_bond	499.37	519.01	**-19.64**
Energy_torsion	1074.95	1108.73	**-33.78**
Backbone_vdwclash	-3.17	-2.39	-0.78
Helix dipole	10.13	9.88	0.25
Disulfide	-95.07	-95.22	0.15
kn electrostatic	-6.27	-5.55	-0.72
Energy ionization	2.92	2.71	0.21

Table 6: Table showing various energy parameters associated with both complexes.

3.3.6. Interfacial Residues

We ran a python script in the PyMol software interface and obtained the list of interface residues in all the complexes modeled between the BMPs and the antagonists. The interfacial residues of these complexes are listed in table 7 (BMPs & Noggin) and table 8 (BMPs & Gremlin-1).

BMP-2_Noggin interface

Chains	Residues at the receptor-binding site I interface
B	**SERB24**, ASNB29, ASPB30, TRPB31, VALB33, ALAB34, PROB35, **PROB36, ALAB86**, ILEB87, SERB88, METB89, LEUB90, LEUB92, GLUB94, GLUB96, LYSB97, VALB98, VALB99, LEUB100, LYSB101, ASNB102, TYRB103, GLNB104, **METB106**
C	**PHEC49**, PROC50, LEUC51, ALAC52, ASPC53, HISC54, SERC57, ASNC59, ILEC62, VALC63, **LEUC66**
H	METH27, HISH29, TYRH30, LEUH31, HISH32, ILEH33, ARGH34, PROH35, ALAH36, PROH37, SERH38, ASPH39, LEUH43,VALH44, ASPH45, LEUH46, ILEH47, GLUH48, HISH49, PHEH54, PHEH168, ARGH204, TRPH205, ARGH206, CYSH207, GLNH208, ARGH209, ARGH210, ILEH218, PROH219, ILEH220, GLNH221, TYRH222

Chains	Residues at the receptor-binding site II interface
B	**PHEB49**, PROB50, LEUB51, ALAB52, ASPB53, HISB54, SERB57, ASNB59, ILEB62, VALB63, **LEUB66**
C	**SERC24**, ASNC29, ASPC30, TRPC31, VALC33, ALAC34, PROC35, **PROC36**, **ALAC86,** ILEC87, SERC88, METC89, LEUC90, LEUC92, GLUC94, GLUC96, LYSC97, VALC98, VALC99, LEUC100, LYSC101, ASNC102, TYRC103, GLNC104, **METC106**
G	METG27, HISG29, TYRG30, LEUG31, HISG32, ILEG33, ARGG34, PROG35, ALAG36, PROG37, SERG38, ASPG39, LEUG43,VALG44, ASPG45, LEUG46, ILEG47, GLUG48, HISG49, PHEG54, PHEG168, ARGG204, TRPG205, ARGG206, CYSG207, GLNG208, ARGG209, ARGG210, ILEG218, PROG219, ILEG220, GLNG221, TYRG222

BMP-7_Noggin interface

Chains	Residues at the receptor-binding site I interface
A	**ARGA48**, TRPA52, GLNA53, ASPA54, TRPA55, ILEA57, ALAA58, PROA59, **GLUA60**, **SERA113**, LEUA115, TYRA116, ASNA122, VALA123, ILEA124, LEUA125, LYSA126, LYSA127, TYRA128, ARGA129, **META131**
D	**PHED73**, PROD74, LEUD75, ASND76, SERD77, ALAD81, ASND83, ILED86,VALD87, **LEUD90**
H	METH27, HISH29, TYRH30, LEUH31, HISH32, ILEH33, ARGH34, PROH35, ALAH36, PROH37, SERH38, ASPH39, ASNH40, LEUH41, PROH42, LEUH43, VALH44, ASPH45, LEUH46, ILEH47, GLUH48, HISH49, PHEH168, HISH199, ARGH204, ARGH206, GLNH208, ARGH210, ILEH218,PROH219, ILEH220, GLNH221, TYRH222, PROH223

Chains	Residues at the receptor-binding site II interface
A	**PHEA73**, PROA74, LEUA75, ASNA76, SERA77, ALAA81, ASNA83, ILEA86,VALA87, **LEUA90**
D	**ARGD48**, TRPD52, GLND53, ASPD54, TRPD55, ILED57, ALAD58, PROD59, **GLUD60**, **SERD113**, LEUD115, TYRD116, ASND122, VALD123, ILED124, LEUD125, LYSD126, LYSD127, TYRD128, ARGD129, **METD131**
G	METG27, HISG29, TYRG30, LEUG31, HISG32, ILEG33, ARGG34, PROG35, ALAG36, PROG37, SERG38, ASPG39, ASNG40, LEUG41, PROG42, LEUG43, VALG44, ASPG45, LEUG46, ILEG47, GLUG48, HISG49, PHEG168, HISG199, ARGG204, ARGG206, GLNG208, ARGG210, ILEG218, PROG219, ILEG220, GLNG221, TYRG222, PROG223

Table 7: List of amino acid residues at the interface of BMP-2_Noggin complex and BMP-7_Noggin complex.

BMP-2_Gremlin-1 interface

Chains	Residues at the receptor-binding site I interface (site Ia)
B	**PHEB49**, PROB50, ILEB62, LEUB66, SERB69, **VALB70**
C	**SERC24**, ASPC25, VALC26, GLYC27, TRPC28, ASNC29, ASPC30, TRPC31, TYRC91, LEUC92, ASPC93, GLUC94, ASNC95, VALC99, LYSC101, **TYRC103**
G	CYSG108, ASNG109, SERG110, ARGG111, THRG112, ILEG114, LYSG148, THRG150, THRG151, METG152, METG153, THRG155, LEUG156, ASNG157, PROG164, THRG165, LYSG167, ARGG169, LYSG174

Chains	Residues at the receptor-binding site I interface (site Ib)
B	**SERB24**, ASPB25, VALB26, GLYB27, TRPB28, ASNB29, ASPB30, TRPB31, TYRB91, LEUB92, ASPB93, GLUB94, ASNB95, VALB99, LYSB101, **TYRB103**
C	**PHEC49**, PROC50, ILEC62, LEUC66, SERC69, **VALC70**
L	CYSL108, ASNL109, SERL110, ARGL111, THRL112, ILEL114, LYSL148, THRL150, THRL151, METL152, METL153, THRL155, LEUL156, ASNL157, PROL164, THRL165, LYSL167, ARGL169, LYSL174

BMP-7_Gremlin-1 interface

Chains	Residues at the receptor-binding site I interface (site-Ia)
A	**PHEA73**, PROA74, LEUA75, ASNA76, ILEA86, LEUA90, PHEA93, **ILEA94**
D	**ASPD49**, LEUD50, GLYD51, TRPD52, GLND53, ASPD54, **TRPD55**, **ASPD118**, ASPD119, SERD120, SERD121, LYSD126, **TYRD128**
G	ARGG111, THRG112, ILEG113, ILEG114, ARGG116, LYSG148, THRG150, THRG151, METG152, METG153, VALG154, THRG155, ASNG157, THRG165, LYSG167, ARGG169, ARGG172, LYSG174

Chains	Residues at the receptor-binding site I interface (site-Ib)
A	**ASPA49**, LEUA50, GLYA51, TRPA52, GLNA53, ASPA54, **TRPA55**, **ASPA118**, ASPA119, SERA120, SERA121, LYSA126, TYRA128
D	**PHED73**, PROD74, LEUD75, ASND76, ILED86, LEUD90, PHED93, **ILED94**
L	ARGL111, THRL112, ILEL113, ILEL114, ARGL116, LYSL148, THRL150, THRL151, METL152, METL153, VALL154, THRL155, ASNL157, THRL165, LYSL167, ARGL169, ARGL172, LYSL174

Table 8: List of amino acid residues at the interface of BMP-2_Gremlin-1 complex and BMP-7_Gremlin-1 complex.

3.3.7. Mutation

BMP-2_Noggin complex

We investigated mutations of all the interfacial residues and tried to study the effect of these mutations on the stability of the complexes. They are listed in table 10. We also graphically plotted these mutations and the change in energy of the complex structures caused by a mutation (fig. 13). The mutations are considered significant only when the change in energy value is more than the average of all the maximum values for changes in energy values upon mutation of all the interfacial residues.

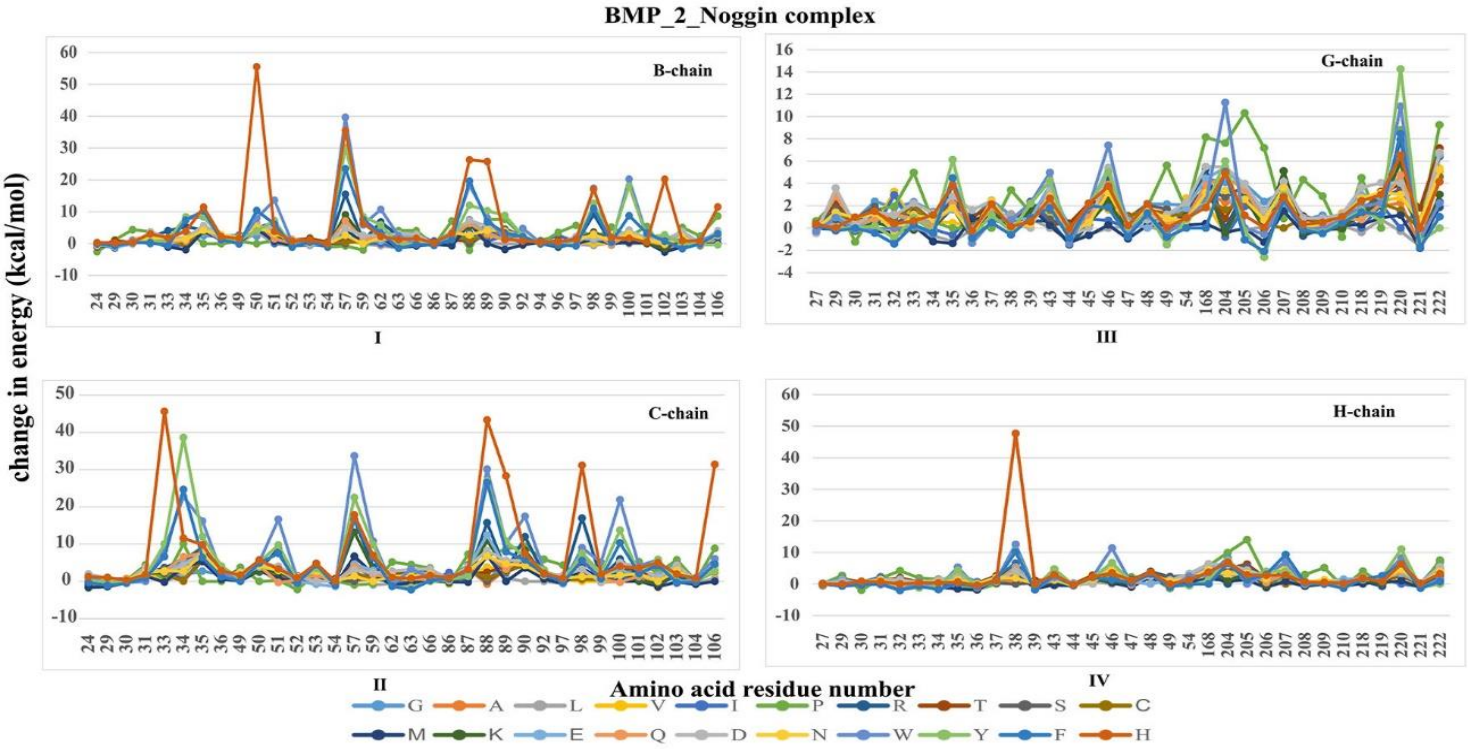

Fig. 13: Plot depicting the effect of the mutation in BMP-2_Noggin complex.

Essential residues	Significant mutations	Factors destabilizing the complex	Change in energy (kcal/mol)
PROB50	HIS	LEUG31, HISG32: Steric association with HISB50	**55.5424**
SERB57	TRP	LEUB51, ALAB61, THRB65, ALAB77, and CYSB113: Steric association with TRPB57	**39.6903**
SERB88	HIS	ILEH47, ASPH45: Steric association with HISB88	26.3057
METB89	HIS	ILEB32. ALAB34: Steric association with HISB89	25.7775
VALC33	HIS	LEUC90, ARGG204: Steric association with HISC33	**45.5906**
ALAC34	TYR	GLUG48, PROC35, and ILEG47: Steric association with TYRC34	38.5911
SERC57	TRP	CYSC113, ALAC61, ALAC57: Steric association with TRPC57	33.6944
SERC88	HIS	LEUG43, VALG44, ASNC102: Steric association with HISC88	**43.3159**
ARGG204	TRP	ARGG167: Steric association with TRPG204	11.2555
TRPG205	PRO	ARGG167: Steric association with PROG205	10.3154
ILEG220	TYR	LEUC100: Steric association with TYRG220	14.2581
SERH38	HIS	ASNB102, TYRB103: Steric association with HISH38	**47.6814**
LEUH46	TRP	GLUH48: Steric association with TRPH46	11.3471
TRPH205	PRO	ARGH167: Steric association with PROH205	14.0096

Table 9: Table showing the effect of steric hindrance in destabilization upon mutation of various interfacial amino acid residues.

Mutations can destabilize a structure in various ways including disruption of various interactions such as hydrogen bond interactions, alkyl-alkyl interactions, pi-alkyl interactions, etc. The list of interfacial residues in the BMP-2_Noggin complex, which upon mutation can induce destabilization due to steric reasons, are listed in table 9.

Analysis from Fig. 13, table 9 and table 10 suggests that PROB50, SERB57, VALC33, SERC88, and SERH38 upon mutation can cause maximum destabilization for the BMP-2_Noggin complex. For PROB50, mutation to HIS causes maximum destabilization as it gets in very close vicinity of

LEU31 (G chain) and HIS32 (G chain). Mutation to TRP, in the case of SER 57, introduces TRP nearby of LEUB51, ALAB61, THRB65, ALAB77, and CYSB113 enabling steric interactions. Mutation of VALC33 to HIS brings LEUC90 and ARGG204 close to HISC33, again enabling steric interactions and causing destabilization. Similarly, in the case of SERC88, the destabilization is caused by a mutation to HIS. HISC88 gets near LEUG43, VALG44, and ASNC102 causing steric hindrance. Upon mutation to HIS, in the case of SERH38, destabilization is mediated by the steric association of HISH38 with ASNB102 and TYRB103.

As mentioned earlier, destabilization occurs due to disruption of interactions. We could see such tendencies in the BMP-2_Noggin complex. The mutation of PROB35 to HISB35 was followed by the disruption of an alkyl bond that existed between PROB35 and LEUG41 in the complex. In SERC88, the mutation was accompanied by the disruption of a carbon-hydrogen bond. In SERH38 as well, we observed disruption of hydrogen bond interactions with ALAB36 and GLNB104. We also observed the breakdown of carbon-hydrogen bond interactions with ASNB102 and disruption of inter-chain interactions in SERB38 in the B chain (Fig. 14).

	B	B	B	B	C	C	C	C	G	G	G	H	H	H
	50	57	88	89	33	34	57	88	204	205	220	38	46	205
G	2.30225	1.17988	0.697547	4.76789	3.1248	1.75187	0.396645	0.50694	4.10523	3.95047	4.16392	1.27029	4.48937	5.29025
A	4.28709	0.296868	-0.29238	3.49238	1.69346	0	0.197057	-0.72416	2.2995	2.28426	2.26674	1.0867	3.7259	3.89815
L	3.67162	2.77131	7.28567	0.227934	-0.18455	2.00942	5.62673	7.39342	3.27519	-0.1657	-0.29497	4.81074	0	1.1682
V	5.0851	0.519243	2.33575	1.60135	0	5.29155	1.13073	3.83363	-0.51852	3.00284	2.73121	5.46401	2.32703	4.57342
I	5.44924	1.94138	3.56826	0.752922	3.24233	5.61376	5.10166	6.72667	-0.80772	1.93339	0	6.62512	1.84718	4.12466
P	0	-0.74814	-2.103	7.56353	0.313183	10.0986	-0.97019	6.74626	7.60991	10.3154	8.80711	4.83336	2.31253	14.0096
R	4.978	15.503	7.45557	2.61012	3.67431	5.6496	16.6433	15.7069	0	3.25652	7.9218	3.50082	6.05912	3.5441
T	5.77188	0.740499	0.681854	3.32241	2.49138	4.96618	3.58744	2.45662	0.86309	3.89569	3.88237	1.83353	3.72036	6.27567
S	4.92962	0	0	3.38759	3.34264	0.316083	7.67E-12	-6.82E-13	2.78869	3.74622	3.47816	0	4.9645	5.60477
C	5.2192	0.370469	1.15806	2.67771	1.85373	0.149786	2.37865	1.01612	1.62404	2.46222	1.5886	3.01391	3.33655	3.55061
M	4.5065	4.4918	6.2235	0	-0.23628	3.93174	6.73044	7.06817	-0.40568	-0.03767	1.14742	4.20754	0.383394	1.25646
K	4.69617	9.08744	5.41709	3.42069	2.26928	4.28671	13.2293	10.9533	-0.45185	2.7835	5.90305	5.71568	0.944611	3.33936
E	4.50477	4.62598	6.88302	3.63652	2.81356	4.96589	4.60408	12.4557	5.39866	3.35922	4.76728	5.40325	5.28085	4.40374
Q	6.43366	7.17553	6.37347	2.98739	2.78181	6.55756	4.05582	7.03866	4.61318	3.4324	4.7547	4.70892	4.14374	3.78978
D	5.61506	4.88172	7.30163	5.45122	2.54995	4.19399	3.0708	8.26357	5.48543	3.91284	4.02481	4.04899	5.95293	4.35776
N	5.1983	2.66956	2.70273	4.15581	2.82328	2.77598	1.35991	6.78363	3.36642	2.56654	3.00818	1.84705	4.5429	3.33886
W	7.95923	39.6903	18.2577	8.08941	8.48835	22.6933	33.6944	30.0998	11.2555	0	10.9219	12.542	11.3471	0
Y	4.01654	30.0804	12.0729	10.3377	10.0042	38.5911	22.4852	26.9751	5.9927	-0.29842	14.2581	10.338	6.74163	2.40281
F	10.4213	23.5281	19.6677	6.82771	6.63786	24.6557	16.6467	26.5205	5.05564	-1.06572	8.44487	10.1468	1.33614	1.25784
H	55.5424	35.5378	26.3057	25.7775	45.5906	11.5667	17.8366	43.3159	4.93141	1.12907	6.52558	47.6814	3.48883	2.85048

Table 10. List of interfacial residues in BMP-2_Noggin and the change in energy value upon mutation.

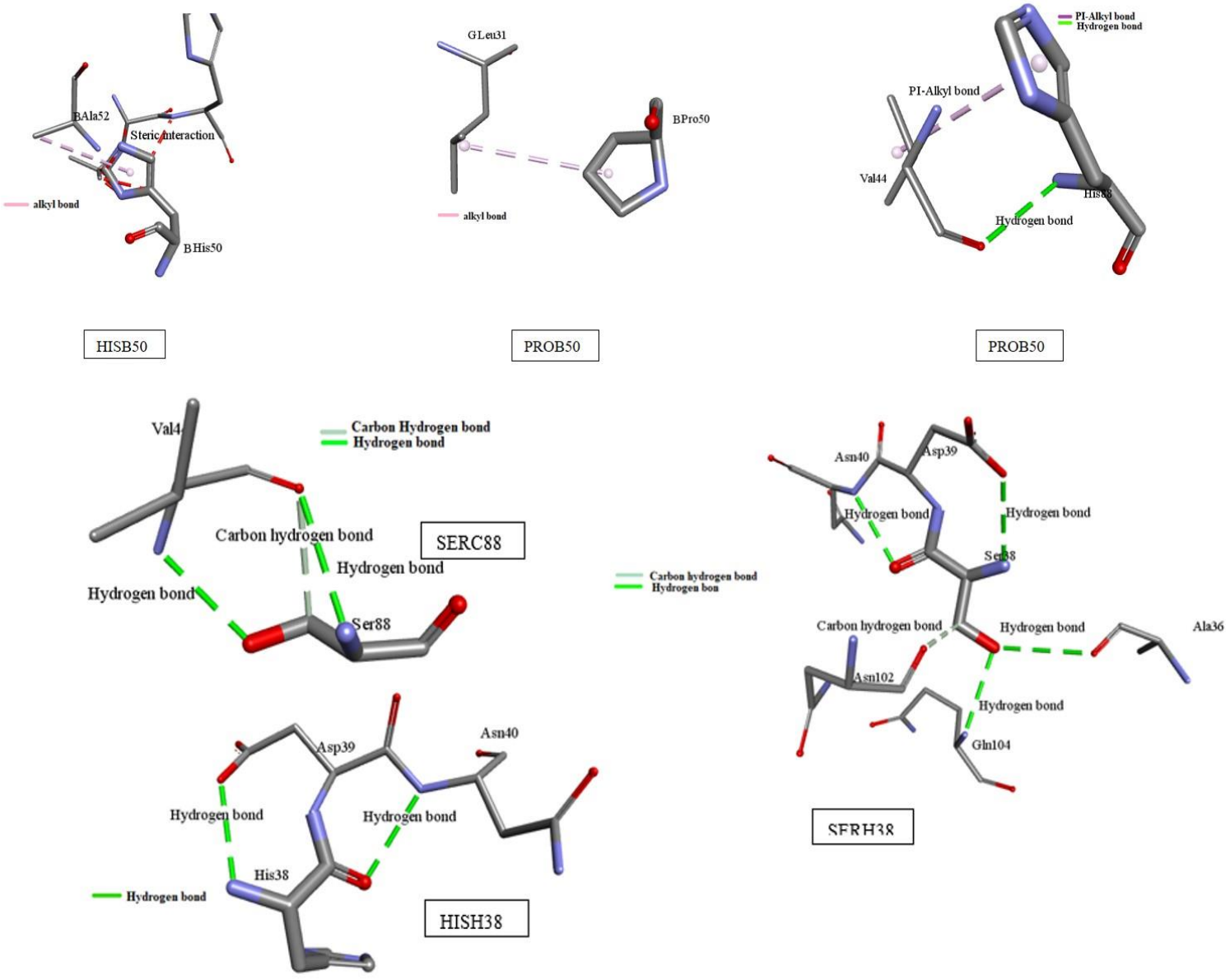

Fig. 14: Figure showing the disruption of the interactions associated with the mutation in the case of PROB50, SERC88, and SERG38.

BMP-7_Noggin

Similarly, we have investigated the effect of a mutation on the complexation between BMP-7 and Noggin (Table 11, Table 12, fig. 15).

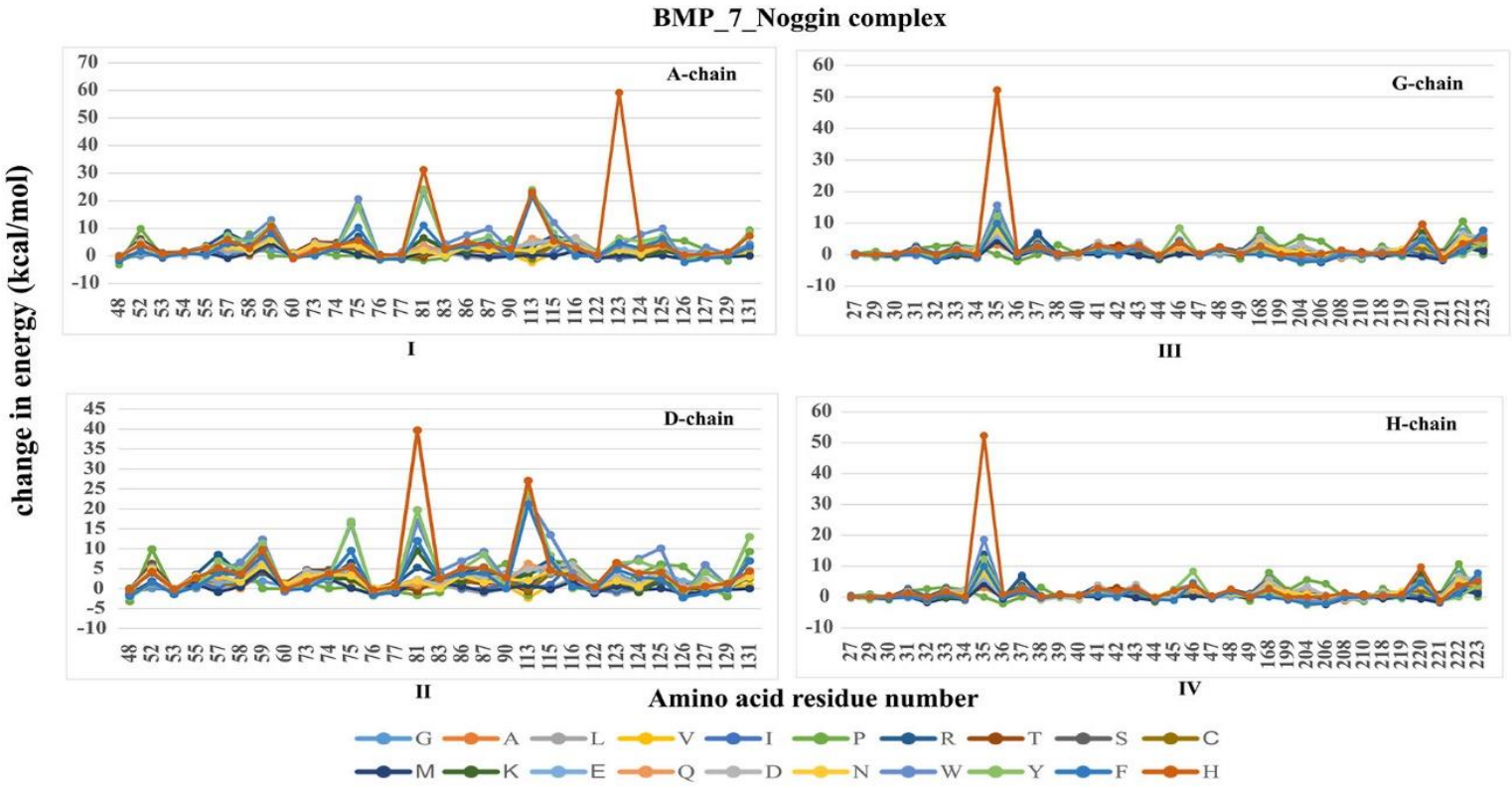

Fig. 15: Plot depicting the effect of mutation in BMP-7_Noggin complex.

Essential residue	Significant mutation	Factors destabilizing the complex	Change in energy (kcal/mol)
LEUA75	TRP	THRA138: Steric association with TRPA75	20.6504
ALAA81	HIS	ILEA86, THRA82: Steric association with HISA81	31.2201
SERA113	TYR	LEUH43: Steric association with TYRA113	23.9505
VALA123	HIS	ILEH220, PROH219: Steric association with HISA123	**59.1864**
LEUD75	TYR	CYSD71: Steric association with TYRD75	16.8951
ALAD81	HIS	ILED86, THRD82: Steric association with HISD81	**39.7236**
SERD113	HIS	VALG44, LEUG43: Steric association with HISD113	27.0922
LEUD115	TRP	Disruption of interactions with VALD123, ILED57, ARGD204	13.4846
PROG35	HIS	ASNA83 167, HISA84: Steric association with HISG35	**52.2049**
ILEG220	HIS	Disruption of interactions with LEUD115, and VALD123	9.6786
TYRG222	PRO	Disruption of interaction with ASNG162, ASPG45, and LEUG200. LEUG200: Steric association with PROG222	10.5963
PROH35	HIS	ASND83, HISD84: Steric association with HISH35	**52.2782**
ILEH220	HIS	Disruption of interaction with LEUA115 and VALA123	9.69101
TYRH222	PRO	Disruption of interaction with ASNH162, ASPH45, and LEUH200 LEUH200: Steric association with PROH222.	10.7257

Table 11: Table listing out the destabilizing factors upon mutation of interfacial residues in the BMP-7_Noggin complex.

	A	A	A	A	D	D	D	D	G	G	G	H	H	H
	75	81	113	123	75	81	113	115	35	220	222	35	220	222
G	3.95264	1.38435	0.566941	4.11863	4.07756	1.41685	0.453907	6.19144	4.62774	4.20069	7.4985	4.63691	4.19732	7.63157
A	2.6132	0	-1.14639	2.25066	2.90825	0	-0.82346	4.55461	3.03783	2.84783	5.88052	3.04629	2.84459	6.02926
L	0	2.60522	0.414906	-1.05333	0	1.71239	0.650367	0	9.46561	1.36188	1.54933	9.85481	1.32334	1.8349
V	1.77469	0.276115	-2.42428	0	2.01143	-0.08628	-2.35634	1.0558	6.51761	0.617825	4.06437	6.50855	0.615251	4.20793
I	2.7073	0.970857	0.08063	-0.64269	2.86436	0.959826	-0.0707	1.02365	7.99323	0	2.98231	8.00373	0	3.20646
P	0.073298	-1.67228	-1.34086	-0.10067	0.30522	-1.70611	-1.70995	6.91877	0	4.83626	10.5963	0	4.83183	10.7257
R	7.05797	6.53467	3.3881	3.20376	6.55265	5.29427	4.01516	7.3581	13.8608	6.90248	1.83844	13.8387	5.25771	1.97052
T	2.06341	-0.73097	-0.59223	1.85392	2.21498	-0.7244	-0.75344	3.75823	7.48266	2.63432	5.69434	7.41025	2.63171	5.82724
S	3.07328	0.528044	0	2.41956	3.1924	0.523436	0	5.89963	5.01771	3.21599	6.48228	5.01036	3.21332	6.60978
C	2.42131	0.724137	-0.86442	1.01022	2.37002	0.468112	-0.27748	3.64996	6.30228	2.10964	5.00355	6.28407	2.10646	5.13672
M	0.38322	1.58648	0.273722	0.20811	0.176465	1.73634	0.871123	-0.18864	4.30478	-0.65742	2.12068	4.30402	-0.65977	2.25363
K	2.72204	6.41974	3.8428	2.669	2.43621	9.49456	3.56997	5.98769	11.4758	6.95461	3.21288	11.4902	7.42743	3.34582
E	5.28343	2.08291	4.5468	1.95122	4.99675	1.86154	4.95459	3.95395	6.03145	3.80542	5.61502	6.0193	3.81681	5.74048
Q	3.26977	3.95624	6.27366	2.53289	3.64941	0.846047	6.30778	4.47704	7.43953	3.45245	4.1006	7.43652	3.45021	4.23384
D	4.63335	2.30857	4.83336	3.09957	5.50391	2.31581	4.8765	5.75387	7.07006	5.2451	6.49457	7.0732	5.24077	6.61986
N	3.7678	1.91785	1.90504	1.96378	3.17808	1.92313	2.053	4.49301	7.82197	3.78796	5.01228	7.82522	3.78417	5.14568
W	20.6504	22.9318	22.4503	3.72912	16.2428	16.7493	22.2163	13.4846	15.6889	5.50101	3.01259	18.6333	5.49887	3.15899
Y	17.6641	24.2116	23.9505	6.41816	16.8951	19.7417	24.709	8.36708	12.3429	5.00875	0	12.3491	5.00273	0
F	10.2816	11.0017	21.5266	4.67289	9.50405	12.0238	21.1894	7.28338	9.93503	4.63024	0.977004	9.93248	4.58784	1.11087
H	5.59146	31.2201	23.0991	59.1864	5.3855	39.7236	27.0922	4.61711	52.2049	9.6786	3.52101	52.2782	9.69101	3.6599

Table 12: Table showing the change in energy values that is calculated using FoldX, upon mutation of the interfacial residues in the BMP-7_Noggin complex.

From Fig. 15, Table 11, and Table 12 we can observe that VALA123, ALAD81, PROG35, and PROH35 upon mutation cause maximum destabilization for the BMP-7_Noggin complex. Besides steric hindrance, the mutation in VALA123 to HIS is accompanied by the disruption of the alkyl-alkyl association with ILEA57 and ILEH220 (H chain) and the disruption of the pi-alkyl association is observed with PHEA117. Mutation of ALA81 to HIS is associated with the disruption of the alkyl-alkyl association with CYSD138 and ILED86. In mutation of PRO35 to HIS, there occurs the disruption of the alkyl-alkyl association with TYRD128, METD131, and TRPD52. A similar situation is observed in PROH35 (Fig. 16).

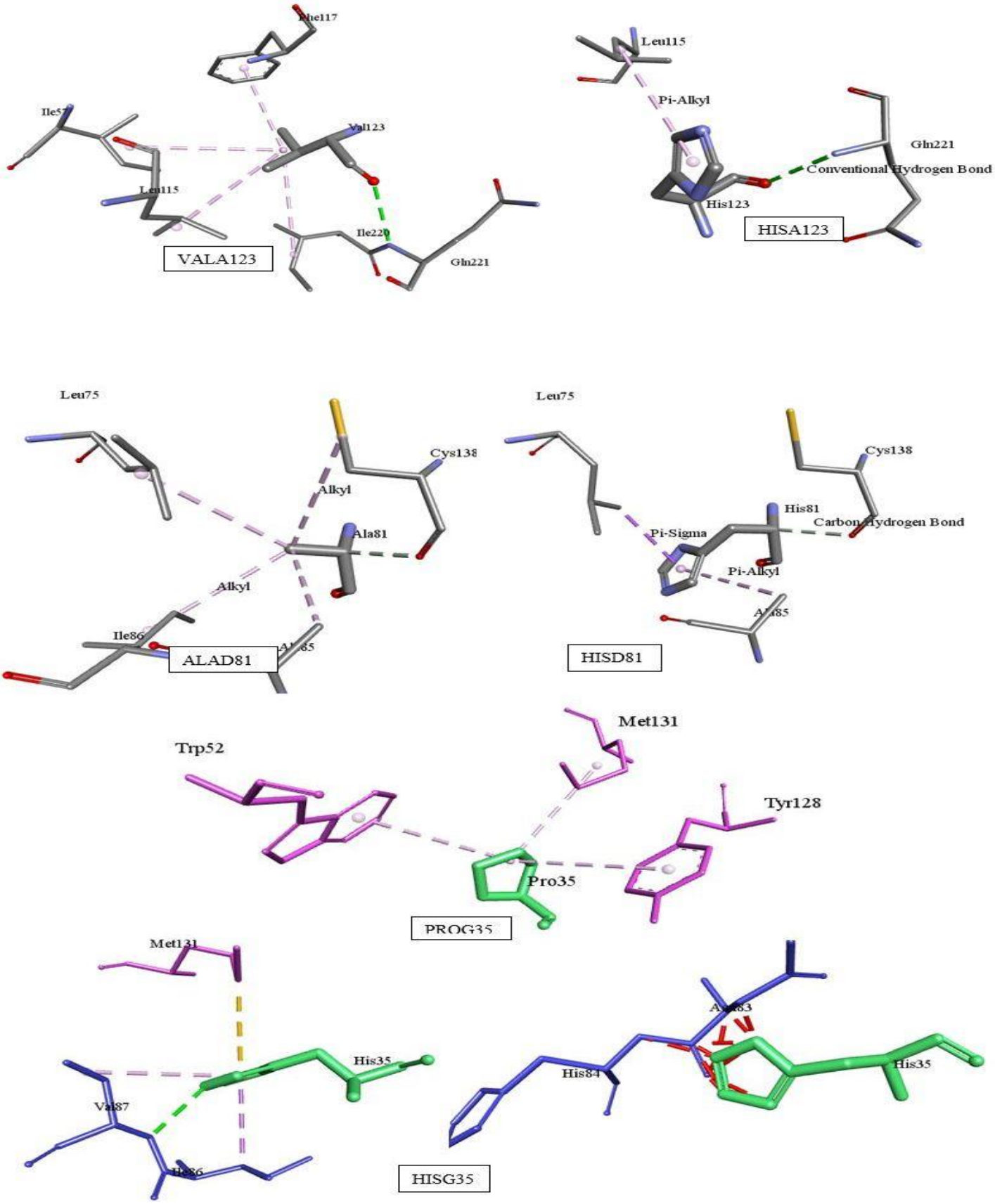

Fig. 16: Figure showing the disruption of interactions, due to mutations, in the BMP-7_Noggin complex. The mutation of VALA123, ALAD81, and PROG35 to histidine is shown. In PROG35 and HISG35, A-chain is colored blue, the D chain is colored pink and the G chain is colored green.

BMP-2_Gremlin-1

We mutated the interfacial residues and inferred residues which are significantly essential for the BMP-2_Gremlin-1 complex. From fig. 17, Table 13, and Table 14, it can be interpreted that ASPB93, GLYC27, CYSG108, THRG150, and CYSL108 are significantly essential for the BMP-2_gremlin-1 complex.

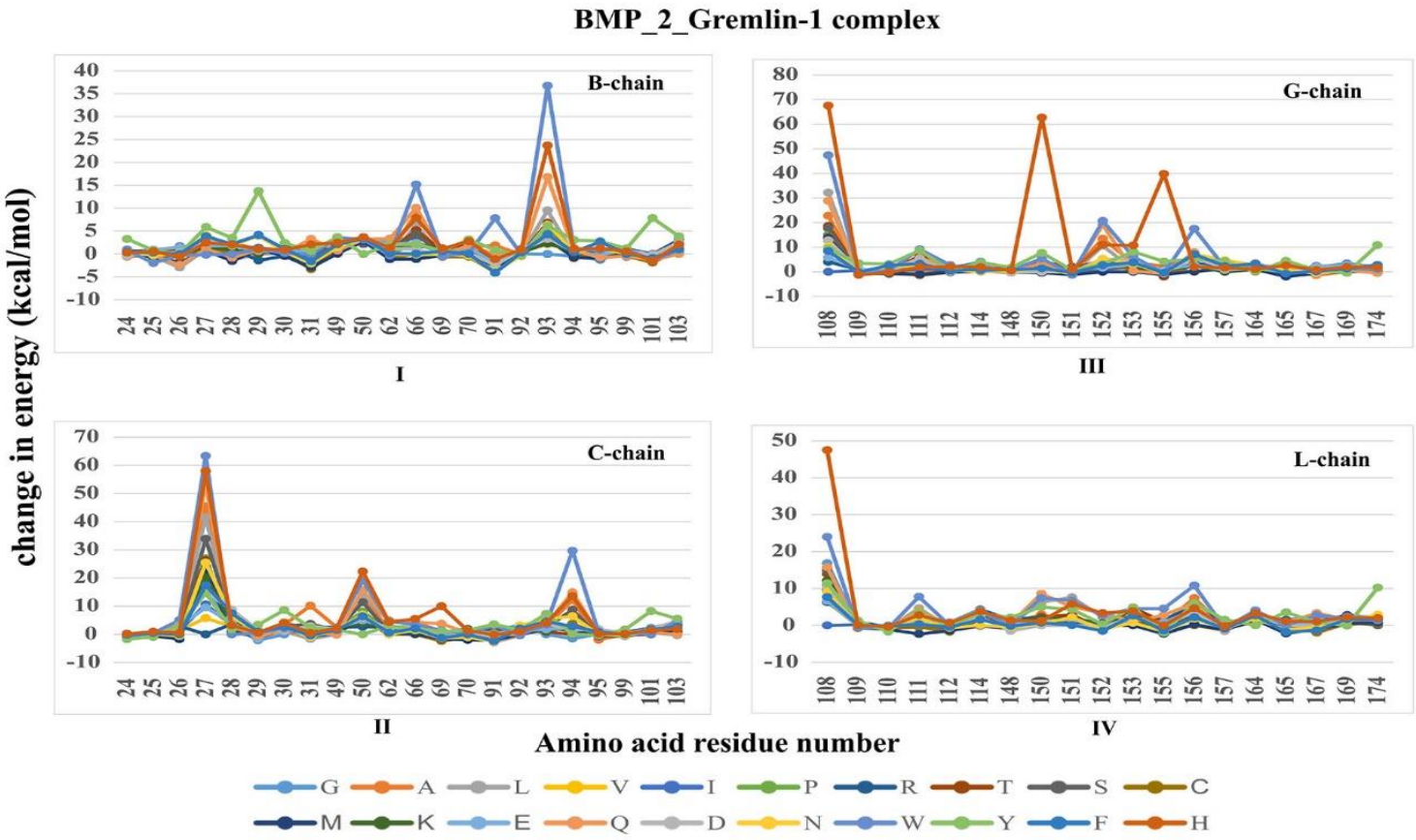

Fig.17: Plot depicting the effects of mutations in BMP-2_Gremlin-1.

	B	B	B	C	C	C	G	G	G	L	L	L
Mutation	29	93	66	27	94	50	108	150	155	108	156	174
D	0.92	0	4.26	15.9	-1.54	4.87	15.11	3.02	-0.13	16.83	4.35	1.97
R	0.96	6.4	8.85	45.39	12.19	13.97	22.8	1.43	2.42	15.25	7.43	1.37
F	0	9.54	6.31	41.53	13.99	14.08	32.17	3.31	-0.42	14.1	3.55	1.33
A	1.11	2.15	1.96	5.78	0.86	3.97	5.68	0.8	-0.42	6.36	3.77	1.69
C	1.38	2.74	1.69	10.6	1.09	4.48	0	0.78	-0.8	0	2.39	2.39
Q	0.56	5.04	2.51	26.97	2.25	8.08	17.46	2.23	-0.26	10.46	2.82	1.47
G	-1.39	2.35	3.77	0	2.13	2.71	4.04	1.73	-0.28	6.28	5.02	1.95
E	0.77	6.84	5.2	26.36	0	5.28	18.65	4.35	-1.98	13.93	3.97	1.58
K	1.07	6.42	4.29	33.92	8.71	11.39	17.94	2.05	0.39	14.85	2.46	0
L	1.13	3.84	0	24.08	3.79	6.91	14.32	0.07	1.13	10.67	0	0.43
M	1.01	3.24	-1.09	22.91	1.79	5.95	13.79	-0.42	-1.09	9.55	0.24	0.75
N	0	2.3	2.19	20.12	2.72	4.09	12.71	3.27	0.48	12.12	2.45	1.94
S	0.65	3.51	2.46	9.51	2.47	4.97	5.86	0.8	0.84	6.64	4.18	2.45
Y	0.94	16.8	10.08	53.45	14.88	15.75	28.89	3.57	-0.78	15.78	6.04	1.41
T	3.94	3.27	1.07	15.2	1.5	5.83	12.78	0	0	10.28	3.67	2.19
I	4.01	6.39	-0.11	25.46	6.44	6.96	10.34	1.58	-0.67	9	1.76	2.88
W	1.04	**36.74**	**15.15**	**63.34**	**29.62**	19.03	47.4	5.3	-0.52	23.95	**10.81**	1.32
P	**13.73**	6.19	2.13	14.6	0.11	0	9.46	7.72	4.22	11.39	6.04	**10.22**
V	4.13	4.28	0.06	17.44	2.8	6.41	8.44	1.45	-0.44	7.65	2.22	1.81
H	1.07	23.7	7.86	57.97	13.63	**22.31**	**67.57**	**62.7**	**39.81**	**47.5**	4.65	2

Table 13: Table showing the change in energy values that is calculated using FoldX, upon mutation of the interfacial residues in the BMP-2_Gremlin-1 complex.

Essential residue	Significant mutation	Factors destabilizing the complex	Change in energy (kcal/mol)
ASNB29	PRO	GLYB27: Steric association with PROB29	13.73
LEUB55	TRP	TRPC28: Steric association with TRPB55	15.15
ASPB93	TRP	Disruption of hydrogen bond interaction with ASNB95, TYRB91. Disruption of salt bridges with LYSL174 and LYSB101	36.74
GLYC27	TRP	THRG150 and VALC26: Steric association with TRPC27	**63.34**
PROC50	HIS	LEUC51: Steric association with HISC50	22.31
GLUC94	TRP	SERG110: Steric association with TRPC94	29.62
CYSG108	HIS	ASNG157, GLUC94: Steric association with HISG108	**67.57**
THRG150	HIS	GLYC27, VALC26: Steric association with HISG150	**62.7**
THRG155	HIS	TRPC31, TYRC103: Steric association with HISG155	39.81
CYSL108	HIS	ASNL157, LEUL156: Steric association with HISL108	**47.5**
LEUL156	TRP	LYSL168: Steric association with TRPL156	10.81
LYSL174	PRO	Disruption of hydrogen bond interaction with LYSL148 and PHEL149. Disruption of salt bridges with ASPB93 and GLUB94	10.22

Table 14: Table listing out the destabilizing factors upon mutation of interfacial residues in the BMP-2_Gremlin-1 complex.

It can be observed from Table 13 and Table 14 that GLYC27, CYSG108, THRG150, and CYSL108 are essential for the BMP-2_Gremlin-1 complex. Further investigations into the mutation study suggest that the destabilization of the BMP-2_Gremlin-1 complex is mostly mediated by steric interactions. This would suggest that maximum destabilization is caused by steric hindrance, which in turn might be caused by the presence of a bulky amino acid residue(s) in the immediate neighborhood where the mutation has taken place.

BMP-7_Gremlin-1

Similarly, we have tried to infer amino acid residues significantly crucial for the complexation between BMP-7 and Gremlin-1. This is graphically depicted in Fig. 18.

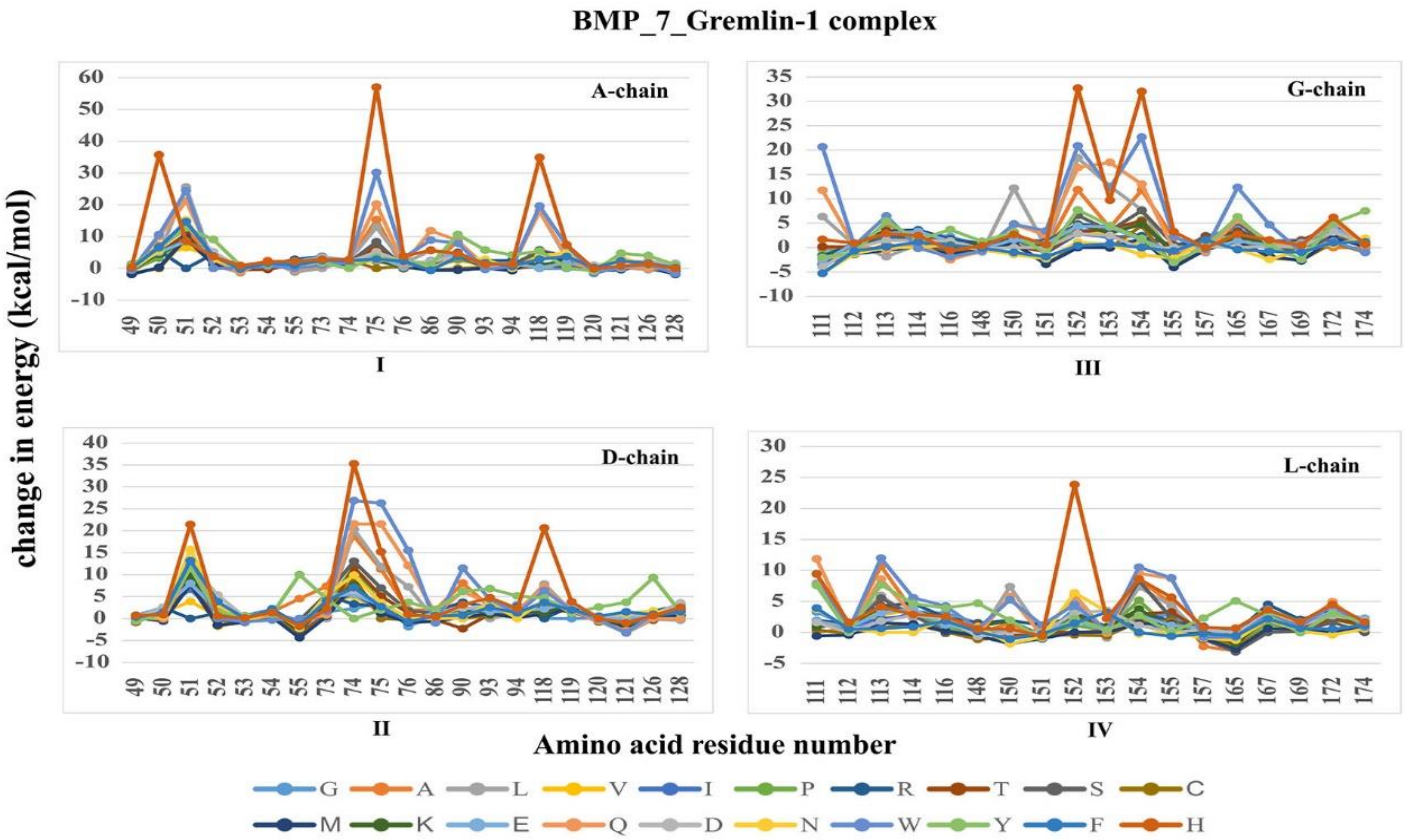

Fig.18: Plot depicting the effects of mutations in BMP-7_Gremlin-1 complex.

Essential residue	Significant mutation	Factor destabilizing the complex	Change in energy (kcal/mol)
LEUA50	HIS	LEUB90,TRPA52: Steric association with HISA50	**35.719**
GLYA51	PHE	META153: Steric association with PHEA51	25.606
LEUA75	HIS	CYSA138, CYSA71, ALAA72: Steric association with HISA75	**56.987**
ASPA118	HIS	ASPA119, TYRA116: Steric association with HISA118	34.82
GLYD51	HIS	LEUD50, THRG150: Steric association with HISD51	21.41
PROD74	HIS	ARGL172, ILEL114: Steric association with HISD74	**35.267**
LEUD75	HIS	ALAD81: Steric association with HISD75	26.299
ASPD118	HIS	ASPD119, TYRD116: Steric association with HISD118	20.61
ARGG111	TRP	TYRD128: Steric association with TRPG111 Disruption of Hydrogen bonds with THRG155, ASPD118, and PHED117. Disruption of electrostatic bond with ASPD119.	20.648
METG152	HIS	VALG154, ARGG111: Steric association with HISG152	**32.685**
VALG154	HIS	TRPD55: Steric association with HISG154	31.994
ARGL111	TYR	THRL115: Steric association with TYRL111. Disruption of Hydrogen bonds with THRL155, THRL112. Disruption of electrostatic bond with PHED93	11.853
ILEL113	HIS	VALL70: Steric association with HISL113	11.986
METL152	HIS	TRPA52: Steric association with HISL152	23.834

Table 15: Table listing out the destabilizing factors upon mutation of interfacial residues in the BMP-7_Gremlin-1 complex.

We observed from Table 15, that LEUA50, LEUA75, ASPA118, and PROD74 are significantly crucial for the stability of the complex between BMP-7 and gremlin-1. Detailed investigations suggest that destabilization in the complex structure of BMP-7_Gremlin-1 is mediated significantly by steric interactions. In other words it means that the maximum destabilization is caused by steric hindrance, which in turn might be caused by the presence of a bulky amino acid residue(s) in the immediate neighborhood where the mutation has taken place.

	A	A	A	A	D	D	D	D	G	G	G	L	L	L
Mutation	50	51	75	118	51	74	75	118	111	152	154	111	113	152
D	5.07	8.777	3.686	0	7.985	2.219	3.777	0	-0.32	3.648	4.861	3.29	1.411	3.772
R	7.212	12.165	15.306	4.618	11.061	18.772	11.26	1.649	0	11.833	11.78	0	10.69	2.847
F	4.303	25.606	12.919	18.003	12.835	20.305	11.846	7.826	6.325	18.407	7.735	7.945	5.957	5.711
A	4.057	6.537	2.148	0.15	3.855	5.033	1.498	1.142	-3.481	3.037	0.235	1.785	2.84	1.917
C	3.75	8.426	2.351	0.21	6.674	5.668	1.83	1.982	-3.942	2.823	2.45	1.304	2.224	1.77
Q	3.218	8.725	5.899	5.155	8.547	11.925	3.072	2.916	-1.475	4.6	5.669	1.5	3.843	1.116
G	5.527	0	3.506	1.019	0	3.307	2.787	-0.008	-1.778	4.782	2.213	1.891	4.292	2.377
E	4.817	10.778	6.884	0.801	7.724	11.647	5.124	2.505	0.2	3.114	5.438	1.712	4.231	-0.034
K	4.907	8.97	8.348	5.767	10.527	13.023	6.925	1.255	-3.768	6.588	7.574	1.353	5.505	2.872
L	0	9.285	0	4.572	7.743	9.289	0	3.483	-3.399	0.468	4.533	0.433	0.747	-0.401
M	0.289	9.727	2.649	3.652	7.843	7.612	1.159	1.011	-3.189	0	1.823	-0.582	1.509	0
N	4.461	8.808	2.957	1.03	9.679	7.681	2.386	1.072	-2.169	4.777	4.769	0.831	3.844	3.098
S	5.103	8.506	3.909	0.228	7.99	5.519	3.033	2.191	-2.996	4.409	1.532	1.842	3.156	1.824
Y	9.88	21.177	20.161	17.996	11.82	21.551	21.508	7.283	11.738	16.389	12.992	11.853	8.587	6.126
T	6.605	13.41	5.191	3.246	12.269	6.316	3.621	4.087	-4.024	2.85	-0.182	1.59	1.812	3.071
I	5.484	15.208	2.608	3.958	15.712	9.858	3.613	4.169	-5.274	1.133	-1.474	3.726	0	6.358
W	10.556	24.464	30.125	19.577	12.289	26.871	26.299	6.351	20.648	20.842	22.632	9.477	11.986	4.505
P	6.286	12.737	3.656	5.462	11.557	0	1.925	4.636	-2.022	7.707	1.847	7.586	7.675	2.237
V	6.617	14.662	2.881	2.878	13.178	7.052	2.686	3.652	-5.306	0.375	0	3.92	0.631	1.496
H	35.719	8.601	56.987	34.82	21.41	35.267	15.197	20.61	1.674	32.685	31.994	9.415	4.116	23.834

Table 16. Table showing the change in energy values that is calculated using FoldX, upon mutation of the interfacial residues in the BMP-7_Gremlin-1 complex.

3.4. Discussion

After a detailed study on the interactive nature of the BMPs with their antagonists, we were able to identify interfacial residues which could cause maximum destabilization in the protein-protein complex interactions upon mutations. These residues can be classified as hot spot residues and be used to investigate small molecule protein-protein interaction modulators (PPIMs), through pharmacological modeling and virtual screening, which can be used to destabilize these complex protein-protein interactions.

We have found in the BMP-2_Noggin complex that interfacial residues namely PROB50, SERB57, SERH38 in the receptor-binding site I and VALC33, SERC88 in the receptor-binding site II are very crucial for the structural stability of the complex. In BMP-7_Noggin, we found interfacial residues VALA123, ALAD81, PROH35 in the receptor-binding site I, and PROG35 essential for maintaining the stability of the complex. In BMP-2_gremlin-1, we observed that interfacial residues GLYC27, CYSG108, THRG150, and CYSL108 are crucial for its stability. In BMP-7_Gremlin-1, we found that amino acid residues LEU50 (A chain), LEU75 (A chain), PRO74 (D chain), and MET152 (G chain) on the interface were significant for maintaining its stability. These amino acid residues if point-mutated, will be able to destabilize the complex structures as seen before. Besides this, we have found that Gremlin-1-complex destabilization factors upon mutation, are directed by steric hindrance solely which is unlikely in the case of Noggin-complexes. Noggin, upon mutation follows destabilization which is associated with the breakdown of various interactions such as hydrogen bonds, salt bridges, etc.

Our study also revealed that the energy change upon mutation across the binding sites is different from one another. From this observation, it can be suggested that a hierarchical binding of antagonists can exist across the binding sites of the BMPs. We further compared the energy change upon mutations at each receptor-binding site, of all the interfacial residues, for these complexes (Fig. 19).

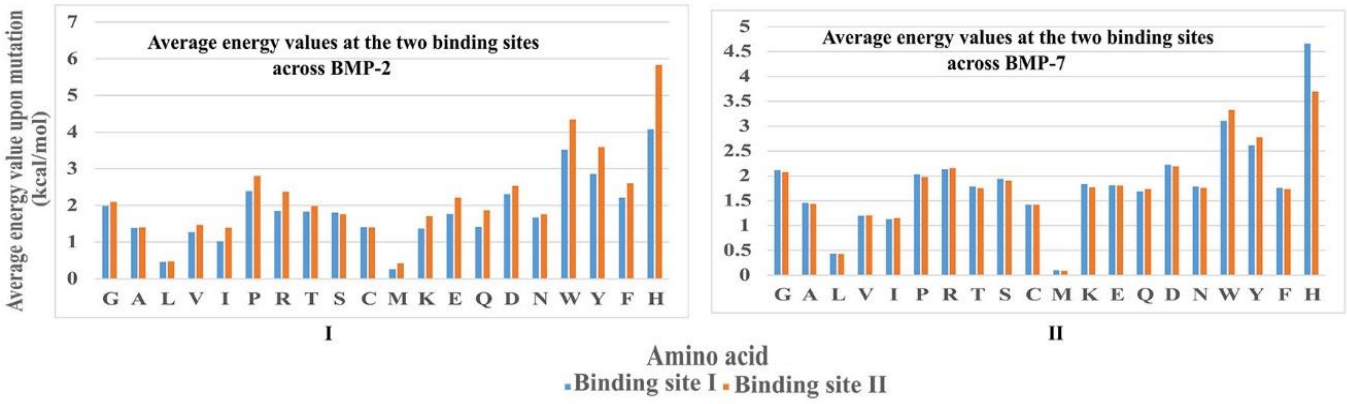

Fig 19: Average of change in energy (for all the mutations) across the two receptor-binding sites.

From the energy plot in Fig.19 and Fig. 20, we could observe a distinct trend of hierarchical binding in the case of BMP-2_Noggin, BMP-2_Gremlin-1, and BMP-7_Gremlin-1 complexes. Although, the same trend was not clearly distinct in the case of BMP-7_Noggin complex. In the case of BMP-2_Noggin, preferential binding across receptor-binding site II over the receptor-binding site I could be observed.

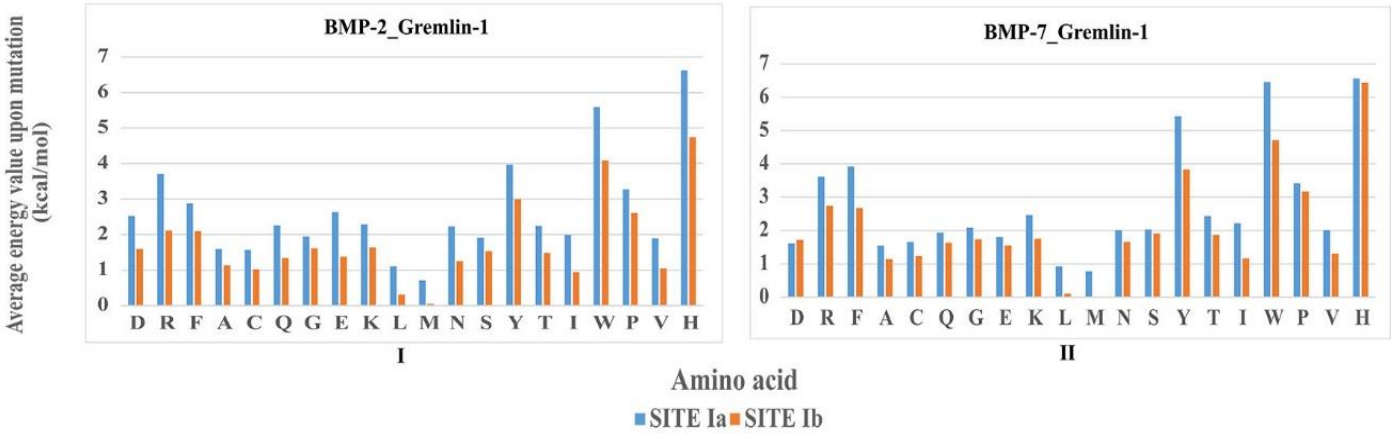

Fig. 20: Average of change in energy (for all the mutations) across both the type-I receptor-binding sites (Site Ia and Site Ib, “a’ and “b” are used to distinguish the two type-I receptor binding sites of BMPs, across which Gremlin-1 binds).

Based on our understanding of the interaction between both the BMPs and Gremlin-1, if the BMPs and Gremlin-1 were to form a closely bound oligomeric structure, the simplest model would be a structure with a consecutive cis-trans configuration as depicted in Fig. 21. This would consider the hierarchical pattern of binding that exists in these interactions as we have observed earlier and would further indicate that both the antiparallel conformer of Gremlin-1 binding across BMPs and the parallel conformer might exist simultaneously for a cis-trans configuration to exist. The vertices in Fig.21 represent a differential binding environment while alternate edges can be representative of either BMP or Gremlin-1

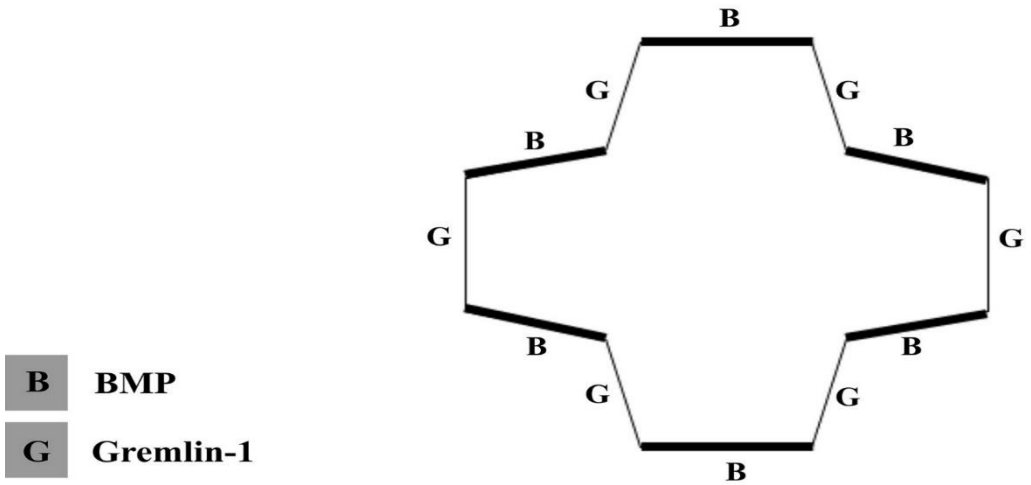

Fig. 21: A model in which Gremlin-1 can bind across BMPs and form a closed ended structure.

.

3.5. Reference

1. K. Lavery, et al., J. Biol. Chem. 283 (30) (2008) 20948.
2. M. Kawabata, T. Imamura, K. Miyazono, Cytokine Growth Factor Rev. 9 (1) (1998) 49.
3. Massague J, Chen YG. Controlling TGF-b signaling. Genes Dev 2000; 14(6):627–44.
4. Canalis E, Economides AN, Gazzerro E. Bone morphogenetic proteins, their antagonists, and the skeleton. Endocr Rev 2003; 24(2):218–35.
5. Reddi AH. Interplay between bone morphogenetic proteins and cognate binding proteins in bone and cartilage development: noggin, chordin and DAN. Arthritis Res 2001; 3(1):1–5.
6. Avsian-Kretchmer O, Hsueh AJ. Comparative genomic analysis of the eight-membered ring cystine-knot-containing bone morphogenetic protein antagonists. Mol Endocrinol 2004; 18(1):1–12.
7. Avsian-Kretchmer, O., and Hsueh, A.J. (2004). Comparative genomic analysis of the eight-membered ring cystine knot-containing bone morphogenetic protein antagonists. Mol. Endocrinol. 18, 1–12.
8. Rosen, V. (2006). BMP and BMP inhibitors in bone. Ann. N Y Acad. Sci. 1068, 19–25.
9. Hsu DR, Economides AN, Wang X, Eimon PM, Harland RM. The Xenopus dorsalizing factor Gremlin identifies a novel family of secreted proteins that antagonize BMP activities. Mol Cell 1998; 1(5):673–83.
10. Pearce JJ, Penny G, Rossant J. A mouse Cerberus/Dan-related gene family. Dev Biol 1999; 209(1):98–110.
11. Topol LZ, Marx M, Laugier D, Bogdanova NN, Boubnov NV, Clausen PA, *et al.* Identification of drm, a novel gene whose expression is suppressed in transformed cells and which can inhibit growth of normal but not transformed cells in culture. Mol Cell Biol 1997; 17(8):4801–10.
12. Oelgeschlager M, Larrain J, Geissert D, De Robertis EM. The evolutionarily conserved BMP-binding protein twisted gastrulation promotes BMP signaling. Nature 2000; 405(6788):757–63.
13. Ross JJ, Shimmi O, Vilmos P, Petryk A, Kim H, Gaudenz K, *et al.* Twisted gastrulation is a conserved extracellular BMP antagonist. Nature 2001; 410(6827):479–83.

14. Scott IC, Blitz IL, Pappano WN, Maas SA, Cho KW, Greenspan DS. Homologues of Twisted gastrulation are extracellular cofactors in antagonism of BMP signaling. Nature 2001; 410(6827): 475–8.
15. Chang C, Holtzman DA, Chau S, Chickering T,Woolf EA, Holmgren LM, *et al.* Twisted gastrulation can function as a BMP antagonist. Nature 2001; 410(6827):483–7.
16. Dionne MS, Brunet LJ, Eimon PM, Harland RM. Noggin is required for correct guidance of dorsal root ganglion axons. Dev Biol 2002; 251(2):283–93.
17. Groppe J, Greenwald J, Wiater E, Rodriguez-Leon J, Economides AN, Kwiatkowski W, *et al.* Structural basis of BMP signaling inhibition by the cystine-knot protein Noggin. Nature 2002; 420(6916):636–42.
18. Warren SM, Brunet LJ, Harland RM, Economides AN, Longaker MT. The BMP antagonist noggin regulates cranial suture fusion. Nature 2003; 422(6932):625–9.
19. Minabe-Saegusa C, Saegusa H, Tsukahara M, Noguchi S. Sequence and expression of a novel mouse gene PRDC (protein related to DAN and Cerberus) identified by a gene trap approach. Dev Growth Differ 1998; 40(3):343–53.
20. Topol LZ, Modi WS, Koochekpour S, Blair DG. DRM/GREMLIN (CKTSF1B1) maps to human chromosome 15 and is highly expressed in adult and fetal brain. Cytogenet Cell Genet 2000; 89(1–2):79–84.
21. Topol LZ, Bardot B, Zhang Q, Resau J, Huillard E, Marx M, *et al.* Biosynthesis, post-translation modification, and functional characterization of Drm/Gremlin. J Biol Chem 2000; 275(12):8785–93.
22. Bell E, Munoz-Sanjuan I, Altmann CR, Vonica A, Brivanlou AH. Cell fate specification and competence by Coco, a maternal BMP TGF-b and Wnt inhibitor. Development 2003; 130(7):1381–9.
23. Ozaki T, Sakiyama S. Molecular cloning and characterization of a cDNA showing negative regulation in v-src-transformed 3Y1 rat fibroblasts. Proc Natl Acad Sci USA 1993; 90(7):2593–7.
24. Ozaki T, Sakiyama S. Tumor-suppressive activity of N03 gene product in v-src-transformed rat 3Y1 fibroblasts. Cancer Res1994; 54(3):646–8.

25. Riikka Laurila, Seppo Parkkila, Jorma Isola, Anne Kallioniemi, Emma-Leena Alarmo. The expression patterns of gremlin 1 and noggin in normal adult and tumor tissues. Int J Clin Exp Pathol 2013; 6(7):1400-1408.
26. Derynck, R., Zhang, Y.E. *Nature.* 2003, 425(6958), 577-584.
27. Yan, K., Wu, Q., H, D., Yan, Lee, C.H., Rahim, N., Tritschler, I., Vecchio, J.D., F,M., Kalady, B, A., Hjelmeland, and Rich, J.N. *GENES & DEVELOPMENT.* 2014, 28, 1085–1100.
28. Rider, C.C. and Mulloy, B., *Biochem. J.* 2010, 429, 1–12.
29. Hsu, M.Y., Rovinsky, S.A., Lai, C.Y., Qasem, S., Liu, X., How, J., Engelhardt, J.F., Murphy, G.F. *Lab Invest.* 2008, 88(8), 842-55.
30. Secondini, C., Wetterwald, A., Schwaninger, R., Thalmann, G.N., Cecchini, M.G. *PLoS One.* 2011, 6(1), e16078.
31. Kenneth Yan, Qiulian Wu, Diana H. Yan, Christine H. Lee, Nasiha Rahim, Isabel Tritschler, Jennifer DeVecchio, Matthew F. Kalady, Anita B. Hjelmeland, and Jeremy N. Rich. Glioma cancer stem cells secrete Gremlin1 to promote their maintenance within the tumor hierarchy
32. Groppe, J., Greenwal, J., Wiater, E., Rodriguez-Leon, J., Economides, A.N., Kwiatkowski, W., Affolter, M., Vale, W.W., Izpisua Belmonte, J.C., Choe, S. *NATURE.* 2002, 420, 636-642.
33. Miglė Kišonaitė, Xuelu Wang, et al., Structure of Gremlin-1 and analysis of its interaction with BMP-2, Biochem J. 473(11) (2016) 1593–1604
34. Vajda S, Yueh C, Beglov D, Bohnuud T, Mottarella SE, Xia B, Hall DR, Kozakov D. New additions to the ClusPro server motivated by CAPRI. *Proteins: Structure, Function, and Bioinformatics.* 2017 Mar; 85(3):435-444.
35. Kozakov D, Hall DR, Xia B, Porter KA, Padhorny D, Yueh C, Beglov D, Vajda S. The ClusPro web server for protein-protein docking. *Nature Protocols.* 12(2) (2017):255-278
36. Kozakov D, Beglov D, Bohnuud T, Mottarella S, Xia B, Hall DR, Vajda, S. How good is automated protein docking? *Proteins: Structure, Function, and Bioinformatics.* 2013 Dec; 81(12):2159-66.
37. Krissinel E., Henrick K., 2005. Detection of Protein Assemblies in Crystals. In: R. Berthold M., Glen

38. E. Krissinel and K. Henrick, 2007. Inference of macromolecular assemblies from crystalline state. J. Mol. Biol. 372, 774--797.

R.C., Diederichs K., Kohlbacher O., Fischer I. (eds) Computational Life Sciences. CompLife 2005. Lecture Notes in Computer Science, vol 3695. Springer, Berlin, Heidelberg.

39. E. Krissinel, 2010. Crystal contacts as nature's docking solutions. J Comput Chem. 31(1), 133-43.
40. Hildebrand, P.W. et al., 2009. SuperLooper--a prediction server for the modeling of loops in globular and membrane proteins. Nucleic Acids Res. 37 W571—4.
41. Ismer J, Rose AS et al., 2016. SL2: an interactive web tool for modeling of missing segments in proteins Nucleic Acids Res. 44(W1), W390-4.
42. A. Fiser, R.K.G. Do, A. Sali, 2000. Modeling of loops in protein structures. Prot Sci. 9, 1753-1773.
43. Fiser, A. and Sali, A., 2003. ModLoop: automated modeling of loops in protein structures. Bioinformatics. 19, 2500—2501.
44. Joost Schymkowitz, Jesper Borg et al., 2005. The FoldX web server: an online force field Nucleic Acids Research, Web Server issue. Vol. 33, W382–W388.
45. De Caestecker, M. *Cytokine Growth Factor Rev.* 2004, 15(1), 1–11.
46. Rachel H. Church, Arjun Krishnakumar et al., Gremlin1 preferentially binds to bone morphogenetic protein-2 (BMP-2) and BMP-4 over BMP-7 Biochem. J. 466 (2015) 55–68.
47. The PyMOL Molecular Graphics System, Version 1.1r1, Schrödinger, LLC.
48. *Dassault Systèmes BIOVIA, Discovery Studio Modeling Environment, Release 2017, San Diego: Dassault Systèmes, 2016.*

Chapter 4
Structural and in vitro investigations into the protein-protein complex interaction between BMP heterodimer (BMP-2/7) and antagonists (Noggin, Gremlin-1)

4.1. Introduction

BMPs or Body Morphogenetic proteins, as mentioned in the previous chapters, are a part of the TGF-β superfamily of signaling proteins (1-6). Studies have found that BMPs can exist as both homodimers as well as heterodimers (7), but less is known about these heterodimers and their interactions with the BMP antagonists. Few studies have been reported on BMP-2/7 heterodimer and its interaction with Noggin. In a study, led by Buijs *et al.* in 2012, it was observed that the BMP activity upon co-incubation of BMP-2/7 heterodimer, along with Noggin, was inhibited by only 30%, while the BMP activity was inhibited by 96% in the case of BMP-2 homodimer and by 69% in the case of BMP-7 homodimer (8). In another study, it was observed that the stimulation of the BMP-2/7 heterodimer has resulted in a significant decrease in the expression levels of Noggin, compared to when either BMP-2 or BMP-7 homodimers had been activated together (9). It was also reported in another study that, BMP-2 when co-expressed with BMP-7 exhibited 20-fold higher activity as compared with either of the BMP homodimers (*in vitro* ALP induction assay) (10). Thus, it is evident that BMP-2/7 heterodimer is weakly antagonized by Noggin as compared to the BMP homodimers. But it is not known if BMP-2/7 is weakly antagonized by Gremlin-1 as well. Gremlin-1, like Noggin, is known to regulate the BMP signaling pathway by binding to BMP homodimers and inhibiting the BMP cycle, thereby inhibiting cell differentiation and maintaining tumor hierarchy (11-16). But unlike Noggin, Gremlin-1 plays a much more crucial role as a major and dominant driving force in maintaining glioblastoma proliferation and hierarchies (17). Thus in this study, we investigate the protein-protein interaction between the BMP-2/7 heterodimer and Gremlin-1. We simultaneously observe the structural interactions between the heterodimer and Noggin proteins and compare both these interactions with the interaction between homodimers and the antagonists.

4.2. Materials and methods

4.2.1. Modeling BMP-2/7 heterodimer complex structure

We used InterEvDock2 for modeling the BMP-2/7 heterodimer complex structure (18-22). We initially tried modeling with ClusPro 2.0, but we were unable to locate the disulfide bond between each chain of the heterodimers, which is crucial for the stability of the complex. InterEvdock2

integrates evolutionary information with a residue-based multi-body statistical potential in the docking process and give us a much precise result. We uploaded the A-chain of BMP-7 with PDB ID 2QJ9 and the B-chain of BMP-2 with PDB ID 1M4U in the InterEvDock2 web-server. We obtained around 150 models. We have optimized all these structures and considered the one which had the least free energy value following optimization.

4.2.2. Modeling BMP-2/7_Noggin and BMP-2/7_Gremlin—1 complex structure

We used InterEvDock2 to model the complex protein structure between BMP-2/7 heterodimer and Noggin. For BMP-2/7_Gremlin-1, we used both InterEvDock2 as well as ClusPro 2.0. Docking gave us approximately 150 models, of which the structure with the least free energy following optimization was considered for further analysis.

4.2.3. Neurospheres formation assay and the effect of BMP-2/7 heterodimer on the neurospheres

We wanted to investigate if the introduction of the BMP-2/7 heterodimer in the human glioblastoma cells was able to induce an active BMP signaling pathway. The idea was to understand the extent of antagonizing effect, the antagonists (Noggin and Gremlin-1) have on BMP-2/7 heterodimer in context to the BMP signaling pathway. For our study, we have considered the SK-N-SH cell line. The SK-N-SH human glioblastoma cell line was used to generate and culture neurospheres (NSs) as mentioned in one of the previous studies (23). The cells were de-differentiated under EGF and BFGF-supplemented NSs formation media for 5 weeks. After 5 weeks, the neurospheres were treated with commercially procured BMP-2/7 heterodimer and its effect was recorded.

4.3. Results

4.3.1. BMP-2/7 heterodimer complex model

InterEvDock2 web-server gave us around 150 docked structures for the BMP-2/7 heterodimer. The structure having the minimum energy value following optimization was taken for further analysis. In Table 1, the top three least energy structures has been highlighted.

Models	Energy value post-optimization (kcal/mol)
Model_X	163.477
Model_Y	182.342
Model_Z	221.732

Table 1: Table showing the energy values of the topmost least energy structures.

Once we optimized the structure, we looked into the intricate details within the structure. We observed that both BMP-2 and BMP-7 form a 12-membered cysteine knot which is connected by a disulfide bond. The disulfide bond is observed between the seventh cysteine present in either of the chains, which are CYS103 in the A chain (BMP-7) and CYS78 in the B chain (BMP-2) (Fig. 1).

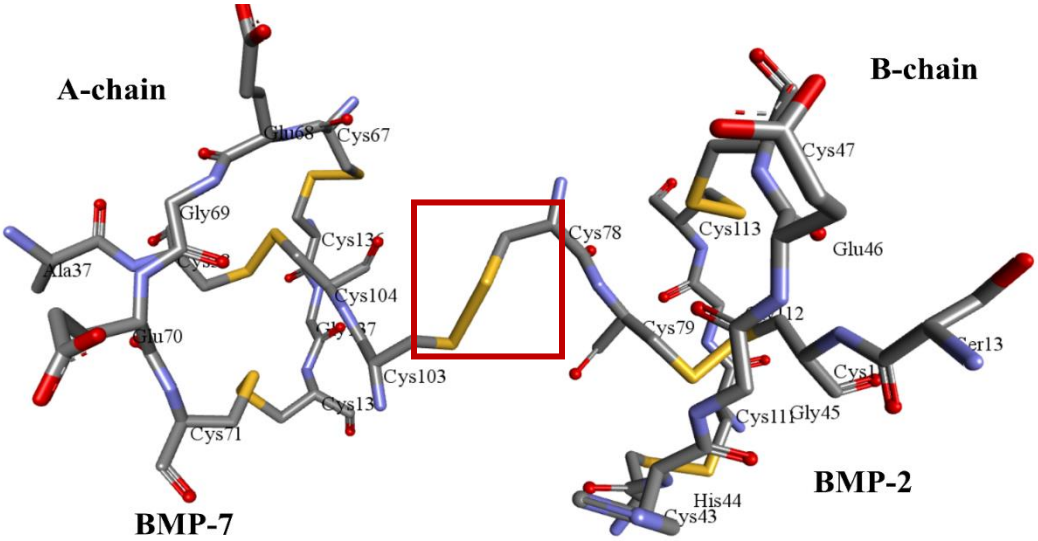

Fig 1. Image depicting how the cysteine knots in both BMP-2 and BMP-7 connected by a disulfide bond between CYS103 and CYS78. The disulfide bond is represented by a yellow color in the image. The nitrogen atoms are represented by blue color while red color is used to denote both the hydrogen atoms as well and the oxygen atoms. The disulfide bond stabilizes the heterodimer.

4.3.2. BMP-2/7_Noggin complex model

We obtained 150 docked structures from InterEvDock2. The optimization of structural energy was carried out by FoldX and the complex with the least energy value was considered, for further analysis. We have listed out the topmost three least energy structures in Table 2.

Models	Energy value post-optimization (kcal/mol)
Model_X	662.897
Model_Y	720.159
Model_Z	828.162

Table 2: Table showing the three topmost least energy structures.

The interface of the complex indicates that the interfacial residues ranging from M27 to N40 in the Noggin are engaged in binding with the interfacial residues ranging from R48 to E60 and S-113 to Y128 in the A chain (finger 1 and finger 2 region) of the heterodimer (Table 3, Fig. 2). This indicates that the binding between the BMP-7 monomeric subunit of the heterodimer and the Noggin, occurs at the receptor binding site I. This is contrary to the fact that BMP-7 prefers binding at the receptor binding site II (7). We observe a similar trend where the BMP-2 monomeric subunit of the heterodimer binds at the receptor binding site II instead of the receptor binding site I. This might be the reason why this heterodimer_Noggin complex has higher free energy post-optimization when compared to homodimer_Noggin (BMP-2_Noggin: 336.532 kcal/mol, BMP-7_Noggin: 592.438 kcal/mol), indicating weaker antagonization of the heterodimer by Noggin, compared to the homodimer.

BMP-2/7_Noggin interface (Receptor binding site-I)

CHAINS	INTERFACIAL RESIDUES
A	**R48,** W52, D54, W55, I57, A58, **E60**, **S113**, L115, Y116, F117, D118, D119, S120, S121, N122, V123, I124, L125, K126, **Y128**
B	F49, P50, L51, A52, D53, H54, S57, N59, I62, L66
G	**M27**, Q28, H29, Y30, L31, H32, I33, R34, P35, A36, P37, S38, **N40**, F168, H199, R204, R206, Q208, R210, I218, P219, I220, Q221, Y222, P223

BMP-2/7_Noggin interface (Receptor binding site-II)

CHAINS	INTERFACIAL RESIDUES
A	S77, N83
B	**N29,** D30, W31, V33, A34, P35, **P36**, **S88**, L90, Y91, L92, D93, E94, E96, K97,V98, L100, K101, N102, Y103, **Q104**
H	**L43,** V44, D45, L46, I47, E48, H49, **F53**, F168, H199, R204, R206, Q208, R210, I218, P219, I220, Q221, Y222, P223

Table 3: The interfacial residues at both the receptor binding sites in the BMP-2/7_Noggin complex

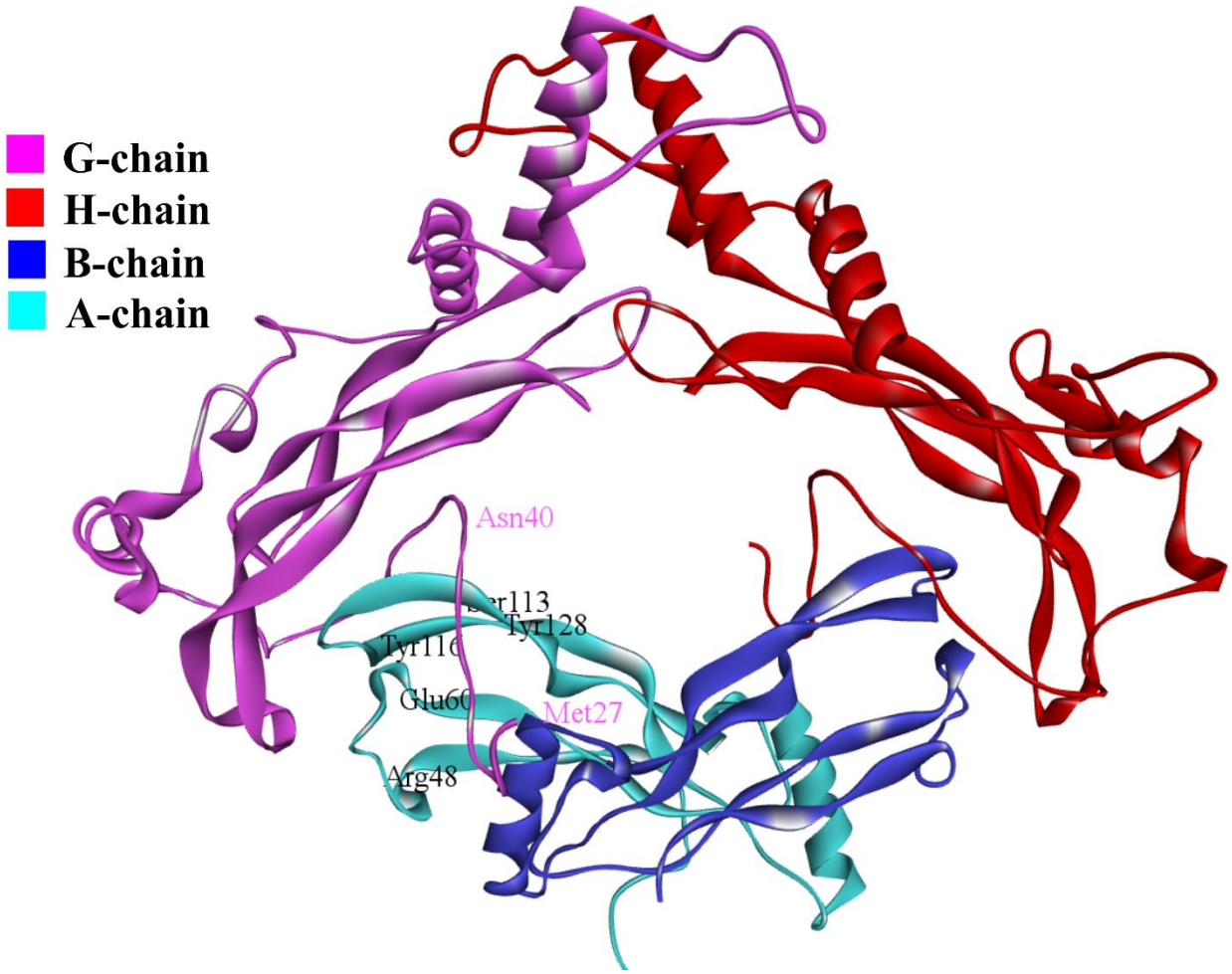

Fig. 2: Image showing the interactions between the A chain (BMP-7 monomeric subunit of the heterodimer) and the G chain (Noggin).

4.3.3. BMP-2/7_gremlin-1 complex model

We initially used InterEvDock2 for modeling the complex structure, but the structures we obtained as outputs were highly asymmetric. We then performed blind docking using ClusPro 2.0 to investigate if we still got asymmetric structures. The outputs obtained from ClusPro 2.0 were highly symmetrical. We also observed the two distinctive conformers similar to the one found in the case of the homodimers: parallel and anti-parallel binding. We have listed out the topmost three least energy structures, in each category of the conformers, in Table 4.

Models	Energy value post-optimization (Parallel) (kcal/mol)
Model_X	510.714
Model_Y	511.127
Model_Z	512.959

A

Models	Energy value post-optimization (anti-parallel) (kcal/mol)
Model_X	499.12
Model_Y	501.214
Model_Z	508.728

B

Table 4: (A) Energy values of the topmost three least energy structures in case of parallel binding conformer. (B) Energy value of the topmost three least energy structures, in case of anti-parallel binding conformer.

The least energy value in the case of both the conformers seems to be higher than the least energy value of the modelled BMP-2(homodimer)_Gremlin-1 complex and the modelled BMP-7(homodimer)_Gremlin-1 complex (BMP-2_Gremlin-1: 365.401 kcal/mol, BMP-7_Gremlin-1: 386.06 kcal/mol).

When we looked into the structures further, we observed that in the case of both the conformers, the BMP-7 monomeric subunit of the heterodimer and the BMP-7 monomeric subunit of the heterodimer binds to Gremlin-1 at the receptor binding site I and the receptor binding site II (Fig.3). This is the same trend in the binding that we also observed in the case of the BMP-2/7_Noggin complex structure. We can therefore suggest that the weak antagonism by Noggin and Gremlin-1, could be because of binding at the less preferable binding sites of the BMPs.

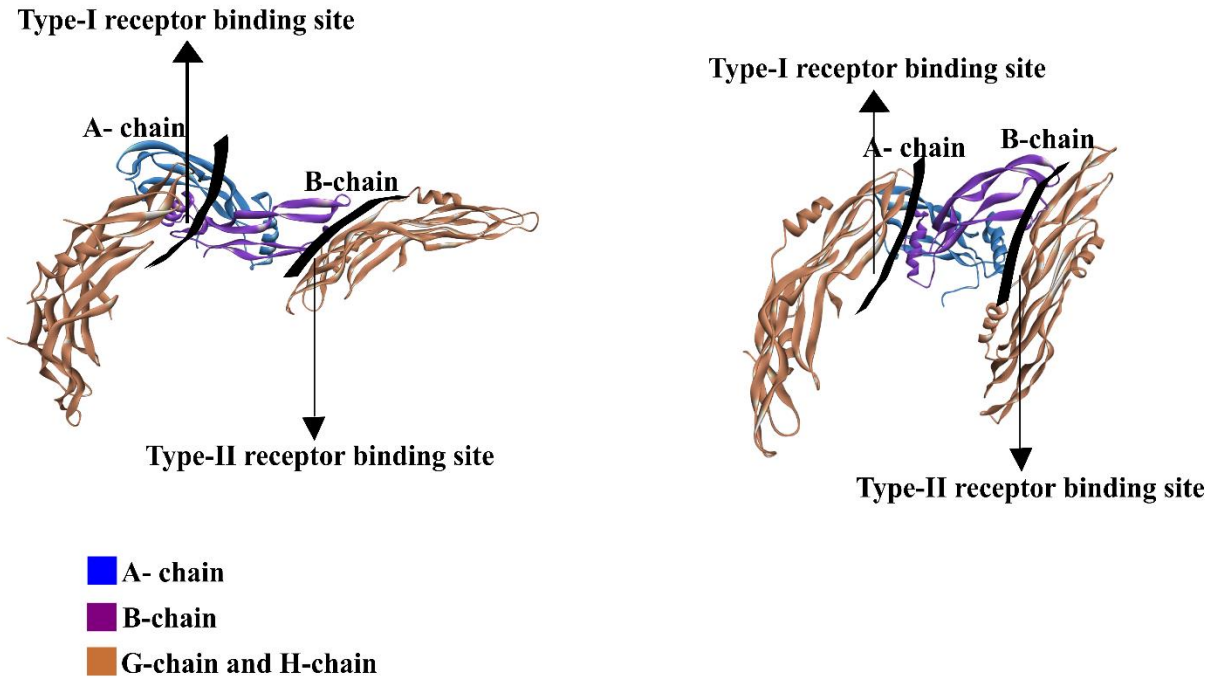

Fig. 3: The possible conformers of BMP-2/7 heterodimer and Gremlin binding after analysis of the ClusPro docking results. Structures represent both parallel binding and anti-parallel binding of the antagonist across the BMP-2/7 heterodimer.

4.3.4. Effect of BMP-2/7 heterodimer on neurospheres (NSs)

The high free energy value post-optimization for the heterodimer_antogonists complexes compared to the homodimer_antagonists complex indicate that the heterodimer is weakly antagonized by Gremlin-1 and Noggin, compared to the antagonism we observed in the case of the homodimers. This could suggest that if the BMP-2/7 heterodimer is to be introduced in the glioblastoma cells externally we might be able to re-initiate an active BMP cycle, which can promote differentiation and suppress the tumorigenic nature of the GICs (Glioblastoma Initiating Cells). After 5 weeks of de-differentiation of the SK-N-SH cells under EGF and BFGF-supplemented NSs formation media, approx. 30 ng/ml of BMP-2/7 heterodimer was injected to see its effect on the neurospheres. The area of the neurospheres was calculated using software called ImageJ. We observed a decrease of approx. 39.70% in the size of the neurospheres on the seventh day of the treatment (Fig. 4). We further went on to check the consequences, if we prolonged the treatment and observed a gradual decrease and after 14 days of treatment, we were able to visualize only cell clumps.

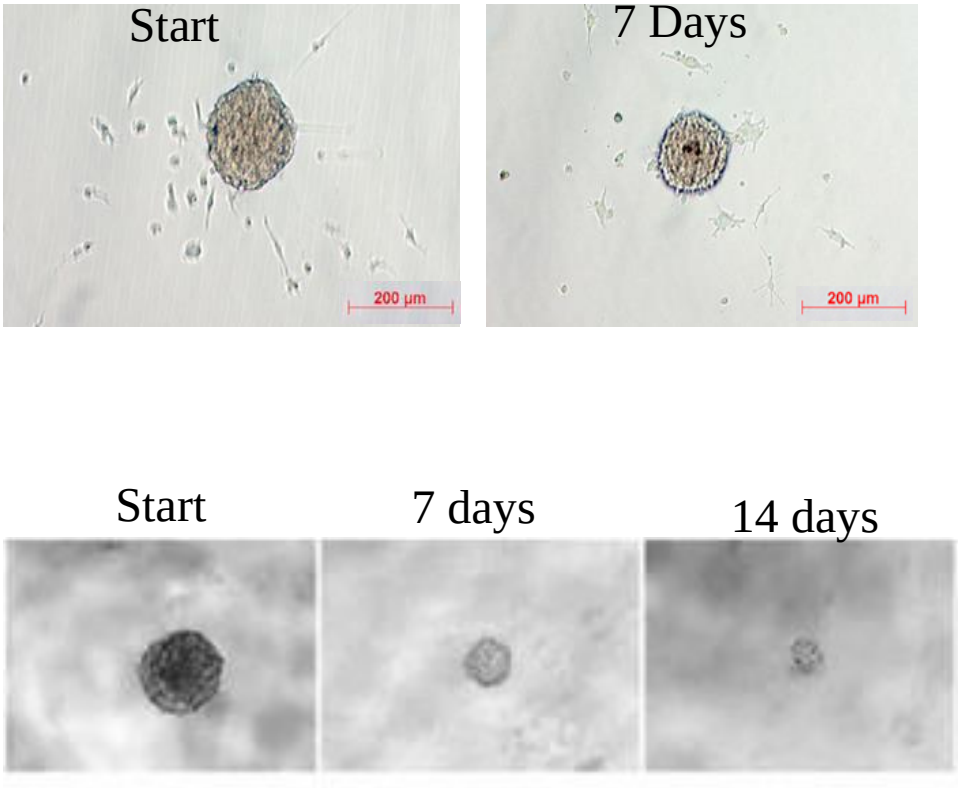

Fig 4. Image showing the disruption of neurospheres upon treatment with BMP-2/7 heterodimer.

4.4. Conclusion

In this study, we observed that the heterodimer_antoginists complexes have higher free energy value following optimization compared to the respective homodimer_antagonists complexes. These results indicate that the heterodimer is weakly antagonized by Gremlin-1 and Noggin as compared to the homodimers. While investigating the structures of the heterodimer_antagonists complexes, we observed that the BMP-7 monomeric subunit chain is interacting with the antagonists at the receptor binding site I. On the other hand, the BMP-2 monomeric subunit chain was found interacting with the antagonists at the receptor binding site II. This event is in contrary to the fact that BMP-7 preferentially binds at the receptor binding site II and BMP-2 prefers binding at the receptor binding site I. We also observed that in the case of Gremlin-1 binding across the heterodimer, both the receptor binding sites are being exhausted, which is not the same case when we compare with Gremlin-1 binding across either BMP-2 or BMP-7 homodimers. We also

tried to investigate the effect of the heterodimer on glioblastoma cells, after we observed that the heterodimer might be weakly antagonized. The treatment of BMP-2/7 heterodimer on glioblastoma neurospheres led to disruptive effect, thereby suggesting its use as a potential therapeutic strategy against glioblastoma.

Reference

1. K. Lavery, et al., J. Biol. Chem. 283 (30) (2008) 20948.
2. M. Kawabata, T. Imamura, K. Miyazono, Cytokine Growth Factor Rev. 9 (1) (1998) 49.
3. M.R. Urist, Science 150 (698) (1965) 893.
4. WagnerD.O. , et al., Sci. Signal. 3 (107) (2010) mr1.
5. A.H.Reddi, BMPs: from bone morphogenetic proteins to body morphogenetic proteins, Cytokine Growth Factor Rev.16 (2005) 249–250.
6. Javelaud D., Mauviel A, Mammalian transforming growth factor-*β*s: smad signaling and physio-pathological roles, *International Journal of Biochemistry and Cell Biology.* 36(7) (2004) 1161–1165.
7. De Caestecker, M. *Cytokine Growth Factor Rev.* **2004**, 15(1), 1–11.
8. Buijs JT, van der Horst G, van den Hoogen C *et.al* The BMP2/7 heterodimer inhibits the human breast cancer stem cell subpopulation and bone metastases formation, Oncogene. 2012, 2164-74.
9. Granjeiro JM, Oliveira RC, Bustos-Valenzuela JC *et.al* Bone morphogenetic proteins: from structure to clinical use, Braz J Med Biol Res. 2005, 1463-73.
10. Beatriz Gámez, Edgardo Rodriguez-Carballo and Francesc Ventura. BMP signaling in telencephalic neural cell specification and maturation**,** Front. Cell. Neurosci. 7 (2013) 87.
11. Derynck R, Zhang YE., 2003. Smad-dependent and Smad independent pathways in TGF-beta family signalling. Nature. 425(6958), 577-584.
12. Rider, C.C. and Mulloy, B., 2010. Bone morphogenetic protein and growth differentiation factor cytokine families and their protein antagonists. Biochem. J. 429, 1–12.
13. Walsh DW, Godson C, Brazil DP, Martin F., 2010. Extracellular BMP antagonist regulation in development and disease: tied up in knots. Trends Cell Biol. 20(5), 244-256.

14. Hsu MY, Rovinsky SA, Lai CY, Qasem S et al., 2008. Aggressive melanoma cells escape from BMP7-mediated autocrine growth inhibition through coordinated Noggin upregulation. Lab Invest. 88(8), 842-55.
15. Kenneth Yan, Qiulian Wu, Diana H. Yan et al., 2014. Glioma cancer stem cells secrete Gremlin1 to promote their maintenance within the tumor hierarchy. GENES & DEVELOPMENT. 28, 1085–1100.
16. Secondini C, Wetterwald A, Schwaninger R et al., 2011. The role of the BMP signaling antagonist noggin in the development of prostate cancer osteolytic bone metastasis. PLoS One. 6(1), e16078.
17. Kenneth Yan, Qiulian Wu *et al.* Glioma cancer stem cells secrete Gremlin1 to promote their maintenance within the tumor hierarchy 2014 Genes & development 28(10).
18. Quignot C, Rey J, Yu J, Tufféry P, Guerois R, Andreani J. InterEvDock2: an expanded server for protein docking using evolutionary and biological information from homology models and multimeric inputs. Nucleic Acids Res. 2018 Jul 2;46(W1):W408-16.
19. Yu J, Vavrusa M, Andreani J, Rey J, Tufféry P, Guerois R. InterEvDock: A docking server to predict the structure of protein-protein interactions using evolutionary information. Nucleic Acids Res. 2016 Jul 8;44(W1):W542-9.
20. Andreani J, Faure G, Guerois R. InterEvScore: a novel coarse-grained interface scoring function using a multi-body statistical potential coupled to evolution. Bioinformatics. 2013 29(14):1742-9.
21. Ramirez-Aportela E, Lopéz-Blanco JR, Chacon P. FRODOCK 2.0: fast protein-protein docking server. Bioinformatics. 2016;32(15):2386-8.
22. Dong GQ, Fan H, Schneidman-Duhovny D, Webb B, Sali A. Optimized atomic statistical potentials: assessment of protein interfaces and loops. Bioinformatics. 2013;29(24):3158-66.
23. Elaine Reguera-Nuñez , Carlota Roca ,et al., Implantable controlled release devices for BMP-7 delivery and suppression of glioblastoma initiating cells, Biomaterials 35 (2014) 2859e2867.

Chapter 5
Nanocapsule formulation studies based on structural investigations

5.1. Summary of first and second objectives

The study under our first objective allowed us to identify residues that are essential for the complex structure formation between BMP homodimers (BMP-2 and BMP-7) and the antagonists (Gremlin-1 and Noggin). These interfacial residues would facilitate us to design small-molecule modulators (inhibitors) known as protein-protein interaction modulators (PPIMs), which could essentially bind at the essential sites of the protein structures and inhibit the protein-protein interactions. This designing of small molecule PPIMs can be done through pharmacology modeling followed by high throughput virtual screening.

The study under our second objective suggested that BMP heterodimer (BMP-2/7) is weakly antagonized by Gremlin-1 and Noggin compared to their respective homodimers. This weak antagonism could mean that upon treatment of the glioblastoma cells with the heterodimer, we might be able to re-initiate an active BMP cycle, which would promote cell differentiation and suppress the tumorigenic nature of the glioblastoma initiating cells. We investigated the effect of treating glioblastoma neurospheres (NSs) with BMP-2/7 heterodimer in vitro and observed a gradual size reduction leading to disruption of the neurospheres. Thus for the study under our third and final objective, we would consider the use of BMP-2/7 heterodimer as a potential therapeutic strategy against glioblastoma. In that regard, we would like to propose the design of a nanocapsule that could encapsulate the BMP-2/7 heterodimer and deliver it at our desired location. The nanocapsule can be implanted upon surgical resection of the primary tumor. The advantage of using such an implantable device would be the fact that it does not need to cross the Blood-Brain Barrier (BBB).

5.2. Materials and methods

5.2.1. Nanocapsule formulation

We considered PLGA [poly(lactic-co-glycolic acid)] as a biodegradable carrier device for the encapsulation of the heterodimer BMP-2/7. For the encapsulation process, we followed the procedure described in a previous study undertaken to investigate the combination of Polyoxomer with PLGA in designing microspheres or nanoparticles capable of forming a controlled-release system (1, 2). Briefly, 2µg of rhBMP-2/7 heterodimer was initially dissolved in 300 µl of sterile

water and kept for thirty minutes at room temperature (RT). Then, we added 2.5 mg of Tetronic 701 into this solution and kept it at RT for thirty minutes which was later lyophilized. The resultant product was re-suspended in 400 mL of acetonitrile that contained 20 mg of PLGA. This constituted the organic phase which was then added to a 4mL solution of cottonseed oil containing 0.5% (w/v) of soybean lecithin. We sonicated the resultant suspension for twenty seconds twice and then it was stirred for 45 min. 2mL of petroleum ether was then added to harden immature particles and the suspension was stirred for 20 min in the extraction hood. Finally, the suspension was filtered under vacuum using nitrocellulose membrane and the protein-encapsulated particles were collected. These particles were then washed using petroleum ether, lyophilized, and stored at 4ºC until further use.

5.2.2. Characterization of the protein encapsulated device

Characterization of the encapsulated protein carrier device includes investigating the particle size, morphology, and size distribution of the particles formed upon encapsulation. Field Emission Scanning Electron Microscope (FESEM) (Carl Zeiss, Ultra 55, Oxford instrument) was used to investigate the particle size and morphology, while Dynamic Light Scattering (DLS) (Anton Paar, Litesizer 500) was done to characterize the size distribution of the PLGA-Protein encapsulated implantable device.

5.2.3. Characterization of heterodimer protein encapsulated in the biodegradable implant using Western Blot

The released samples were run on 12% SDS-PAGE (Sodium dodecyl sulphate-polyacrylamide gel electrophoresis) under non-reducing conditions. The same gel was used to transfer proteins on nitrocellulose membranes. The membrane was subsequently blocked with 5% skimmed milk and incubated overnight at four degrees Celcius with the primary antibody; Anti-Human mouse Bmp2/7(MAB3229). Then the membrane was incubated with an alkaline phosphatase-conjugated secondary antibody for three hours. The blot was then developed with BCIP/NBT in the dark at room temperature.

5.2.4. Release study using ELISA

Around 1 mg of sample (loaded with BMP-2/7 heterodimer) was incubated with PBS (pH 7.4) (that contained 1% (w/v) of BSA) as well as neurospheres (NSs)-culturing medium (mitogen-free) at 37º C and under agitation (100 rpm). The particles were centrifuged at 7000 RCF (for 10 min, 4º C) and the supernatants were collected at various periods ranging from 12 hours to 30 days. The BMP-2/7 heterodimer released from the protein-encapsulated particles to the supernatants, was estimated using enzyme-linked immunosorbent assay (ELISA).

ELISA was performed by coating NUNC flat bottomed 96 well plates with different concentrations of recombinant BMP2/7 incubating overnight at 4°C. The wells were subsequently blocked with 5% skimmed milk and incubated overnight at 4°C with the primary antibody; Anti-Human mouse Bmp2/7(MAB3229). ELISA was then developed with biotinylated secondary antibody (SAB3701278) and HRP conjugated streptavidin.

5.2.5. Scratch wound healing assay

To observe the effect of BMP2/7 heterodimer over SK-N-SH cell movement and division, a wound healing assay was performed. The cells were allowed to grow up to 100% confluency in a monolayer. Then scratch was induced by a scraper to make a visible discontinuity in the monolayer. The wound healing (due to cell migration and division) was observed microscopically. The initial time point (24 hrs.) explores the cell migration and the next two time points explore cell division. Thus the effect of BMP2/7 heterodimer on both cellular properties was explored.

5.3. Results

5.3.1. BMP-2/7 loaded PLGA carrier device and its characterization

BMP-2/7 heterodimer loaded PLGA particles were prepared by the oil-oil (O/O) emulsion-solvent evaporation method. The use of PLGA usually requires the application of shearing forces to encapsulate a protein that can affect the structural integrity of the protein and can also lead to protein denaturation. Also, PLGA tends to degrade very easily affecting the controlled nature of

drug release. Thus, copolymers or polyoxomers are usually used to mend the disadvantages associated with only PLGA encapsulation of proteins (3, 4). In this study, we have used Tetronic 701 as polyoxomer. The initial encapsulation of the protein by Tetronic will mostly lead to nano-complexation as pointed out in a former study (5). Although our study suggests that these Tetronic encapsulations of the BMP-2/7 protein will give rise to complexes of varying sizes. This might be because of the use of heterodimer as the encapsulating protein, which might cause a lack of homogeneity in its interaction with the polyoxomer and explain the resultant heterogeneous encapsulation. The design of the encapsulation process is explained in the manner of a flowchart in Fig.

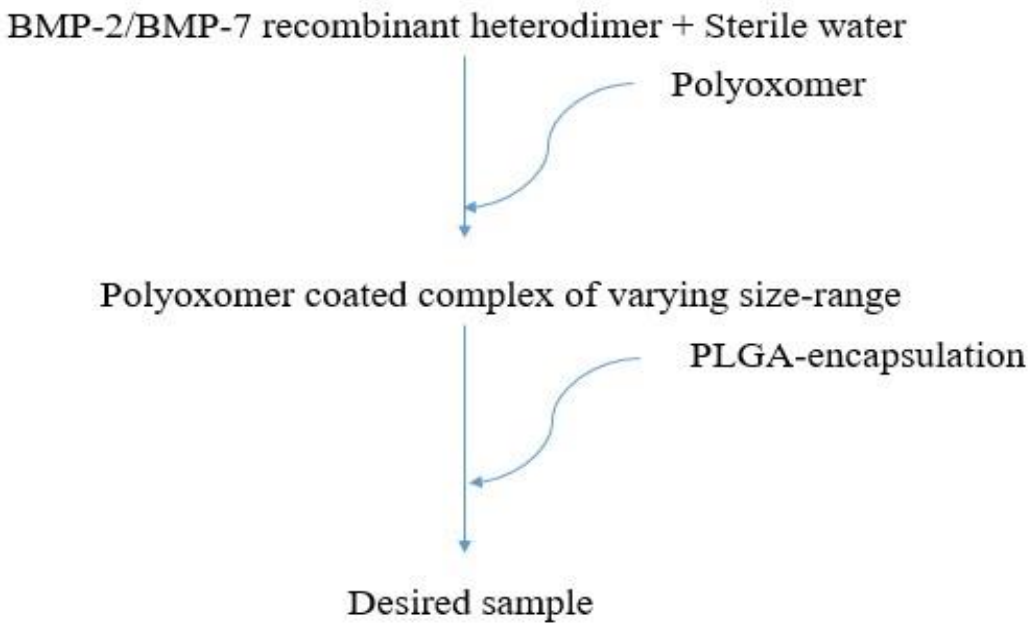

Fig. 1: A flowchart of the design of biodegradable implantable PLGA device encapsulating BMP-2/7 heterodimer.

The relative frequency intensity weighted (%) vs particle diameter size (nm) plot from the DLS study indicate the prevalence of two distinctive peaks distributed over a variable particle size ranging from 125.899 nm- 460.086nm and 1681.330 nm – 3779.304 nm with peak values corresponding to 246.0 nm and 2605 nm respectively and polydispersity index of 0.25. The plot also indicates a higher prevalence of particle with size diameter 246.0nm (>0.075%) when compared to size diameter 2605 nm (<0.025%) (Fig. 2).

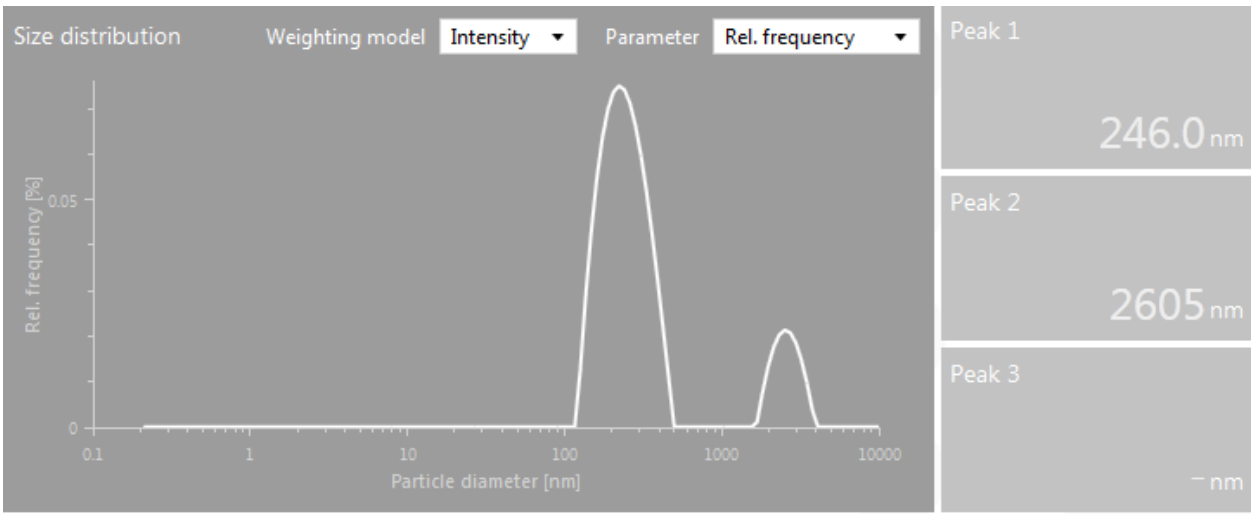

Fig. 2: The output from the DLS experiment showing two peaks in a relative frequency intensity weighted (%) vs particle diameter (nm) plot, representing the two most prevalent particle sizes in the target sample.

FESEM is a technique used to visualize and characterize minute details of objects under study. In our study, we visualized minute details of our encapsulated implant. FESEM imaging revealed that these encapsulated particles form core-shell type characterizations (Fig. 3).

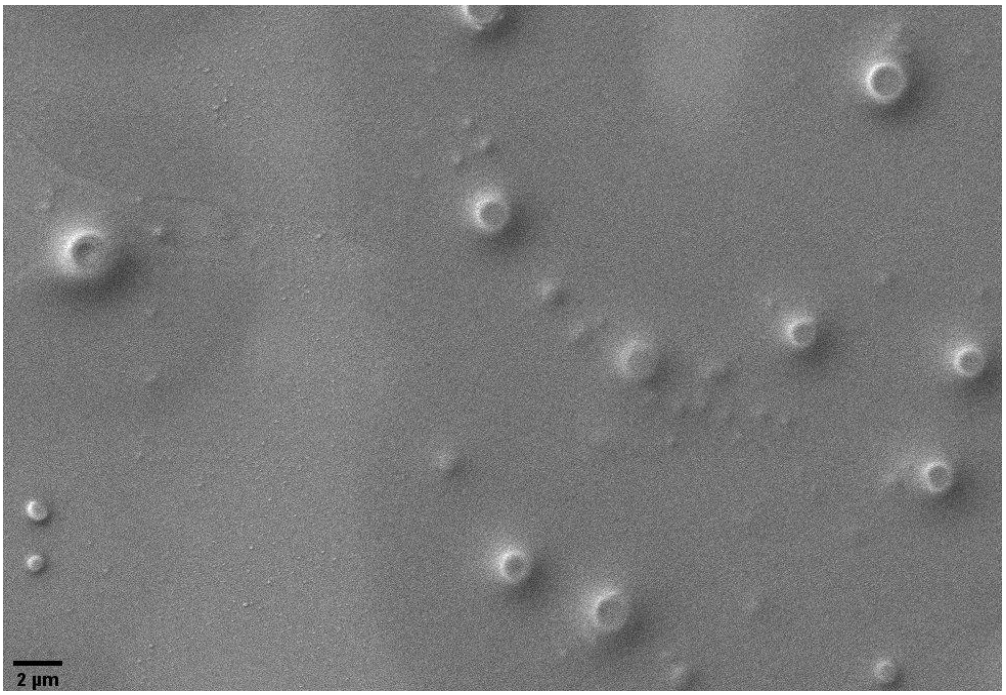

Fig. 3: FESEM imaging of the BMP-2/7 heterodimer encapsulated PLGA target sample**5.3.2.**

Characterization of the BMP-2/7 heterodimer protein using western blot

Western Blot was done to investigate the integrity of the protein used upon encapsulation. As per R and D (Research and Diagnostic) systems, SDS-PAGE visualization for BMP-2 and BMP-7 is at 12.9kDa and 15.8kDa, respectively. The SDS-PAGE visualization for the BMP-2/7 heterodimer is at approximately 40kDa. The BMP-2/7 heterodimer has a disulfide bond between its two monomeric subunits. So in the presence of beta-mercaptoethanol (BME) the disulfide bonds between the two monomeric subunits of the heterodimer would degrade and show two bands. But, again, since the difference between BMP-2 and BMP-7 is around 3 kDa, we would instead be getting a smudged broad-band that would represent both the monomeric subunits in the western blot (Fig. 4). The released nonreduced (-BME) protein heterodimer represent the same molecular weight as the BMP2/7 unloaded heterodimer. While BME treatment has given a broad band that has three plausible explanations. At first, the antibody used to identify the heterodimer is suggested to be not used for post sample reduction, but it was done nonetheless to be assertive of the dimeric form post nanocapsule preparation. Secondly, the BMP7 heterodimer contains three glycosylation sites that can lead to differential glycosylation in secreted protein and give rise to protein molecules with a little varying molecular weight. The third and final explanation could be the fact that the SDS-PAGE was not capable of distinguishing 3kDa difference between the monomers.

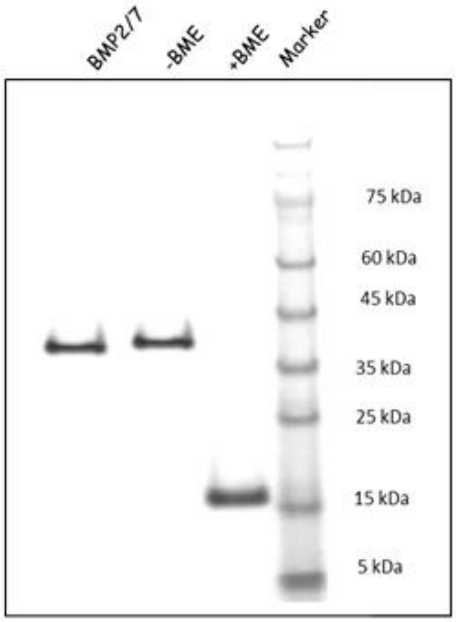

Fig 4. The 30th-day release sample on 12% SDS-PAGE, which was visualized with western blot.

5.3.3. Release study using ELISA

ELISA was done to conduct release studies. We performed an indirect model of ELISA. The recombinant BMP-2/7 heterodimer that we purchased was reconstituted, initially, at different concentrations, and the standard curve was constructed (Fig. 5).

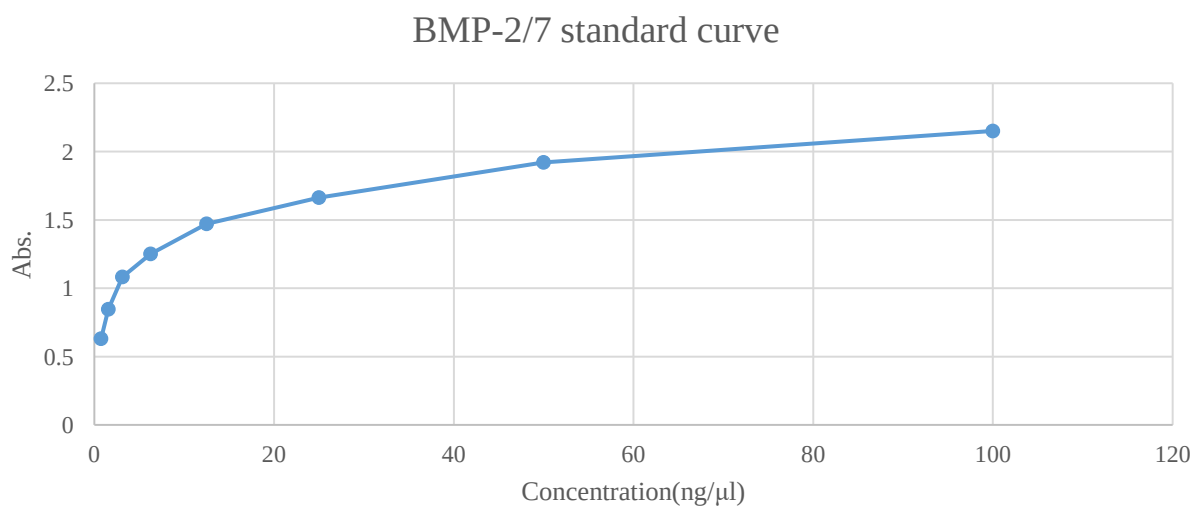

Fig. 5: The BMP-2/7 heterodimer standard curve

The release study was conducted in both PBS (Phosphate buffered saline) and DMEM/F-12 (Dulbecco's Modified Eagle Medium/F-12) supplemented release media. In both cases, we observed a gradual increase in the released protein concentration over a prolonged period (Table 1).

	Buffer (PBS)			Media (DMEM/F-12)		
	30th day	20th day	10th day	30th day	20th day	10th day
Absorbance	1.83	1.583	1.2	1.67	1.492	1.259
Concentration	0.306196	0.197953	0.053008	0.257134	0.138502	0.064678

Table 1: The heterodimer's concentration upon its release from the encapsulation in PBS and DMEM/F-12 supplemented release media.

5.3.4. Scratch wound healing assay

The wound area was calculated using the ImageJ 1.51K free software. We initially calculated the intensity of the wound area (pixels/cm) and then the readings of the scale bar numerical value was converted into a percentage of signals. The experiment's wound area was then shown as a percentage of the total area (Fig 6). From the wound healing assay, we can conclude that the treatment of SK-N-SH cells with the BMP-2/7 heterodimer affects the adhesion or the cell division.

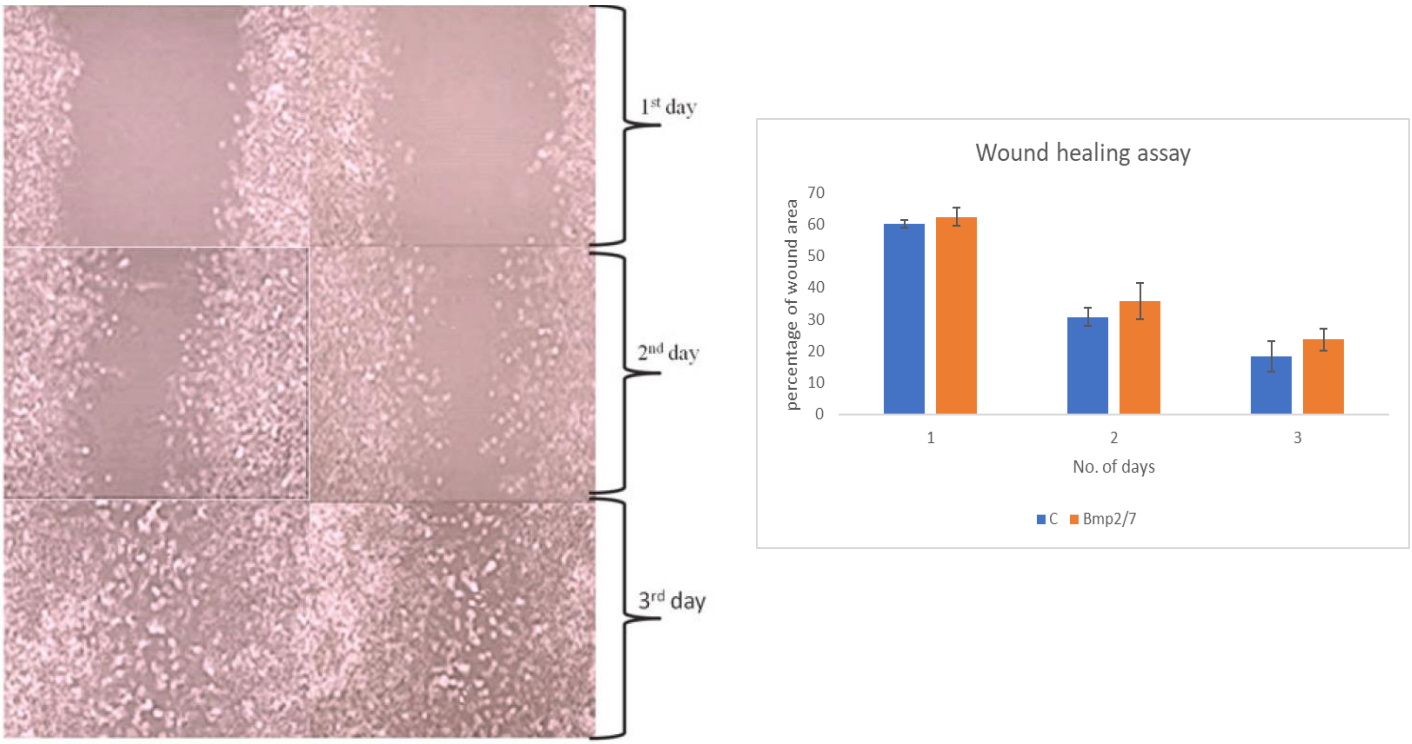

Fig. 6. Image reflecting the percentage of the wound area against the number of days post-scratch.

5.4. Conclusion

Our study could successfully design the desired BMP2/7 heterodimer encapsulated nanocapsule. We also observed trace amounts of microspheres formed along with our selected sample. This heterogeneity could be because of the heterodimer interacting with the polyoxomer in a varied manner. Although, this heterogeneity could also be advantageous as it could prolong the duration of release. The study also established a steady release of the heterodimer from the biodegradable implant for a minimum of 30 days. We are also planning further studies by increasing the number of days and investigating the maximum number of days, in which we expect a steady release of

the desired protein. The scratch wound healing assay study suggested that the heterodimeric protein release can either cause cell adhesion or cell division in the SK-N-SH cells. Our future studies could include a clonogenic index study to investigate the effect of the released protein on NSs (Neurospheres) formation assay and to identify the dosage required for an effective response and a FITC (Floroscein isothiocyanate) study, to detect the path followed by the heterodimer upon its release in the NSs formation assay.

5.5. Reference

1. Parajó Y, d'Angelo I, Horváth A, Vantus T, György K, Welle A, *et al.* PLGA: poloxamer blend micro- and nanoparticles as controlled release systems for synthetic proangiogenic factors. Eur J Pharm Sci 2010;41:644e9.
2. Tobío M, Nolley J, Guo Y, McIver J, Alonso MJ. A novel system based on a poloxamer/PLGA blends as a tetanus toxoid delivery vehicle. Pharm Res 1999;16:682e8.
3. Marco van de Weert, Wim E. Hennink, and Wim Jiskoot, Protein Instability in Poly(Lactic-co-Glycolic Acid) Microparticles, Pharmaceutical Research, Vol. 17, No. 10, 2000.
4. Hirenkumar K. Makadia and Steven J. Siegel, Poly Lactic-co-Glycolic Acid (PLGA) as Biodegradable Controlled Drug Delivery Carrier, Polymers (Basel). 2011 September 1; 3(3): 1377–1397.
5. Elaine Reguera-Nuñez, Carlota Roca , Eugenio Hardy , Maria de la Fuente , Noemi Csaba, Marcos Garcia-Fuentes, Implantable controlled release devices for BMP-7 delivery and suppression of glioblastoma initiating cells, Biomaterials 35 (2014) 2859e2867

Chapter 6: Conclusions and Discussions

Glioblastoma is one of the most aggressive form of cancers ever known to mankind. Even with several research studies and outputs in this topic every year, it still remains one of the prominent diseases without a cure. Our lab is also invested in designing a therapeutic strategy in dealing with Glioblastoma and this thesis therefore tries to engage with the question of a possible treatment that can be recommended in dealing with Glioblastoma or GBM. We have considered the BMP signaling pathway as the focus of our study and divided our entire study into three objectives. Our first objective was structurally investigate the protein-protein interactions between BMP homodimers and their antagonists (Gremlin-1 and Noggin).

In our first objective, we found several essential insights into the complex interactions between the BMPs (BMP-2, BMP-7) and the antagonists (Gremlin-1, Noggin). We were able to distinguish interfacial residues that were crucial for the interactions. In the BMP-2_Noggin complex, PROB50, SERB57, SERH38 in the Type-I receptor binding site and VALC33, SERC88 in the Type-II receptor binding site of BMP-2 are recognized as essential residues for the binding. In BMP-7_Noggin, VALA123, ALAD81, PROH35 in the Type-I receptor binding site and PROG35 in the Type-II receptor binding site of BMP-7 are found essential. In the interactions between BMP and Gremlin-1, amino acid residues GLYC27, CYSG108, THRG150, CYSL108 in BMP-2_Gremlin-1 and amino acid residues LEUA50, LEUA75, PROD74, METG152 in BMP-7_Gremlin-1 are found to be very crucial for maintain the stability of the complexes formed. These interfacial residues upon mutation can cause maximum destabilization to the complexes. Thus, these interfacial residues can be treated as hot-spot residues which can be used to design pharmacology and by high throughput virtual screening, we would be able to design small molecule modulators which can inhibit the interactions between these complexes. As mentioned before in chapter 1, an active BMP signaling pathway can benefit a Glioblastoma patient, promoting differentiation, reducing GBM proliferation and thereby suppressing the tumorigenic nature of the Glioblastoma Initiating Cells (R. Galli *et al. Cancer Research* 2004, S. G. M. Piccirillo *et al. Nature* 2006, Z. Zhou *et al. Cancer Biotherapy and Radiopharmaceuticals* 2011). Apart from that we also obtained insights into the nature of binding. We observed that while mutational destabilization in case of the interactions between the BMPs and Gremlin-1 is predominantly driven by steric hindrance, the same cannot be said in case of the interactions between the BMPs and Noggin. The interactions between the BMPs and Noggin is also

destabilized because of breakdown of bonds such as hydrogen bonds, alkyl-alkyl interactions, pi-alkyl interactions etc. We also observed hierarchical binding in case of the interactions between the BMPs and Gremlin-1. We could observe the same phenomenon in the interactions between the BMPs and Noggin as well, but it was much clearly visible in BMP-2_Noggin with BMP-2 favoring Type-II receptor binding site as compared to Type-I receptor binding site. We already knew that Gremlin-1 formed oligomeric complexes with the BMPs (Kišonaitė, M. *et al.* Biochem J. 2016), and we further wondered how large a oligomeric complex it can form with the BMPs if the complex structure has to be confined in a closed ended manner if it had to terminate the process of polymerization on its own. Our study suggests that a simplest model of such a close ended structure would be a cis-trans model where both the parallel conformation of binding by Gremlin-1 across the BMPs and the anti-parallel conformation of binding has to simultaneously engage in the process of oligomeric complex formation.

Our second objective was to investigate the complex interactions between BMP-2/7 heterodimer and antagonists (Noggin, Gremlin-1). There are reports suggesting weaker antagonism of BMP-2/7 heterodimer by Noggin, and we wanted to understand if it was the same case in the case of Gremlin-1 as well. It was essential as Gremlin-1 as compared to Noggin, plays a much predominant role in maintaining tumor hierarchy (Kenneth Yan *et al.* Genes & development 2014). We also wanted to compare the nature of binding between BMP-2/7_Noggin and BMP-2/7_Gremlin-1. We observed that even in context to Gremlin-1, there is a weaker antagonizing affect towards the heterodimer as compared to the homodimers. We observed that in both situations of binding, the BMP-7 monomeric subunit of the heterodimer is engaged in binding with the antagonists at the Type-I receptor binding site, while the BMP-2 monomeric unit engaged at the Type-II receptor binding site. This is contrary to the preferential binding site for both BMP-7 and BMP-2, which could probably be the reason for forming weaker interactions. We, therefore, tried to do an in vitro study to see the significance of these weaker antagonisms. We treated human glioblastoma cells (SK-N-SH) with the BMP-2/7 heterodimer and observed that in the initial 7 days of the treatment, the area of the neurospheres was reduced by approximately 40 %. Upon further treatment, we were gradually not able to visualize any neurospheres (Only cell clumps were visualized). This might have been because of the weaker antagonism by the antagonists. This

finding can therefore be used to design a prominent therapeutic strategy against glioblastoma which becomes the aim of our third and final objective.

In the final objective, we successfully designed a nanocapsule which can be implanted upon surgical resection. We encapsulated the BMP-2/7 heterodimer with polyoxomer-PLGA. We observed trace amount of microspheres as well but comparatively their existence wasn't much significant. We also observed a steady release of the heterodimer from the nanocapsule implant for a minimum of 30 days and we are planning to do further studies to quantify the maximum number of days it is required for the release of the entire heterodimer from the nanocapsule. Our further studies in this context would include a clonogenic index study which will help us to identify the effective dosage and also a FITC study to show the path through which the heterodimer travels upon its release in the neurospheres formation assay.

.

Publications

Received: 19 February 2020 | Revised: 3 June 2020 | Accepted: 2 August 2020
DOI: 10.1002/jcc.26407

FULL PAPER

Journal of COMPUTATIONAL CHEMISTRY WILEY

Structural basis of BMP-2 and BMP-7 interactions with antagonists Gremlin-1 and Noggin in Glioblastoma tumors

Kesaban Sankar Roy Choudhuri | Seema Mishra

- Kesaban Sankar Roy Choudhuri, Seema Mishra. Structural basis of BMP-2 and BMP-7 interactions with antagonists Gremlin-1 and Noggin in Glioblastoma tumors. J Comput Chem. 2020;1–18.

BMP nanocapsule formulation in treating Glioblastoma and BMP-antagonists interaction studies

by Kesaban Sankar Roy Choudhuri

BMP nanocapsule formulation in treating Glioblastoma and BMP-antagonists interaction studies

ORIGINALITY REPORT

7%	2%	7%	1%
SIMILARITY INDEX	INTERNET SOURCES	PUBLICATIONS	STUDENT PAPERS

PRIMARY SOURCES

1	Kesaban Sankar Roy Choudhuri, Seema Mishra. "Structural basis of BMP-2 and BMP-7 interactions with antagonists Gremlin-1 and Noggin in Glioblastoma tumors", Journal of Computational Chemistry, 2020 Publication	3%
2	Submitted to Washington University in St. Louis Student Paper	1%
3	Beth Bragdon, Oleksandra Moseychuk, Sven Saldanha, Daniel King, Joanne Julian, Anja Nohe. "Bone Morphogenetic Proteins: A critical review", Cellular Signalling, 2011 Publication	<1%
4	Elaine Reguera-Nuñez, Carlota Roca, Eugenio Hardy, Maria de la Fuente, Noemi Csaba, Marcos Garcia-Fuentes. "Implantable controlled release devices for BMP-7 delivery and suppression of glioblastoma initiating cells", Biomaterials, 2014 Publication	<1%

5	Venkanna Bhanothu, Anand Kumar Kondapi. "Status of topoisomerase-2β protein in all-trans retinoic acid–treated human neuroblastoma (SK-N-SH) cells", Journal of Cellular Biochemistry, 2018 Publication	<1 %
6	Sonia B. Jakowlew. "Transforming Growth Factor-β in Cancer Therapy, Volume I", Springer Science and Business Media LLC, 2008 Publication	<1 %
7	Ahmed, S.. "Virtual screening and selection of drug-like compounds to block noggin interaction with bone morphogenetic proteins", Journal of Molecular Graphics and Modelling, 201004 Publication	<1 %
8	Toril Holien, Anders Sundan. "The role of bone morphogenetic proteins in myeloma cell survival", Cytokine & Growth Factor Reviews, 2014 Publication	<1 %
9	Adrian E Harrington, Samantha A Morris-Triggs, Brandon T Ruotolo, Carol V Robinson, Shin-ichi Ohnuma, Marko Hyvönen. "Structural basis for the inhibition of activin signalling by follistatin", The EMBO Journal, 2006 Publication	<1 %

papyrus.bib.umontreal.ca

10	Internet Source	<1 %
11	Jessica Jann, Suzanne Gascon, Sophie Roux, Nathalie Faucheux. "Influence of the TGF-β Superfamily on Osteoclasts/Osteoblasts Balance in Physiological and Pathological Bone Conditions", International Journal of Molecular Sciences, 2020 Publication	<1 %
12	Schreuder, H.. "Crystal structure of recombinant human growth and differentiation factor 5: Evidence for interaction of the type I and type II receptor-binding sites", Biochemical and Biophysical Research Communications, 20050415 Publication	<1 %
13	theses.gla.ac.uk Internet Source	<1 %
14	Ramesh Prasad, Prosenjit Sen. "Computational Approach to Identify Differential Behaviours of Soluble Tissue Factor and Full-length Tissue Factor towards Factor VIIa", Phys. Chem. Chem. Phys., 2017 Publication	<1 %
15	www.ijritcc.org Internet Source	<1 %

16	parasitol.kr Internet Source	<1 %
17	Zhang, J.I.. "Crystal Structure Analysis Reveals How the Chordin Family Member Crossveinless 2 Blocks BMP-2 Receptor Binding", Developmental Cell, 20080513 Publication	<1 %
18	Submitted to University of Hong Kong Student Paper	<1 %
19	cancerci.biomedcentral.com Internet Source	<1 %
20	Submitted to La Trobe University Student Paper	<1 %
21	mafiadoc.com Internet Source	<1 %
22	S J. Lin. "The structural basis of TGF- , bone morphogenetic protein, and activin ligand binding", Reproduction, 08/01/2006 Publication	<1 %

Exclude quotes On

Exclude bibliography On

Exclude matches